UNIVERSITEIT VAN PRETORIA
UNIVERSITY OF PRETORIA
YUNIBESITHI YA PRETORIA

# PROCESS DEVELOPMENT FOR THE REMOVAL OF IRON FROM NITRIDED ILMENITE

by

Jaco Johannes Swanepoel
29613435

Submitted in partial fulfilment of the requirements for
the degree of

**MASTER OF ENGINEERING (Chem Eng)**

in the

**DEPARTMENT OF CHEMICAL ENGINEERING**
**FACULTY OF ENGINEERING, BUILT ENVIRONMENT & INFORMATION TECHNOLOGY**

**UNIVERSITY OF PRETORIA**

**PRETORIA**

**October 2010**



UNIVERSITEIT VAN PRETORIA
UNIVERSITY OF PRETORIA
YUNIBESITHI YA PRETORIA
Faculty of Engineering, Built Environment and Information Technology

**University of Pretoria**

**Department of Chemical Engineering**

**CVD 800**

**Dissertation**

**Process Development for the Removal of Iron from Nitrided Ilmenite**

**Jaco Johannes Swanepoel**

**29613435**

**October 2010**

# SYNOPSIS

The Council for Scientific and Industrial Research (CSIR) in South Africa is developing a process to produce titanium tetrachloride from a low-grade material such as ilmenite. Titanium tetrachloride can then be used as feed material for titanium metal or pigment-grade titanium dioxide production. Titanium tetrachloride is commercially produced by chlorinating synthetic rutile (<92% $TiO_2$) or titanium dioxide slag (<85% $TiO_2$) at ~900 ˚C. A drawback of chlorination at this temperature is that any constituents other than $TiO_2$ will end up as hazardous waste material.

A characteristic step in the CSIR's proposed process is to nitride titanium dioxide contained in the feed material before it is sent for chlorination. The chlorination of the resulting titanium nitride is achieved at a much lower temperature (~200˚C) than that of the existing titanium dioxide chlorination reaction. An added advantage of the low-temperature chlorination reaction is that chlorine is selective mostly towards titanium nitride and metallic iron, which means that any other constituents present are not likely to react with the chlorine. The result is reduced chlorine consumption and less hazardous waste produced. The nitrided ilmenite must, however, be upgraded by removing all iron before it can be sent for chlorination. Commercial ilmenite upgrading processes, called *synthetic rutile production*, also require the removal of iron and other transition metals before chlorination.

A literature review of existing ilmenite upgrading processes revealed four possible process options that could remove iron from nitrided ilmenite. Two of these process options, the Becher and Austpac ERMS SR processes, are proven process routes. The other two are novel ideas – one to passivate iron contained in the nitrided ilmenite against chlorination and the other to use ammonium chloride (as used in the Becher process) as a stoichiometric reactant to produce a ferrous chloride solution. A preliminary experimental evaluation of these process options indicated that the Austpac ERMS SR process is the most viable option for removing iron from nitrided ilmenite. The Austpac ERMS SR process was therefore selected as a template for further process development.

A detailed Austpac ERMS SR process review found that two process units in the Austpac ERMS SR process could be used in a process that separates iron from nitrided ilmenite. These are the Enhanced Acid Regeneration System and the Direct Reduced Iron process units. The review also concluded that another leach unit would have to be developed. It was therefore necessary to further investigate the dissolution of nitrided ilmenite in hydrochloric acid.

A detailed experimental evaluation of nitrided ilmenite dissolution in hydrochloric acid found that hydrochloric acid could be used as the lixiviant to selectively remove iron from nitrided ilmenite. The dissolution of metallic iron in 90 ˚C hydrochloric acid reached levels of at least 96% after only 60 minutes. An average “combined resistance” rate law was found that could be used to describe this dissolution reaction. The observed activation energy and Arrhenius pre-exponential factor were found to be equal to 9.45 $kJ.mol^{-1}$ and 30.8 $s^{-1}$ respectively.

The Austpac ERMS SR process review and experimental results described above were then combined and used to propose a process that could be employed to remove iron from nitrided ilmenite. The proposed process was modelled using the Flowsheet Simulation module in HSC Chemistry 7.0©. The result is a process model that removes most of the iron from nitrided ilmenite and produces a high-quality iron by-product.

**Keywords:** titanium nitride, upgraded nitrided ilmenite, hydrochloric acid leaching, metallic iron dissolution, synthetic rutile, titanium tetrachloride

# ACKNOWLEDGEMENTS

I would like to express my gratitude to The Department of Science and Technology for funding this research and the CSIR for using its facilities.

I would also like to thank the following people for all their help and support, without them I would not have been able to complete this work:

- I want to thank Dawie van Vuuren for his guidance. He is my manager, but also someone who deserves to be called my mentor.
- I want to thank Dr. Mike Heydenrych for his guidance as academic supervisor.
- Finally, a special thanks to my family and fiancée for their never-ending love and support.

# CONTENTS

# LIST OF FIGURES

# LIST OF TABLES

# LIST OF ABBREVIATIONS

| | |
|---|---|
| CSTR | Continuous stirred-tank reactor |
| DRI | Direct Reduced Iron |
| EARS | Enhanced Acid Recovery System |
| EDX | Energy-dispersive X-ray spectroscopy |
| ERMS | Enhanced Roasting and Magnetic Separation |
| FE-SEM | Field-emission scanning electron microscope |
| PSD | Particle size distribution |
| SEM | Scanning electron micrograph/microscopy |
| TGA | Thermo-gravimetric analysis |
| WHIMS | Wet High-Intensity Magnetic Separation |
| XRD | Powder X-ray diffraction |

# CHAPTER 1 – INTRODUCTION

## 1.1 – Background and motivation

The Council for Scientific and Industrial Research (CSIR, 2009) in South Africa is actively seeking an alternative method to produce titanium metal more economically than current practices. Titanium tetrachloride is, however, required as feed for titanium metal production.

The CSIR has proposed a novel low-temperature titanium tetrachloride production method (Van Vuuren & Stone, 2006: 1–12). This process is referred to as the "CSIR's proposed process" for the purpose of this dissertation. Figure 1.1 is a simplified block flow diagram of the CSIR's proposed process and shows only the main process units and major streams in the process. The diagram in Figure 1.1 is for an ideal case where 100% iron is separated in the "upgrade" unit.

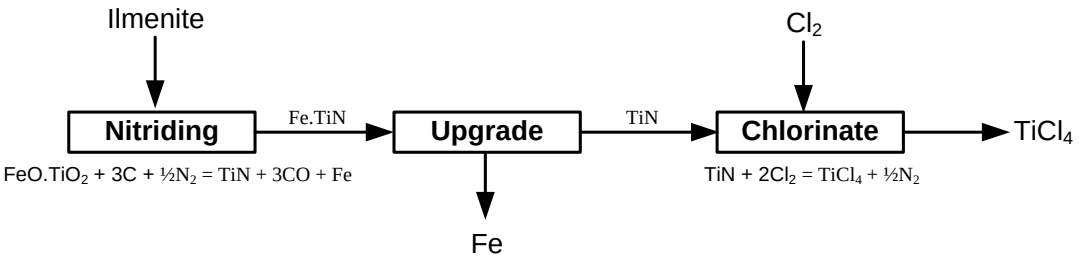


**Figure 1.1: Simplified block flow diagram for an ideal CSIR proposed process**

The CSIR's proposed process recovers titanium dioxide from low-grade feed materials such as ilmenite by first nitriding (Reaction 1.1) the feed and then chlorinating (Reaction 1.2) the titanium nitride contained in the nitrided feed.

Chlorination of the titanium nitride can be achieved at much lower temperatures (ca 200 ˚C) than in the existing (ca 900 ˚C) titanium dioxide chlorination reaction (Van Vuuren & Stone, 2006: 2).

$$FeO.TiO_2 + 3C + \tfrac{1}{2}N_2 = TiN + 3CO + Fe \qquad \text{Reaction 1.1}$$

$$TiN + 2Cl_2 = TiCl_4 + \tfrac{1}{2}N_2 \qquad \text{Reaction 1.2}$$

An advantage of the low-temperature chlorination reaction in the CSIR's proposed process is that chlorine's selectivity towards titanium nitride is higher than towards most of the other constituents in the feed (Van Vuuren & Stone, 2006: 5). This is true except for iron, which chlorinates at the same conditions as titanium nitride. The removal of iron (the "upgrade" block in Figure 1.1) is therefore crucial before chlorinating the nitrided ilmenite.

Commercial processes, which use titanium dioxide instead of titanium nitride, also require the removal of iron and other transition metals from ilmenite (Geetha & Surender, 2000: 42). This is referred to as the "upgrading" of ilmenite (40–60% $TiO_2$) to synthetic rutile (92–95% $TiO_2$) or "synthetic rutile production".

## 1.2 – Purpose of dissertation

The main objective of this dissertation is to develop and propose a process for removing iron from nitrided ilmenite. The following objectives are in support of the main objective:

1. To find and review available ilmenite upgrading processes and select process routes that might be applicable to nitrided ilmenite upgrading (Chapter 2).
2. To standardise a sample of nitrided ilmenite to be used in all experimental investigations (Chapter 3).
3. To experimentally evaluate candidate process routes (i.e. to determine whether they could be used on nitrided ilmenite) and select the most viable option (Chapter 4).
4. To conduct a detailed review of the process option selected in (3) (Chapter 5).
5. To conduct an in-depth experimental evaluation on a unit in the process selected (Chapter 6).
6. To propose a process for removing iron from nitrided ilmenite (Chapter 7).

## 1.3 – Scope of dissertation

The following steps are required in order to meet the objectives stated in Section 1.2:

1. Literature review to identify available process technologies (Chapter 2).
    a. Find commercial process technologies.

   b. Find non-commercial process technologies.
   c. Recommend other possible process options for further investigation.
2. Standardise a sample of nitrided ilmenite to be used in all experimental investigations (Chapter 3).
3. Undertake an experimental evaluation of the process options identified in Chapter 2 to determine whether they are viable (Chapter 4).
   a. Conduct a literature review to determine the appropriate experimental conditions.
   b. Conduct an experiment for each process option.
   c. Select the most viable process option for removing iron from nitrided ilmenite.
4. Conduct a detailed review of the process option selected in Chapter 4 (Chapter 5).
   a. Conduct a literature review to obtain a process description.
   b. Propose a process flow diagram for the process selected.
   c. Determine or estimate material and energy balances for the process selected.
5. Conduct an in-depth experimental evaluation on a unit in the selected process (Chapter 6). In this case the unit selected for experimental work is the leach unit.
   a. Evaluate the effect of acid concentration on reaction rate.
   b. Evaluate the effect of temperature on reaction rate.
   c. Analyse rate data and recommend a rate law that could describe the dissolution reaction.
   d. Evaluate the dissolution of other nitrided ilmenite constituents in hydrochloric acid.
6. Propose a process for removing iron from nitrided ilmenite (Chapter 7).
   a. Compile a process description.
   b. Estimate material and energy balances for the proposed process.

# CHAPTER 2 – LITERATURE REVIEW

## 2.1 – Overview

Titanium tetrachloride is commercially obtained by chlorinating titanium dioxide. Any transition metals present during chlorination lead to chlorine consumption. The removal of iron and other transition metals from a feed source such as ilmenite is therefore crucial before chlorination and is known as “ilmenite upgrading” or “synthetic rutile production” (Geetha & Surender, 2000: 42).

Therefore, various process options already exist to remove transition metals, especially iron if ilmenite is used as feedstock. The aim of this chapter is therefore to find existing process technologies.

The literature review of existing process technologies is discussed in two sections, one for commercial (Section 2.2) and one for non-commercial (Section 2.3) processes. Section 2.4 is a brief discussion of the literature review. The chapter concludes in Section 2.5 with selected processes that require experimental evaluation to determine their practicability.

The result of the literature review is summarised in three figures, Figure 2.1, 2.2 and 2.3. Each process mentioned in these figures is categorised according to the industrial method used. These methods are:

- Hydrometallurgical – This involves separation in an aqueous medium.
- Pyrometallurgical – This involves separation by means of thermal treatment.
- Combination of pyrometallurgical and hydrometallurgical – To upgrade ilmenite, for example, the ore is first thermally treated to change the iron oxidation state from $Fe^{3+}$ to $Fe^{2+}$ or $Fe^{0}$. A hydrometallurgical separation method such as hydrochloric acid leaching is then used as the main separation step.

Process classification is performed to help identify options that could be applied to the CSIR’s nitrided ilmenite upgrading scheme. The combined pyro- and hydrometallurgical

category is of particular interest because the nitriding reaction, Reaction 1.1, entails a thermal processing step.

## 2.2 – Commercial processes used to produce synthetic rutile

Figure 2.1 illustrates commercial processes used to upgrade ilmenite. These processes are only briefly discussed below. Refer to the source articles for more information.

| Separation category | Separation method applied | Products obtained | Process name or description |
|---|---|---|---|
| Hydrometallurgical | Hot sulphuric acid leaching | Waste iron sulphates (Copperas) and pigment grade (+99%) $TiO_2$ | **Sulphate process** |
| Hydro- & Pyrometallurgical | Thermal pre-treatment → Aerated leaching & iron oxides precipitation → Sulphuric acid leaching (refinement) | Waste iron oxides and +92% $TiO_2$ | **Becher process** |
| | Thermal pre-treatment → Hydrochloric acid leaching → Acid regeneration | Waste iron oxides and +92% $TiO_2$ | **Benilite process**<br>**Austpac process** |
| Pyrometallurgical | **Carbothermal reduction and melting** (Arc furnace) | ±85% $TiO_2$ and pig iron | **Smelting process** |

**Figure 2.1: Processes industrially used to produce synthetic rutile from ilmenite**

*The Sulphate process*

In the Sulphate process, ilmenite is treated with concentrated sulphuric acid ($H_2SO_4$) at 150-180 ˚C in a batch process according to the following reaction (Van Dyk, 1999: 2):

$$FeTiO_3(s) + 5H_2O + 2H_2SO_4(aq) = FeSO_4{\cdot}7H_2O(s) + TiOSO_4(aq) \qquad \text{Reaction 2.3}$$

Ferric sulphate can form when leaching ilmenite. If present, ferric sulphate is reduced to ferrous sulphate with the addition of scrap iron (Ward, 1990: 4). The solution is then cooled down to precipitate ferrous sulphate ($FeSO_4{\cdot}7H_2O(s)$ or copperas) after which it is separated from the solution (Ward, 1999: 7). The solution is heated to 90˚C to hydrolyse the titanyl sulphate to insoluble titanyl hydroxide (Van Dyk, 1999: 2):

$$TiOSO_4(aq) + 2H_2O = TiO(OH)_2(s) + H_2SO_4(aq) \qquad \text{Reaction 2.4}$$

The solids are finally calcined at 1°000 to drive off contained water to produce pigment-grade titanium dioxide (Zhang & Nicol, 2009: 146).

The Sulphate process accounts for 40% of world production for pigment grade titanium dioxide (Zhang & Nicol, 2009: 146) but produces large amounts of waste (Ward, 1990: 4). Each ton of titanium dioxide produced results in 2 to 3 tons of iron sulphate waste (Motsie, 2008: 13).

*The Becher process*

The Becher process (Becher, 1963) was developed primarily to upgrade Western Australian ilmenite from approximately 55 to 95% titanium dioxide (Ward, 1999: 4). It is a two-step procedure for upgrading ilmenite. In the first processing step, ferrous and ferric ions are reduced to metallic iron ($Fe^{\circ}$) in a rotary kiln using coal as both fuel and reductant (Ward, 1990: 11). The reduced ilmenite is then leached with aerated water in the presence of ammonium chloride ($NH_4Cl$) to produce synthetic rutile and iron oxides (Bruckard, Calle, Constanti-Carey, Fletcher & Horne, 2003).

The Becher process is a cost-effective method (Noubactep, 2009: 2) for upgrading ilmenite, but it also has disadvantages, the first of which is the slow rate of reaction (Ward, 1990: 12): the aerated leaching step for a 20 ton batch of reduced ilmenite takes approximately 14-20 hours (Ward, 1999: 12). The second disadvantage is the wide range of iron oxides produced as waste (Geetha & Surender, 1997: 214). Extensive research work has been done to characterise the aerated leaching step in an attempt to control the precipitation of different iron oxides (Ward, 1990; Ward, 1999; Geetha & Surender, 1997; Geetha & Surender, 2000).

*Hydrochloric acid leaching of thermally treated ilmenite*

The Benilite and Austpac processes both fall into this category (Lanyon, Lwin & Merrit, 1999: 300; Walpole & Winter, 2002: 1). These are acid leaching processes consisting of a pre-leach thermal treatment step, a hydrochloric acid leaching step, and finally an acid regeneration step (Lanyon *et al.*, 1999: 299).

The Austpac process (Winter, 2008) is the newest hydrochloric acid leaching process and claims to be more cost-effective than the Benilite process (Walpole & Winter, 2002: 1). The Austpac process includes an improved oxidation and reduction unit, as well as an improved acid recovery and acid regeneration section, with the added possibility of producing

metallised iron as a by-product. The Austpac process is, however, not a fully commercial process yet but a 3 000 t/a synthetic rutile plant was built and operated for a year to successfully prove the process's patented technology (Austpac Resources N.L., 2010). The developers of the Austpac process won the 2008 Australian Mining Industry Award for "Applied Technology of the Year" (ABN Newswire, 2008; Austpac Resources N.L., 2010).

The next step for the Austpac process is a 60 000 t/a synthetic rutile plant to be built in Eastern Australia. This plant has an anticipated capital cost of AU$120 million with a three-year payback period and a 30% internal rate of return (Austpac Resources N.L., 2010).

*Carbothermal reduction of ilmenite in a plasma/electric arc furnace*

In this smelting process, ilmenite is carbothermally reduced in a plasma/electric arc furnace to pig iron and a slag rich in titanium (Zhang & Nicol, 2009: 146). The product obtained contains approximately 85% titanium dioxide (Lanyon *et al.*, 1999: 300) and serves as feed to other processes to produce either synthetic rutile or titanium pigment (Mahmoud, Afifi & Ibrahim, 2004: 100).

This process involves high power, capital and maintenance costs but produces pig iron as by-product (Ward, 1999: 5).

Carbothermal reduction of ilmenite or "slagging" is the major method used in South Africa to beneficiate titanium-bearing minerals such as ilmenite. Richards Bay Minerals, situated in South Africa, is the leading producer of titanium slag in the world (Motsie, 2008: 3).

## 2.3 – Non-commercial processes for synthetic rutile production

Figure 2.2 illustrates the non-commercial processes developed to upgrade ilmenite. These processes are only briefly discussed below. Refer to the source articles for more information regarding these processes.

| Separation category | Separation method applied | Products obtained | Process name or description |
|---|---|---|---|
| Hydrometallurgical | Sulphuric acid leaching → Solvent extraction | Waste iron sulphates and +92% $TiO_2$ | **Solvent extraction** |
| Hydro- & Pyrometallurgical | Thermal pre-treatment → Leaching Fe with $Fe^{3+}$ → Electrolytic or oxidative ($O_2$) regeneration of $Fe^{3+}$ | Electrolytic $Fe^{3+}$ regeneration → Iron product and +92% $TiO_2$<br>Oxidative ($O_2$) $Fe^{3+}$ regeneration → Iron oxides and +92% $TiO_2$ | **Summit process** |
| | Thermal pre-treatment → Sulphuric acid leaching → Acid regeneration | Waste iron sulphates and +92% $TiO_2$ | **Isihara process** combined with **Sulphate process** |
| | Thermal pre-treatment → Hydrochloric acid leaching → Acid regeneration | Waste iron oxides and +92% $TiO_2$ | **Murso process**<br>**Laporte process**<br>**Tiomin Synthetic Rutile** (TSR) **process** |

**Figure 2.2: Non-commercial processes available for producing synthetic rutile from ilmenite**

*Solvent extraction*

Solvent extraction was tested on South African ilmenite feedstocks as a possible hydrometallurgical method for separating titanium from the iron titanate complex (Sole, 1999a; Sole, 1999b). The investigation led to a continuous mini-plant trial run (Sole, Feather & Connell, 1999). However, from the results it was concluded that a slow rate of reaction and poor titanium-stripping capabilities are limitations on the commercial application of solvent extraction (Sole, Feather & Connell, 1999: 283).

*The Summit process*

The Summit process consists of three main steps (Shiah, 1966). The first step is the thermal reduction of ferrous and ferric ions to the metal state. The second step uses ferric chloride ($FeCl_3$) to leach metallic iron from ilmenite to result in a solution containing both ferrous and ferric chloride (Ward, 1990: 14). The final step is the regeneration of ferric ions required for the leaching step. The regeneration step can be done in two ways:

1. Oxidation of ferrous chloride with air (Shiah, 1966)
2. Electrochemical oxidation of ferrous chloride to produce ferric and metallic iron (Cunningham, 1958).

The Summit process was found to be not commercially feasible at the time due to high capital and operating costs (Ward, 1999: 6).

*Acid leaching processes*

The Isihara process is a sulphuric acid leaching process that uses waste sulphuric acid, from spent sulphuric acid in the Sulphate process, to produce synthetic rutile (Ward, 1999: 5). Large amounts of waste iron sulphates were, however, produced in the Isihara process which prevented its commercialisation.

The Murso process (Ward, 1999; Lanyon *et al*., 1999, Walpole & Winter, 2002), the Laporte process (Walpole & Winter, 2002; Winter, 2008) and the TSR process (Winter, 2008) are all hydrochloric acid leaching process options with various methods of either leaching or regenerating the acid. None of these processes was, however, commercialised.

## 2.4 – Discussion

The summaries illustrated in Figure 2.1 and Figure 2.2 give an indication of how much work has been done in an attempt to find a suitable process for effectively removing iron from an iron titanate complex such as ilmenite. It is clear from a comparison of Figure 2.2 and Figure 2.1 that the success rate of finding a successful iron removal process is rather small and is dependent on not only the extent of iron removal, but also on keeping the capital and operating costs as low as possible.

The possible process options suitable for the CSIR's proposed process are somewhat reduced when one considers that only process options with a thermal pretreatment step are relevant since the nitriding step of the CSIR's proposed process is similar to the thermal pretreatment step in conventional process options.

The issue of waste generation in most commercial processes may impose another design restriction on new ilmenite upgrading processes, i.e. spend more money to generate less waste and, if possible, produce an iron by-product that can be sold.

Three different approaches are available for consideration when selecting a process for upgrading nitrided ilmenite:

- Apply an existing commercial process, but adapt it to use nitrided ilmenite as feed.

- Improve or modify an existing process to be more economical or to produce iron or iron by-products instead of waste.
- Develop a novel process.

The use of an existing process would be the preferred manner to proceed because the technology already exists. The only requirement would be to adapt the process to use nitrided ilmenite as feed instead of conventionally reduced ilmenite.

Two existing process technologies were selected in Figure 2.1 as candidates that could be adapted and used to upgrade nitrided ilmenite. The Becher process (Becher, 1963) and the Austpac process (Walpole & Winter, 2002: 1–13) were the two process options selected.

The Becher process will most likely work on nitrided ilmenite, because nitriding in the CSIR's proposed process also reduces the iron in ilmenite to its metallic state before it is sent to the next processing step (Van Vuuren & Stone, 2006: 2). The nitrided ilmenite should, however, still be analysed and tested for high concentrations of magnesium and chromium. High concentrations of these species inhibit the aerated leaching reaction and ultimately result in the Becher process not being technically viable (Lanyon *et al*., 1999: 300).

The Austpac process is the second process considered. A thermal treatment section is required in both the Austpac process and the CSIR's proposed process. The thermal treatment step in the Austpac process is called the "Enhanced Roasting and Magnetic Separation" (ERMS) section, with main objective of increasing the magnetic properties of the ilmenite (Walpole & Winter, 2002: 4). This is achieved by first roasting the ilmenite in air to oxidise the $Fe^{2+}$ to produce $Fe^{3+}$, after which the ore is selectively reduced to produce a high ratio of $Fe^{2+}/Fe^{3+}$ (Walpole & Winter, 2002: 4). This practice of oxidisation and then partial reduction is claimed also to increase the leachability of iron in the ilmenite ore (Walpole & Winter, 2002: 5). This thermal treatment differs from that of the CSIR's proposed process in that the ilmenite ore is nitrided (Reaction 2.1) to produce titanium nitride and metallic iron ($Fe^{o}$) (Van Vuuren & Stone, 2006). Experimental work will therefore be required to evaluate the leachability of nitrided ilmenite at the leaching conditions claimed to be possible in the Austpac process. The "Enhanced Acid Recovery System" (EARS) and the "Direct Reduced Iron" (DRI) sections in the Austpac process are the two sections with the most potential to improve economic viability and to reduce environmental impact. This is achieved by producing a 25 wt % hydrochloric acid that is recycled to the leaching section and also a metallised iron by-product that could be sold as feed for steel producers (Walpole & Winter,

2002: 12–13). These two sections will most likely work independently of the thermal treatment step used because the feed stream to these sections will be the same (both will be loaded with ferrous chloride and unreacted hydrochloric acid).

The second category, to improve existing processes, has many possibilities. Processes with the highest likelihood to succeed would be those that conform to the following specifications:

- Economically viable
- Effectively remove as much iron as possible
- If possible, produce a useable by-product from the separated iron.

Two process options with potential areas for improvement and the possibility of complying with the above-mentioned design specifications were identified and are briefly discussed below.

The Becher process is the first process that could possibly be improved. Improvement can be made by ensuring that only one pure iron oxide (e.g. magnetite) precipitates which might be sold as a by-product. This is possible through controlling the pH and redox potential inside the aeration vessel (Ward, 1990: i). Experimental work was conducted to achieve this, which resulted in the selective precipitation of magnetite, hematite and goethite (Ward, 1990:123–141). This work was tested on an industrial-size aeration tank, but the process has thus far not been commercially implemented (Ward, 1990: 307).

The Summit process (see Figure 2.2) is the second process that could potentially be improved. The developers of the process considered two ways to regenerate the ferric ion required to leach the metallic iron in the reduced ilmenite. The first is to oxidise the ferrous iron with oxygen (or air) and the second is to electrolytically regenerate the ferric ions. Pure metallic iron is produced during the electrolytic reaction and therefore creates the possibility of producing iron as a marketable product. The Summit process was never commercially implemented, mainly due to the high operating costs (Ward, 1990: 14). A possible area for improvement is therefore to attempt to reduce these costs. If this process option could be made economically viable, it would produce two products, namely titanium nitride and iron.

The third possibility is to develop an entirely new process. Figure 2.3 illustrates various proposed process schemes that could be tested. These process options are briefly discussed below.

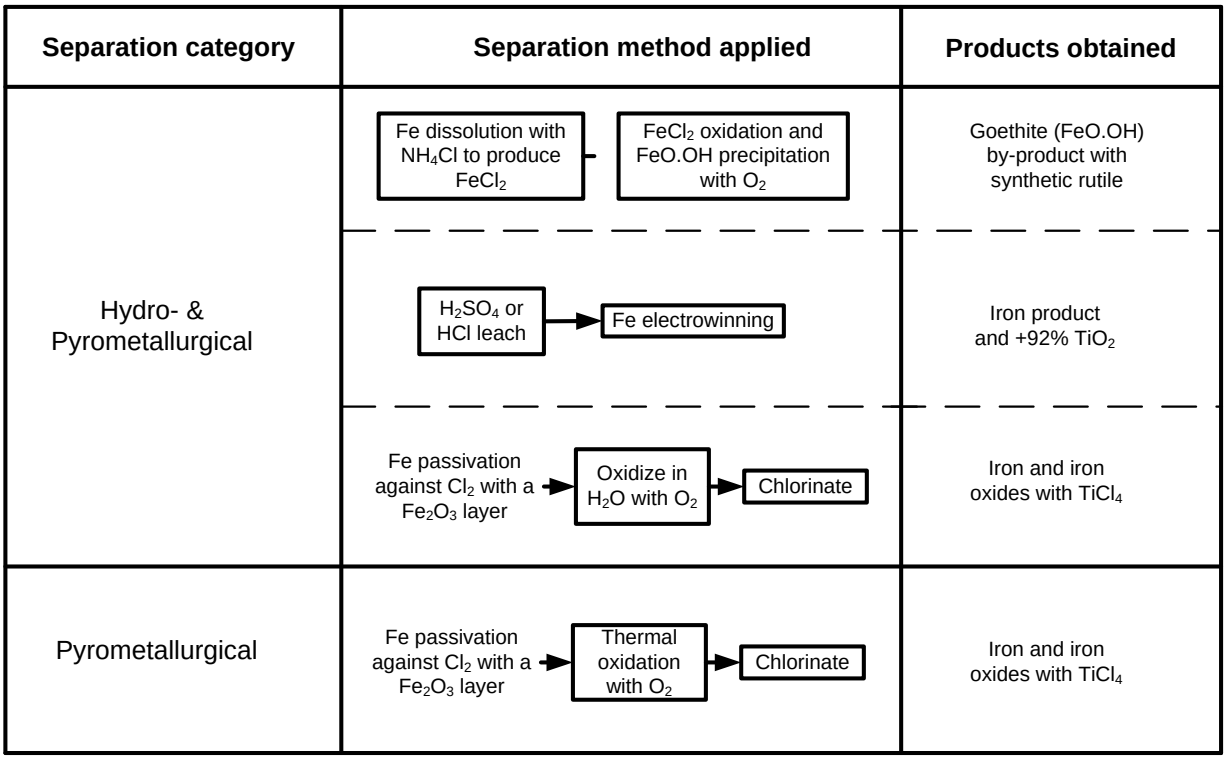


**Figure 2.3: Other possible process options for upgrading nitrided ilmenite**

The first possible process scheme is to use ammonium chloride as a stoichiometric reactant to oxidise metallic iron and produce a ferrous chloride solution, which is then further oxidised in a separate vessel with aerated water to precipitate goethite as the principal iron oxide. The precipitation of goethite would be controlled to ensure a high-quality oxide. If this complied with specifications, it could be sold as a by-product.

The second possible process scheme is to use sulphuric acid to leach metallic iron from the nitrided ilmenite complex. The solid (upgraded) nitrided ilmenite can then be filtered from the solution. The solution is sent to an electrowinning cell house where the iron is electrochemically recovered. The iron can be sold as product.

The third and fourth possible process schemes both propose to passivate the iron contained in nitrided ilmenite against chlorination by first forming a haematite shell around the iron. The nitrided ilmenite with passivated iron is then chlorinated to form titanium tetrachloride from titanium nitride. The solids remaining in the chlorinator are iron encapsulated in a passivated haematite shell. This iron could be treated and sold as product. These two process options differ in the method used to passivate the iron. The first process option suggests using an

aqueous solution to enable “wet corrosion” to occur and the second process option proposes thermal oxidation with air as a passivating step.

## 2.5 – Selected processes for experimental evaluation

Four process routes were identified in the literature review as candidate options for further experimental work. The first two options are existing process technologies and the other two are novel ideas. The two commercial process options selected for experimental evaluation are:

- The Becher process
- The Austpac ERMS SR process.

These two process options should be either adapted to use nitrided ilmenite instead of conventionally reduced ilmenite as feed, or improved to overcome the current process restrictions of waste generation and acid consumption.

The two novel process ideas selected for experimental evaluation are:

- Oxidative passivation of iron in nitrided ilmenite
- Use of $NH_4Cl$ as a stoichiometric reactant with iron in nitrided ilmenite.

The experimental work completed to determine the viability of each process route is reported in Chapter 4.

# CHAPTER 3 – CHARACTERISTICS OF NITRIDED ILMENITE

## 3.1 – Overview

A range of experimental investigations is required to evaluate process options that could possibly be used to remove iron from nitrided ilmenite. These experimental investigations require a standardised nitrided ilmenite sample.

Three steps were used to prepare a standardised nitrided ilmenite sample. The first step was to prepare a batch sample of nitrided ilmenite at fixed nitriding conditions. The second step was to remove residual char from the nitrided ilmenite sample (reported in Appendix 1) and the final step was to characterise the "clean" nitrided ilmenite sample.

The characterisation of a nitrided ilmenite sample is reported in this section and includes the following:

- Particle size distribution (PSD)
- Chemical composition
- Scanning electron microscope (SEM) photographs
- Energy-dispersive X-ray (EDX) spectroscopy with an elemental map
- Powder X-ray diffraction (XRD).

The procedure used to separate the residual char from the nitrided ilmenite is reported in Appendix 1.

## 3.2 – Material, methods and equipment used

### 3.2.1 – Sample preparation

Sample preparation was the first step in the experimental procedure. Nitrided ilmenite was obtained by nitriding unroasted Hillendale ilmenite (with the chemical composition given in Table 3.1 and $d_{50}$ = 125 µm) at approximately 1 325 $^{o}$C with 30% excess bituminous carbon under $N_2$(g) for 6 hours. The nitrided ilmenite was cooled down in an $N_2$(g) atmosphere and

then magnetically separated from the residual char using the procedure described in Appendix 1. This sample served as standard for all investigations, except for the particle size distribution analysis for which samples containing residual char were used.

**Table 3.1: Chemical composition of unroasted Hillendale ilmenite**

| Constituent | Mass % |
|---|---|
| $Fe_2O_3$ | 12.29 |
| FeO | 36.15 |
| $TiO_2$ | 48.40 |
| MnO | 1.06 |
| $SiO_2$ | 0.44 |
| $Al_2O_3$ | 0.27 |
| $P_2O_5$ | 0.01 |
| $V_2O_5$ | 0.25 |
| $ZrO_2$ | 0.08 |
| $Cr_2O_3$ | 0.09 |
| MgO | 0.50 |
| CaO | 0.02 |
| Other | 0.44 |

Figure 3.1 is a photograph of the Hillendale ilmenite particles before nitriding. The sizes of these particles are between 200 and 250 µm. An Olympus SZ61 stereo microscope was used to view the particles at a magnification of approximately 15 times.

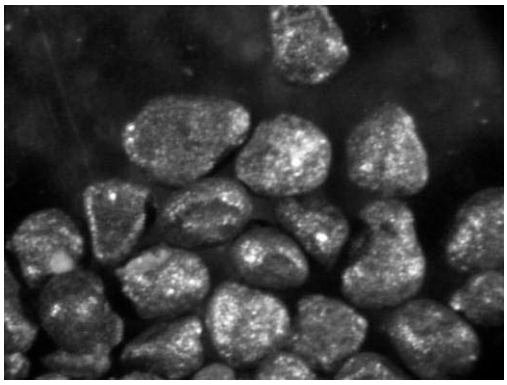

**Figure 3.1: Photograph of Hillendale ilmenite particles between 200 and 350 µm (Approx. magnification x15)**

Figure 3.2 is a photograph of nitrided ilmenite particles at sizes between 125 and 180 µm. These particles were viewed at a magnification of approximately 15 times.

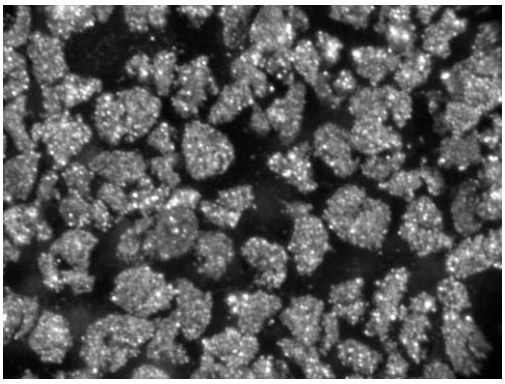

**Figure 3.2: Photograph of nitrided ilmenite particles between 125 and 180 µm (Approx. magnification x15)**

### 3.2.2 – Particle size distribution

The particle size distribution of the nitrided ilmenite sample was measured using a HAVER EML 200 test sieve shaker fitted with 315, 250, 180, 125, 90, 63 and 45 µm DIN 4188 screens.

The procedure used during the analysis of the particle size distribution was as follows:

A 130 g sample was taken from a container with thoroughly mixed nitrided ilmenite. The nitrided ilmenite was mixed for 5 minutes in a Turbula mixer to ensure that a representative sample was taken.

Figure 3.3 illustrates the Turbula mixer.

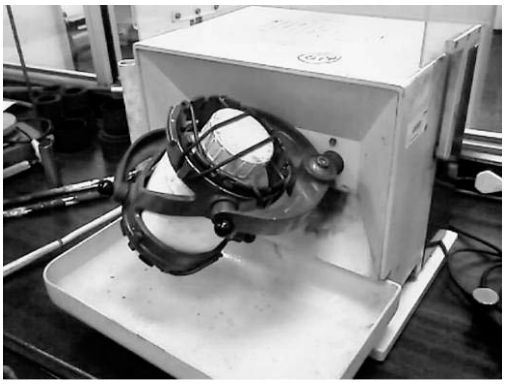

**Figure 3.3: Turbula mixer used for mixing**

The dry magnetic separation procedure described in Appendix 1 was used to remove residual char from the 130 g nitrided ilmenite sample. This sample with residual char removed will be referred to from here onwards as the “clean” nitrided ilmenite sample.

The clean nitrided ilmenite sample was then added to the top screen (315 µm) of the sieve shaker and left for 15 minutes to shake on the “high” setting. The screens were cleaned, weighed and the mass noted before the sample was added to the shaker. The mass of each screen was weighed and noted again after 15 minutes of shaking. This procedure was repeated three times.

A Mettler-Toledo PM30 electronic balance was used to determine the mass of each screen.

### 3.2.3 – Chemical composition

Three standard nitrided ilmenite samples were sent for ICP-OES analysis. UIS Analytical Services (2009) used a Leco CS400 for the chemical composition analysis.

### 3.2.4 – SEM photographs

The samples were viewed using a LEO 1525 field-emission scanning electron microscope (FE-SEM) which was operated at an accelerating voltage of 15 kV. For imaging purposes, the InLens detector was used at a working distance of 5 mm and an aperture size of 60 µm. The SEM photographs were obtained from the National Metrology Institute of South Africa (2009).

### 3.2.5 – EDX with elemental mapping

The LEO 1525 field-emission scanning electron microscope was equipped with an Oxford Link Pentafast EDS detector. The Oxford INCA software suite was used to determine the elemental (X-ray) mapping at the same operating conditions as used for the SEM imaging. The National Metrology Institute of South Africa (2009) conducted the EDX analysis.

### 3.2.6 – Powder X-ray diffraction

The samples were prepared using a back-loading preparation method. They were analysed with a PANalytical X’Pert Pro powder diffractometer with X’Celerator detector and variable divergence and fixed receiving slits with Fe-filtered Co-Kα radiation. The phases were

identified using X'Pert Highscore plus software. The relative phase amounts were estimated using the Rietveld method (Autoquan Program). The analysis was done by XRD Analytical and Consulting (Verryn, 2009).

## 3.3 – Results and discussion

### 3.3.1 – Particle size distribution (PSD) results

The experimental procedure for the PSD analysis (Section 3.2.1.2) entailed the use of the dry magnetic separation procedure (Appendix 1) to remove residual char from the nitrided ilmenite. The result from each attempt was that approximately 9 wt % of the original sample was residual char and 91% nitrided ilmenite. The PSD for the residual char is discussed in more detail in Appendix 1.

A frequency distribution for both nitrided ilmenite and Hillendale ilmenite before nitriding is given in Figure 3.4. The results illustrated in Figure 3.4 present the mass per cent of sample retained for each mean particle size and are the average of three tests.

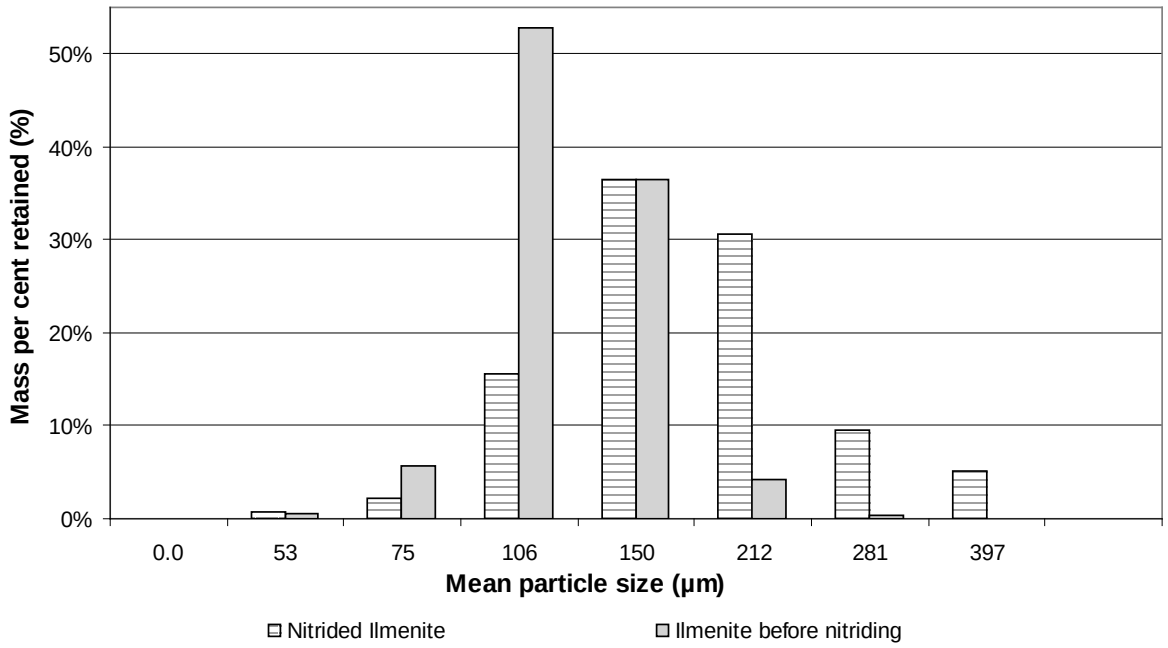


**Figure 3.4: Particle size distributions of ilmenite before and after nitriding**

Equation 3.1 gives the mean particle size of each fraction.

$$Mean\ \text{particle size} = \sqrt{(bottom\ screen\ \text{size} * top\ screen\ \text{size})} \qquad \text{Equation 3.1}$$

The average mass mean particle sizes of Hillendale ilmenite before and after nitriding are 125 and 185 µm respectively.

The spread in particle size of the nitrided ilmenite particles in Figure 3.4 is much wider than that of the ilmenite particles before nitriding. Furthermore, the particle sizes of the nitrided ilmenite sample were larger than those in the original sample.

Visual inspection of the nitrided ilmenite particles between 250 and 315 µm showed larger, complex particles consisting of aggregates of smaller particles (see photograph in Figure 3.5). This indicated that some sintering had occurred between the particles. An Olympus SZ61 stereo microscope was used to view the particles at a magnification of approximately 15 times.

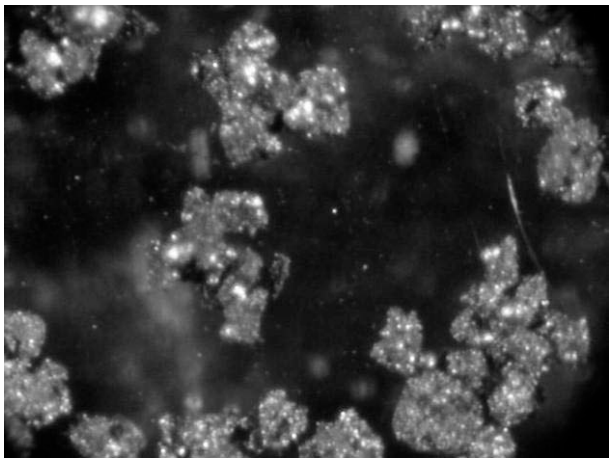

**Figure 3.5: Photograph of nitrided ilmenite particles between 250 and 315 µm (Approx. magnification x15)**

The extent of sintering between the particles was studied by lightly grinding particles of the +250–315 µm fraction. The particles were first screened to ensure they were between 250 and 315 µm. They were then lightly ground for 2 minutes in a mortar and pestle. After grinding, the particle size distribution was again measured.

The result is illustrated in Figure 3.6 as a frequency size distribution. Figure 3.6 also shows the particle size distribution of the nitrided ilmenite before grinding (as in Figure 3.4) for comparison.

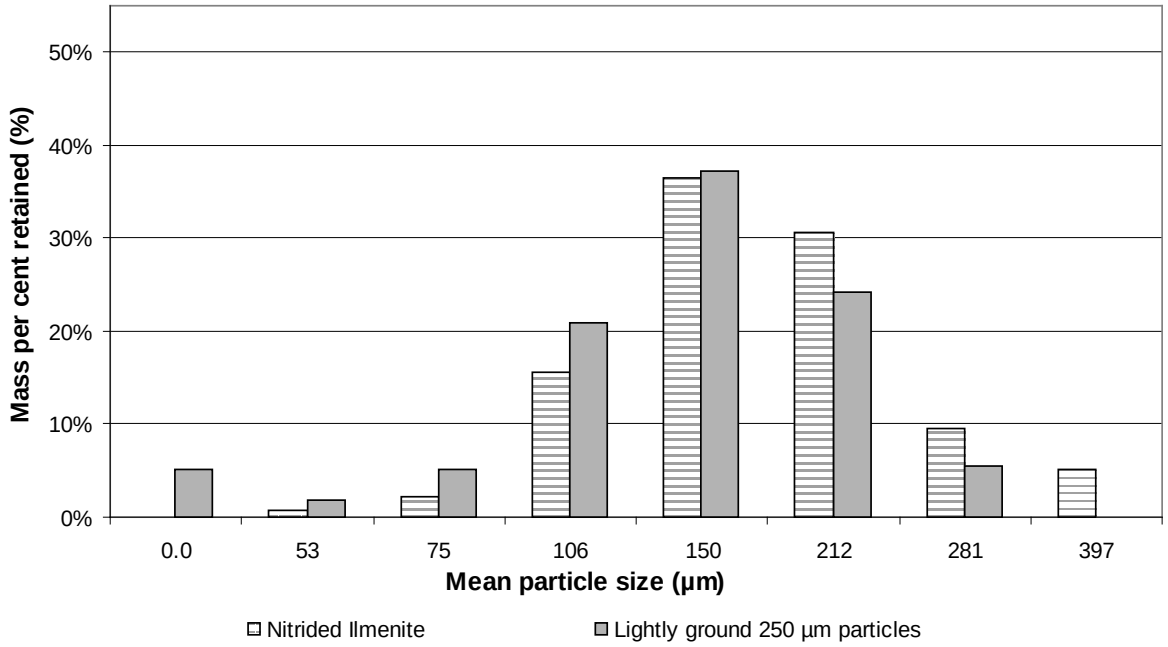


**Figure 3.6: Particle size distribution for lightly ground 250 µm nitrided ilmenite particles**

The mass mean particle size obtained from lightly grinding +250–315 µm particles is 150 µm. This is a substantial reduction from 250 µm after only 2 minutes of lightly grinding the particles.

The results illustrated in Figure 3.6 show a clear reduction of larger particles and an increase in the amount of smaller particles present after only 2 minutes of light grinding. This suggests that the particles were only weakly sintered to each other and that they can be separated from each other relatively easily to produce smaller particles.

The significant fraction of particles smaller than 45 µm also suggests that the ilmenite particles do indeed become smaller during nitriding.

The formation of smaller particles in the nitrided ilmenite sample when physical force is exerted on it leads to some difficulty in obtaining a true particle size distribution. Further work can be considered to reduce these effects in an attempt to analyse the size distribution more accurately.

The data obtained from the particle size distributions were also used to determine the constants in the Rosin-Rammler equation, given in Equation 3.2.

$$Y^{-} = 1 - \exp\left(-\left(\frac{d}{d^*}\right)\right)^n \qquad \text{Equation 3.2}$$

where $Y^{-}$ is the cumulative fraction material passing, d is the screen size and d* and n are both constants, but d* is also the screen size through which 63.2% of the particles pass.

The values of the constants for the PSD of nitrided ilmenite are:

d*= 199 µm
n = 3.28

The cumulative mass per cent of sample passing a given screen size is illustrated in Figure 3.7 for both the PSD experimental data (points on graph) and the Rosin-Rammler equation (line).

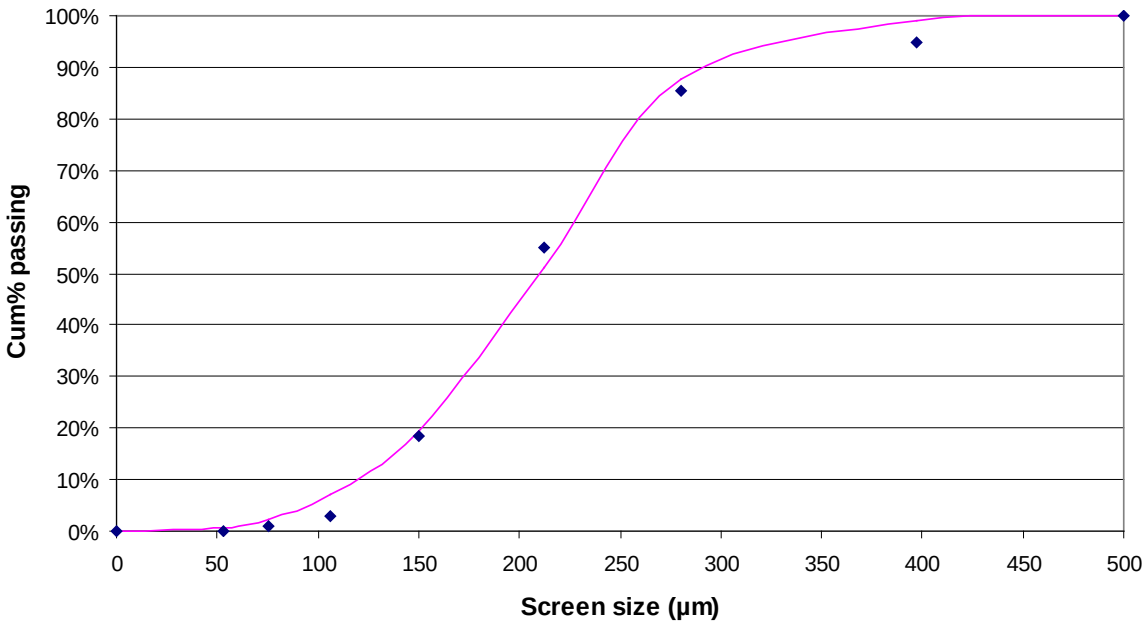


**Figure 3.7: Cumulative size distribution of nitrided ilmenite particles**

The Rosin-Rammler equation predicts that the mean particle size is equal to 178 µm, which compares well with the calculated mass mean particle size of 185 µm.

### 3.3.2 – Chemical composition

Table 3.2 presents the composition of the nitrided ilmenite sample obtained.

**Table 3.2: Chemical composition of nitrided ilmenite**

| Constituent | Mass % |
|---|---|
| $SiO_2$ | 3.54 |
| $Al_2O_3$ | 1.88 |
| Fe (metal) | 45.64 |
| $TiO_2$ | 2.73 |
| TiN | 40.26 |
| CaO | 0.14 |
| MgO | 0.62 |
| $K_2O$ | 0.03 |
| MnO | 1.27 |
| $P_2O_5$ | 0.05 |
| $V_2O_5$ | 0.19 |
| C (total) | 3.40 |
| S (total) | 0.21 |

The results in Table 3.2 (average of three samples) were normalised to include the conversion of $TiO_2$ to TiN. This conversion (~95%) was estimated based on the mass loss of sample during the nitriding reaction. It was assumed that any iron oxide present in the ilmenite sample reduces to Fe during the nitriding reaction. The results of the chemical composition before normalisation for all three nitrided ilmenite samples are given in Appendix 5.

### 3.3.3 – SEM and EDX results

Figures 3.8 to 3.11 are SEM photographs of nitrided ilmenite particles. A brief description is given below each figure, together with the EDX results, to give an estimated elemental composition of what is seen in each SEM photograph.

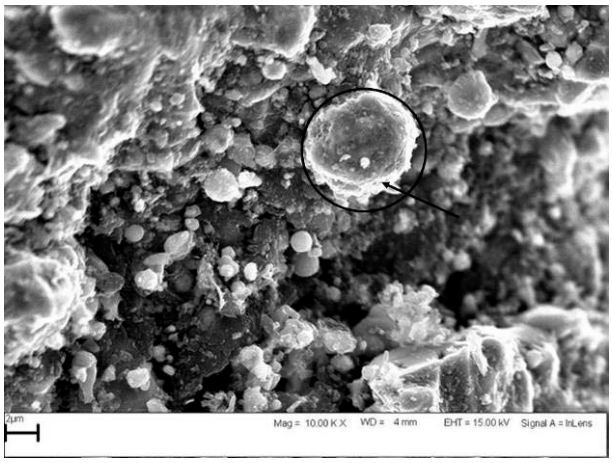


**Figure 3.8: SEM photograph of nitrided ilmenite particle with an iron globule visible**

Figure 3.8 is a SEM photograph of the surface of a nitrided ilmenite particle with what was suspected to be an iron globule attached to the particle. An EDX elemental map confirmed the suspicion with a concentrated area for iron, indicated with an arrow on Figure 3.8. The EDX results for Figure 3.8 are summarised in Table 3.3.

**Table 3.3: EDX results for Figure 3.8 summarised**

| Element | Mass % |
|---|---|
| C | 11.98 |
| Al | 1.26 |
| Ti | 69.00 |
| Fe | 17.77 |

The large presence of carbon in the sample is attributed to the carbon coating of each sample before the EDX analysis is performed.

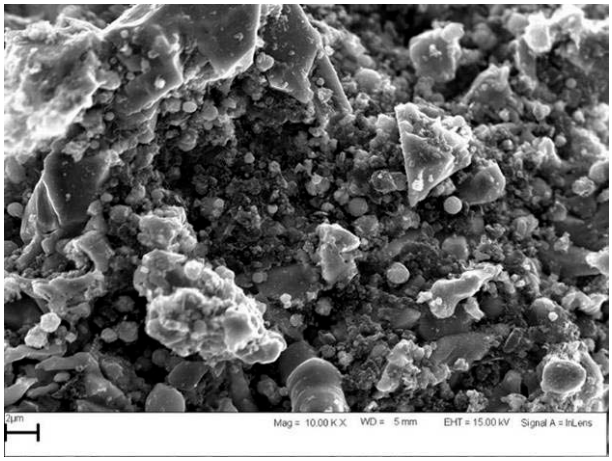


**Figure 3.9: SEM photograph of nitrided ilmenite particle without an iron globule visible**

Figure 3.9 is a SEM photograph of the surface of a nitrided ilmenite particle but without any iron globules visible. The EDX results for Figure 3.9 are summarised in Table 3.4.

**Table 3.4: EDX results for Figure 3.9 summarised**

| Element | Mass % |
|---|---|
| C | 17.54 |
| N | 8.96 |
| O | 16.43 |
| Al | 1.90 |
| Si | 1.28 |
| Ti | 46.31 |
| Fe | 7.59 |

The results summarised in Table 3.4 serve only as an indication of the elemental composition but show that the iron content is much less than in Figure 3.8. The interpretation of the results in Table 3.4 is, however, difficult due to the additional large decrease in titanium content. A more conclusive interpretation of the results could, however be made from the EDX results for Figure 3.10.

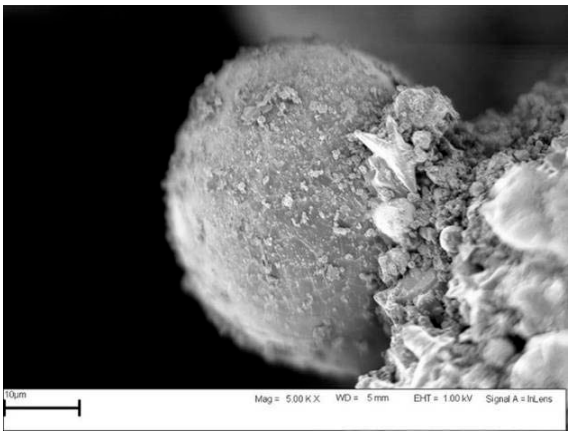


**Figure 3.10: SEM photograph of nitrided ilmenite particle with iron globule visible**

Figure 3.10 is a SEM photograph taken of an iron globule on the surface of a nitrided ilmenite complex but with mostly the globule in focus. The EDX results for Figure 3.10 are summarised in Table 3.5.

**Table 3.5: EDX results for Figure 3.10 summarised**

| Element | Mass % |
|---|---|
| C | 63.69 |
| Si | 0.68 |
| Ti | 4.71 |
| Fe | 30.92 |

From the results summarised in Table 3.5, it is clear that iron globules do indeed form on the surface of nitrided ilmenite complexes.

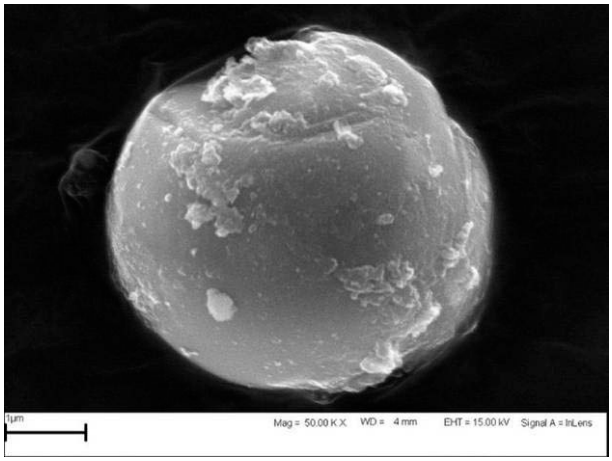


**Figure 3.11: SEM photograph of a round particle not attached to any other particles**

Figure 3.11 is a SEM photograph of a ball-shaped particle that was not attached to a larger particle or complex. The EDX results for Figure 3.11 are summarised in Table 3.6.

**Table 3.6: EDX results for Figure 3.11 summarised**

| Element | Mass % |
|---|---|
| C | 54.80 |
| Al | 6.06 |
| Ti | 39.13 |

The results summarised in Table 3.6 suggest that the particle consists mainly of titanium (not including the excess carbon added). It therefore seems incorrect to assume that all spherical particles in a nitrided ilmenite sample are iron globules – they can also be titanium nitride or carbide particles.

### 3.3.4 – XRD results

The XRD results for a standard nitrided ilmenite sample are summarised in Table 3.7.

**Table 3.7: Quantitative results summarised for XRD analysis of nitrided ilmenite**

| Phase | Mass % |
|---|---|
| $TiO_2$ | 2.35 |
| $Fe_3C$ | 6.50 |
| α-Fe | 39.70 |
| TiN | 51.45 |

## 3.4 – Concluding remarks

A thorough characterisation of a standard nitrided ilmenite sample was completed. A few of the important findings were:

- Nitriding of ilmenite at the "standard" nitriding conditions results in aggregates of smaller particles that are loosely sintered together.
- The standard nitrided sample contains approximately 46% metallic iron and approximately 40% titanium nitride.
- The major phases present in the standard nitrided samples are:
    - TiN
    - α-Fe
    - $Fe_3C$
    - $TiO_2$
- SEM photographs and EDX results indicated that iron globules form on the surface of the nitrided ilmenite complexes, but also that not all the globules in the product are iron.

A few experiments were conducted to try to separate the iron globules, mentioned above, from the nitrided ilmenite complex. These were, however, unsuccessful. These attempts are reported in Appendix 2.

# CHAPTER 4 – PRELIMINARY EXPERIMENTAL EVALUATION

## 4.1 – Overview

Four process options were identified in Chapter 2 for further experimental evaluation. The purpose of the evaluation is to determine the viability of using the process for removing iron from nitrided ilmenite. The following process options are evaluated in this chapter:

- Oxidative passivation of iron in nitrided ilmenite (Section 4.2)
- The Becher process (Section 4.3)
- Use of $NH_4Cl$ as a stoichiometric reactant with iron in nitrided ilmenite (Section 4.4)
- The Austpac ERMS SR process (Section 4.5).

The chapter concludes (in Section 4.6) with a selected process route that proved (from the experimental results) to be the most viable method of removing iron from nitrided ilmenite.

## 4.2 – Oxidative passivation of iron in nitrided ilmenite

Various process options were identified as possible process routes to remove iron from nitrided ilmenite (Chapter 2). One of these process options is a novel attempt to passivate the iron in nitrided ilmenite by thermal oxidation in air to form a haematite “shell” around the iron particles to prevent the iron core from chlorinating during the chlorination step. The products obtained from chlorination would then be a vapour $TiCl_4$ stream and a solids stream consisting of metallic iron and haematite. It might be possible to recover this metallic iron and sell it as a by-product.

The resulting process would then consist of the existing nitriding step, an oxidation step to form the haematite shell, then the $TiCl_4$ production step and finally a treatment step to recover the chlorine gas ($Cl_2$) from the iron that has reacted during chlorination.

The practicability of passivating iron against chlorination through thermal oxidation was investigated in this section. Thermodynamic equilibrium calculations in HSC© predict that

titanium nitride can oxidise to form either titanium dioxide or anatase ($TiO_2$(A)) and that metallic iron can oxidise to form haematite. An experiment was, however, required to determine which species would oxidise first so that conclusions could be drawn as to the practicability of this idea. See Figure 4.1 for the graphical output obtained from HSC©. The simulation describes a system with excess air available to react with 0.5 kmol iron and 0.5 kmol titanium nitride.

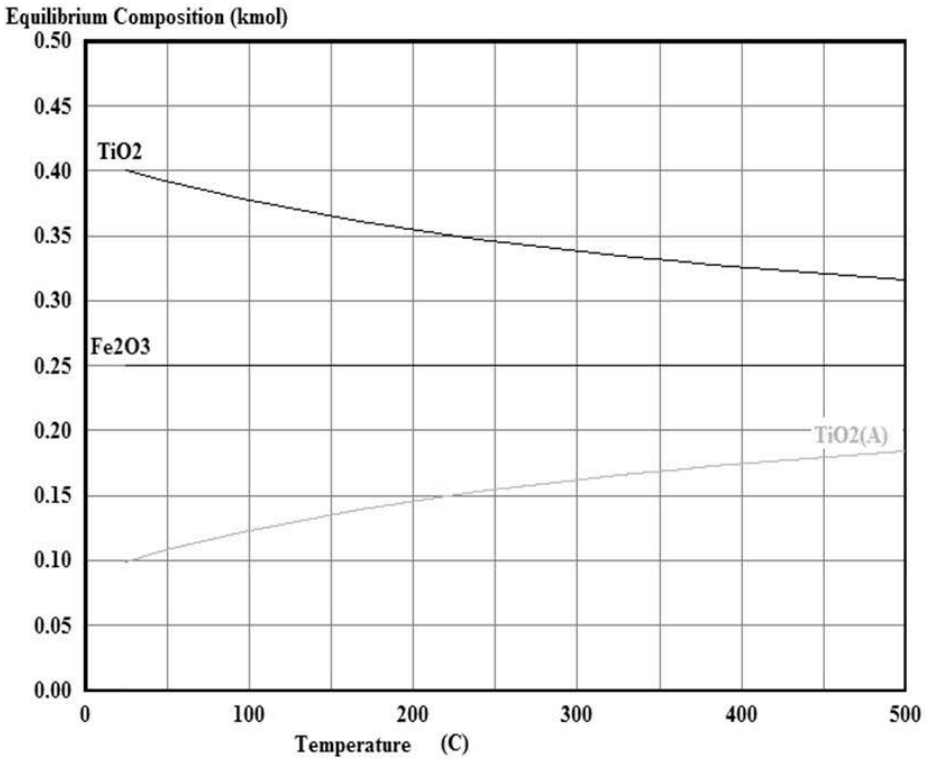


**Figure 4.1: Thermodynamic equilibrium composition according to HSC Chemistry 7.0©**

## 4.2.1 – Experimental

### 4.2.1.1 – Materials and methods

The experimental procedure consisted of four sequential steps.

Sample preparation was the first step in the experimental procedure. Refer to Chapter 3 for a detailed overview of the sample characteristics and the procedures used to obtain the sample.

Thermo-gravimetric analysis (TGA) was used to estimate the temperature at which rapid oxidation of nitrided ilmenite starts. A Mettler Toledo STAR SW 9.01 was used for the thermo-gravimetric analysis. A sample of nitrided ilmenite was loaded into the device with excess air supplied to serve as oxidising an atmosphere. The temperature of the sample was programmed to rise linearly, starting from ambient temperature to 700 ºC. Three samples were tested with different temperature-ramping profiles, namely 2.5, 5 and 10 $^{o}C.min^{-1}$. This was the second step in the experimental procedure.

Thermal oxidation of the nitrided ilmenite was the third step in the experimental procedure. The set-up and procedure used for this experimental apparatus are discussed in Section 4.2.1.2.

The fourth and final step in the experimental procedure was characterisation of the samples obtained from the thermal oxidation experiment (Step 3) by XRD analysis. The samples were prepared using a back-loading preparation method. They were analysed with a PANalytical X'Pert Pro powder diffractometer with X'Celerator detector and variable divergence and fixed receiving slits with Fe filtered Co-Kα radiation.

The phases were identified using X'Pert Highscore plus software. The relative phase amounts were estimated using the Rietveld method (Autoquan program). The analysis was done by XRD Analytical and Consulting (Verryn, 2009).

#### 4.2.1.2 – Experimental apparatus

The thermal oxidation experiment was conducted in a Nabotherm® oven furnace with a Logotherm® Program Controller S17 to control the operating temperature inside the oven. A KNF-Neuberger diaphragm pump was used to supply approximately 8 litres of air per minute to the interior of the oven to provide an oxidising atmosphere. The air was first sent through a coil inside the furnace to preheat it before it came into direct contact with the samples inside the furnace.

A Mettler-Toledo AT400 electronic balance was used to determine the mass of the sample containers used in the experiment. These sample containers were weighed empty, with samples and then again after the experiment. The sample containers were all added to the furnace when the temperature set-point reached the desired value. The position for each container inside the furnace was noted.

Figure 4.2 illustrates the arrangement of sample containers inside the furnace.

**Figure 4.2: Sample containers arranged inside the furnace**

The first sample container was removed from the furnace after one hour. Every 30 minutes after that another sample container was removed. This schedule ensured thermal oxidation data points for 5 hours. The sample containers were then weighed again and noted to determine the mass gained.

## 4.2.2 – Results and discussion

### 4.2.2.1 – Results from thermo-gravimetric analysis

Thermo-gravimetric (TG) analysis was required to estimate the temperature at which thermal oxidation for nitrided ilmenite starts. Three TG analyses were conducted, each with a different step size. Figure 4.3 illustrates the results obtained for the 5 $^{o}C.min^{-1}$ step size.

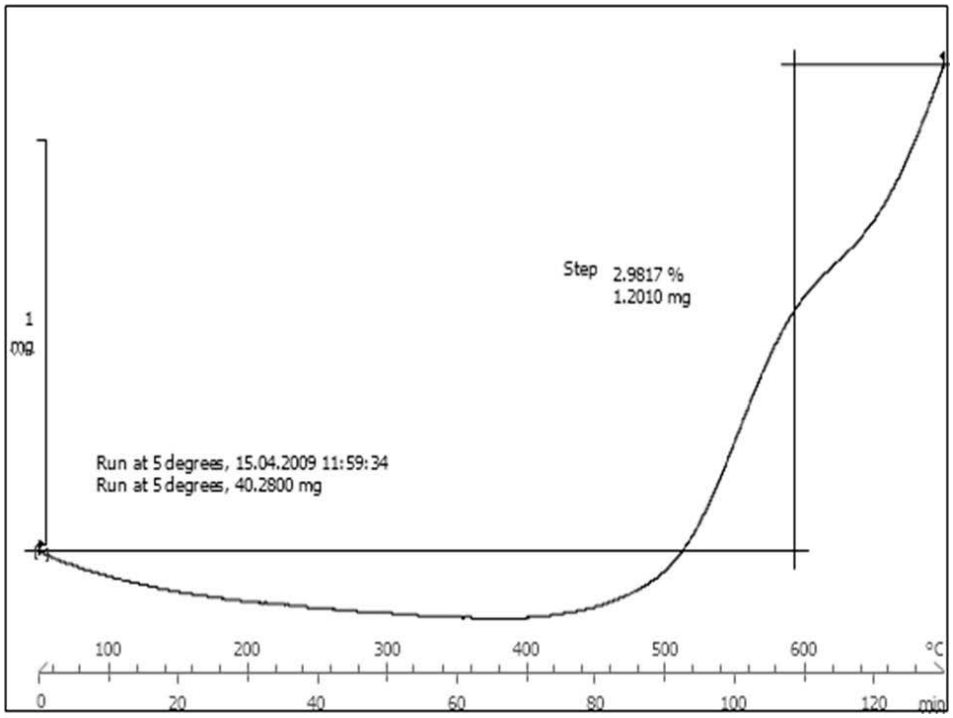


**Figure 4.3: TGA results for nitrided ilmenite oxidation with a 5 ºC.min$^{-1}$ step**

The results illustrated in Figure 4.3 provide the mass change for the nitrided ilmenite sample as a function of both temperature and time. Three different mass change profiles were identified in Figure 4.3. These, as a function of temperature, are:

1. A slow mass decline over the temperature range between 25 $^{o}$C and approximately 350 $^{o}$C
2. Between 350 and 600 $^{o}$C – first an initial slow increase in mass but then a fast increase in mass
3. From 600 $^{o}$C and upwards – first a slower increase in mass and then another fast increase in mass.

The initial decline in mass can be attributed to absorbed moisture present in the sample.

The second and third profiles identified in Figure 4.3 represent stages at which oxidation occurs. The presence of two different profiles might be related to the thermodynamic prediction in HSC© that both titanium nitride and iron can oxidise, but it seems that oxidation is predominant for each at different temperatures. Refer to Figure 4.1 for the results obtained in HSC©.

The TGA results can therefore be interpreted as showing that oxidation of both components does occur, but it is not known which oxidises first. This could be determined only by sending thermally oxidised samples (Section 4.2.2.2) for XRD analysis (Section 4.2.2.3).

The main objective of the TG analysis was to determine the operating temperature for the thermal oxidation experiment. It was found that the first component started to oxidise at approximately 350 $^{o}$C. This would therefore be the selected operating temperature for the thermal oxidation experiment.

### 4.2.2.2 – Results from thermal oxidation run

The purpose of the thermal oxidation experiment was to obtain thermally oxidised nitrided ilmenite samples that could be sent for XRD analysis.

The experimental procedure described in Section 4.2.2.2, with a 350 $^{o}$C operating temperature, was used to conduct the experiment. The results obtained from the thermal oxidation experiment are illustrated in Figure 4.4 as the percentage mass increase for each sample as a function of time in the furnace.

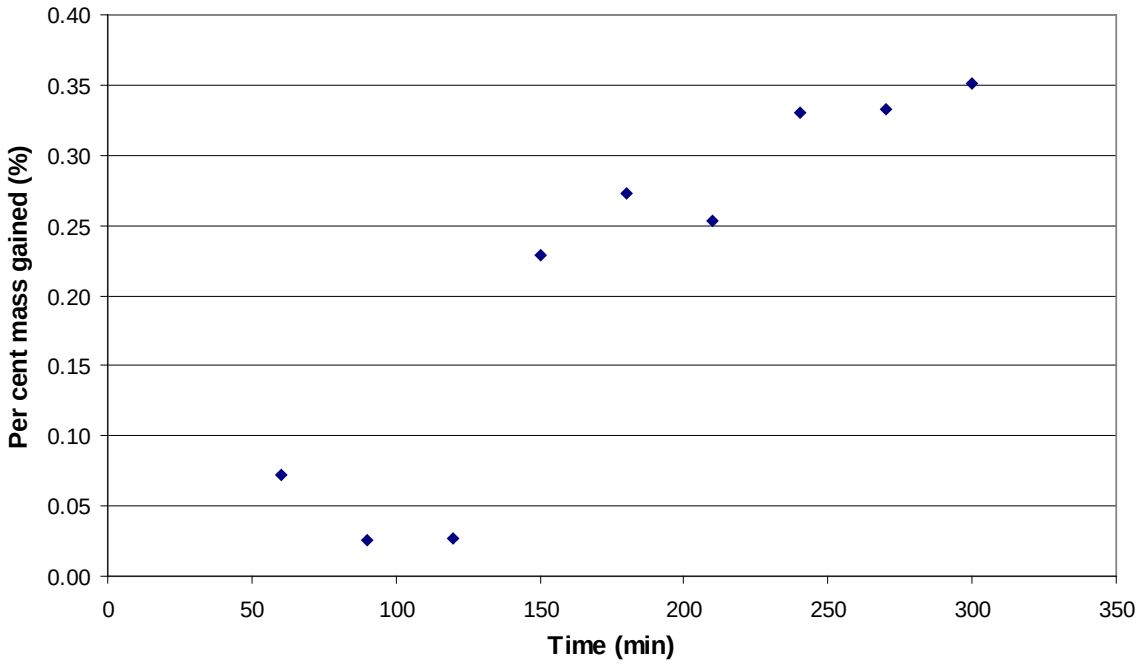


**Figure 4.4: Percentage mass gained during oxidation of nitrided ilmenite as a function of time**

The second (at 90 minutes) and third (at 120 minutes) data points in Figure 4.4 did not fit the linear trend of the other data points. This might be attributed to the same phenomenon found in the TGA results (Figure 4.3) where it was suggested that the presence of moisture in the sample reduced the actual weight of the sample. This would prevent the data from representing the true mass gained due to oxidation.

Further conclusions could not be drawn without knowing which component oxidises first. This could only be determined through XRD analysis. Section 4.2.2.3 discusses the results obtained from XRD analysis.

### 4.2.2.3 – Results from XRD analysis

Three samples were selected for XRD analysis. One was a sample used as feed for the experiment and was therefore not oxidised. The 150 and 300-minute oxidised samples were also selected for XRD analysis.

Table 4.1 summarises the XRD results obtained for thermally oxidised nitrided ilmenite.

**Table 4.1: XRD results for thermally oxidised nitrided ilmenite**

| Constituent | 0 min (mass %) | 150 min (mass %) | 300 min (mass %) |
|---|---|---|---|
| $TiO_2$ | 2.35 | 2.65 | 3.07 |
| $Fe_3C$ | 6.50 | 7.81 | 8.25 |
| Fe | 39.70 | 39.76 | 38.59 |
| TiN | 51.45 | 49.78 | 50.09 |

The results obtained from the XRD analysis cannot be considered as a quantitative answer reflecting the true composition of the material analysed, but they can be used to accurately identify which phases or species are present in the sample.

The results summarised in Table 4.1 show that there is an increase in anatase and cementite as the oxidation reaction continues. Haematite, however, which is the desired oxide, did not form sufficiently during the thermal oxidation to be identified during the XRD analysis. The conclusion is therefore that titanium nitride oxidises before iron in a nitrided ilmenite sample.

### 4.2.3 – Conclusions

Initial thermodynamic investigations (Figure 4.1) predicted that both iron and titanium nitride would oxidise at high temperatures in an oxygen-rich atmosphere. The reaction kinetics were, however, required to determine which oxidises first and this could only be done experimentally.

Thermo-gravimetric analysis showed that two different reactions occur when nitrided ilmenite is oxidised, one presumably iron oxidation and the other titanium nitride oxidation. The quantitative result from the TG analysis revealed that the operating temperature of the furnace should be approximately 350 $^{o}$C, which is the temperature at which the first oxidation reaction starts.

Thermal oxidation experiments were then conducted at 350 $^{o}$C for 5 hours. The results from these tests suggested that the oxidation of titanium nitride with “hot air” is faster than the oxidation of iron.

The conclusion from this study is therefore that the proposed idea of passivating iron against chlorination by means of a thermal oxidation step is not viable.

## 4.3 – The Becher process

The Becher process (Becher, 1963) is a two-step process for upgrading ilmenite. Ferrous and ferric iron oxides are reduced to metallic iron in the first step using coal as reductant. The reduced ilmenite is then leached with aerated water in the presence of ammonium chloride ($NH_4Cl$) to produce synthetic rutile and iron oxides. The aerated water-leaching step is in essence the Becher process. The aerated water-leaching step consists of a single tank equipped with propellers to agitate the reaction solution. The reaction solution is held between 70 and 80 ˚C with air continuously pumped into the solution from the bottom of the tank. The aerated water-leaching step takes approximately 20 hours to complete for each batch of ilmenite. A batch is typically 20 tons of ilmenite in 100 m$^3$ of water (Ward, 1990).

The Becher process is likely to work on nitrided ilmenite, because nitriding in the CSIR’s proposed process also reduces the iron in ilmenite to its metallic state before it is sent to the next processing step. However, it was still necessary to evaluate the aerated water-leaching

step used in the Becher process on nitrided ilmenite to determine whether it can effectively remove the iron. This is the objective of this section.

### 4.3.1 – Materials, methods and equipment used

#### 4.3.1.1 - Sample characteristics

The sample described in Chapter 3 was used in this experiment. Refer to Chapter 3 for a detailed overview of the sample characteristics and the procedures used to obtain the sample.

Analytical-grade $NH_4Cl$ was used in the aerated water-leaching test.

#### 4.3.1.2 – Experimental procedure

Aerated water leaching of nitrided ilmenite was carried out using a 750 ml three-necked glass reactor. The reaction vessel was equipped with two condensers in series and an overhead stirrer fitted with a PTFE-coated shaft and impeller. A temperature-controlled heating mantle regulated the temperature inside the reaction vessel. A glass-gas diffuser connected to a KNF-Neuberger diaphragm pump was used to supply approximately 8 litres of air per minute to the reaction solution. Air leaving the diaphragm pump was, however, first saturated in a water scrubber before it entered the reaction solution. This helped to maintain an approximately constant volume inside the reaction vessel. A schematic diagram of the experimental set-up is illustrated in Figure 4.5.

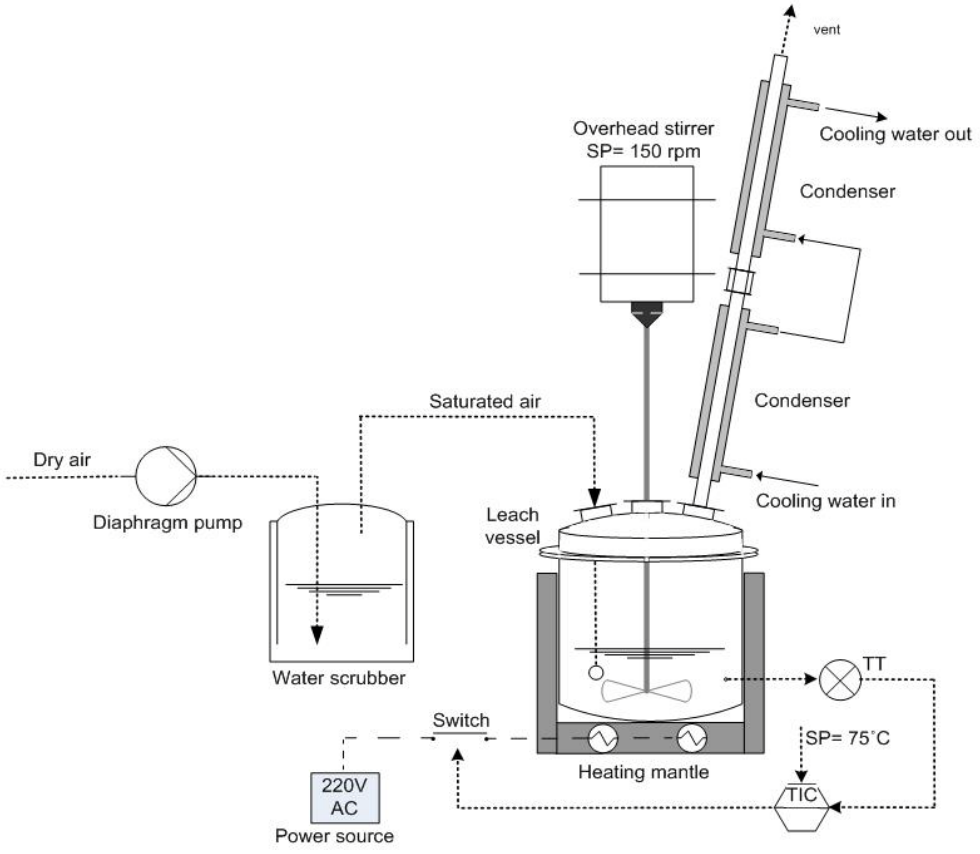


**Figure 4.5: Diagram of experimental set-up for the aerated water-leaching test**

The first step in the experimental procedure was the addition of 500 ml 0.1 M $NH_4Cl$ solution to the reaction vessel. This solution was left in the reaction vessel until it reached the 75 $^oC$ temperature set-point. A 168 g nitrided ilmenite sample was then added to the reactor. This resulted in a 25 wt % slurry. The diaphragm pump and overhead stirrer (~ 150 r/min) were then switched on.

The experiment was stopped after 19 hours and the solution decanted from the reaction vessel. This solution was then filtered. The residue was also removed from the reactor and placed on a 45 µm screen. It was then repeatedly washed with hot water. The water passing the 45 µm screen was also filtered to prevent any loss of material. Both solid fractions (larger and smaller than 45 µm) were dried for 30 minutes at 80 $^oC$. These solid residues were then sent for XRD analysis.

### 4.3.2 – Results

The XRD results showed that the particles smaller than 45 µm were primarily magnetite, and those larger than 45 µm (product residue) contained a mixture of nitrided ilmenite, metallic iron and magnetite. The separation of magnetite from the product residue with the procedure used was therefore not efficient. The XRD results could not, however, quantify the amount of magnetite present in the product residue.

The experiment started with 168 g of nitrided ilmenite. The mass of magnetite (all particles smaller than 45 µm) after 19 hours of aerated water leaching was found to be equal to 29 g. The chemical composition of the nitrided ilmenite (Table 3.2) showed that 45.6% of the sample consists of metallic iron. Therefore, approximately only 27% of the metallic iron was removed from the original nitrided ilmenite sample.

This low conversion can be attributed to the fact that the Hillendale ilmenite originally nitrided contained approximately 20% more total iron than the ilmenite (i.e. Capel ilmenite) typically used in Becher plants (Becher, 1963). The compositions of both the Hillendale ilmenite and the Capel ilmenite (before thermal treatment) are summarised in Table 4.2.

**Table 4.2: Comparison between Hillendale and Capel ilmenite**

| Constituent | Capel ilmenite | Hillendale ilmenite |
|---|---|---|
| $Fe_2O_3$ | 18.16 | 12.29 |
| FeO | 22.51 | 36.15 |
| $TiO_2$ | 55.43 | 48.40 |
| MnO | 1.44 | 1.06 |
| $SiO_2$ | 1.41 | 0.44 |
| $Al_2O_3$ | 0.25 | 0.27 |
| $P_2O_5$ | 0.15 | 0.01 |
| $V_2O_5$ | 0.13 | 0.25 |
| $ZrO_2$ | 0.08 | 0.08 |
| $Cr_2O_3$ | 0.03 | 0.09 |
| MgO | Nil | 0.50 |
| CaO | Nil | 0.02 |
| Other | 0.41 | 0.44 |

The increased iron content in the nitrided ilmenite sample translates to the requirement that each set of five batches (100 $m^3$ each) used in the Becher process would require an extra 100 $m^3$ tank. This results in increased plant inventory and equipment requirements to achieve the same conversion as in the Becher process.

The rate of oxidation achieved in this study can be increased by pumping extra air through the solution to precipitate an iron oxide other than magnetite (Ward, 1990). This was not evaluated, but a mixed range of iron oxides is expected to precipitate.

Another observation is that acid leaching will still be required as a polishing step to remove any iron and iron oxides from the product residue. This is also a requirement for existing Becher processes (Becher, 1963).

### 4.3.3 – Conclusions

The aerated water-leaching step used in the Becher process was evaluated for 19 hours on nitrided ilmenite. The results indicated that only ~27% of the iron was removed. This low conversion was attributed to the 20% extra iron present in Hillendale ilmenite compared with the ilmenite typically used in a Becher plant. It can be overcome by either increasing the airflow rate through the reaction solution (to precipitate other oxides) or by decreasing the slurry wt % in each aerator leach tank.

## 4.4 – Investigating the stoichiometric reaction between $NH_4Cl$ and nitrided ilmenite

The Becher process was identified as a process option that could possibly remove iron from nitrided ilmenite (Chapter 2). This process uses a 1% $NH_4Cl$ solution as catalyst in an aerated water-leaching step to dissolve metallic iron. A disadvantage of the aerated water-leaching step is that it takes approximately 20 hours to complete for each batch ilmenite sample. A novel idea came to mind to use the $NH_4Cl$ as a stoichiometric reactant in an attempt to operate the dissolution reaction continuously. Figure 4.6 illustrates a block flow diagram for the proposed process.

The process illustrated in Figure 4.6 consists of three main vessels: a Ferro Reactor, an ammonia-recovery vessel and a Goethite Precipitator.

In the Ferro Reactor $NH_4Cl$ reacts with metallic iron to produce ferrous ions in solution and a solid titanium nitride stream. The titanium nitride solids are filtered from the solution and serve as the upgraded ilmenite product stream.

The ferrous-rich solution obtained from the Ferro Reactor is send to the Goethite Precipitator where air is blown through the solution (aerated oxidation) to precipitate goethite and produce an aqueous ammonium chloride solution that can be recycled back to the process.

The elevated temperatures used in the Ferro Reactor cause ammonia to evaporate from the reaction vessel. This vapour stream is sent to the ammonia-recovery vessel where ammonia is recovered and recycled back to the Goethite Precipitator to maintain appropriate pH levels.

The purpose of this section is to do an experimental evaluation of the process route described above.

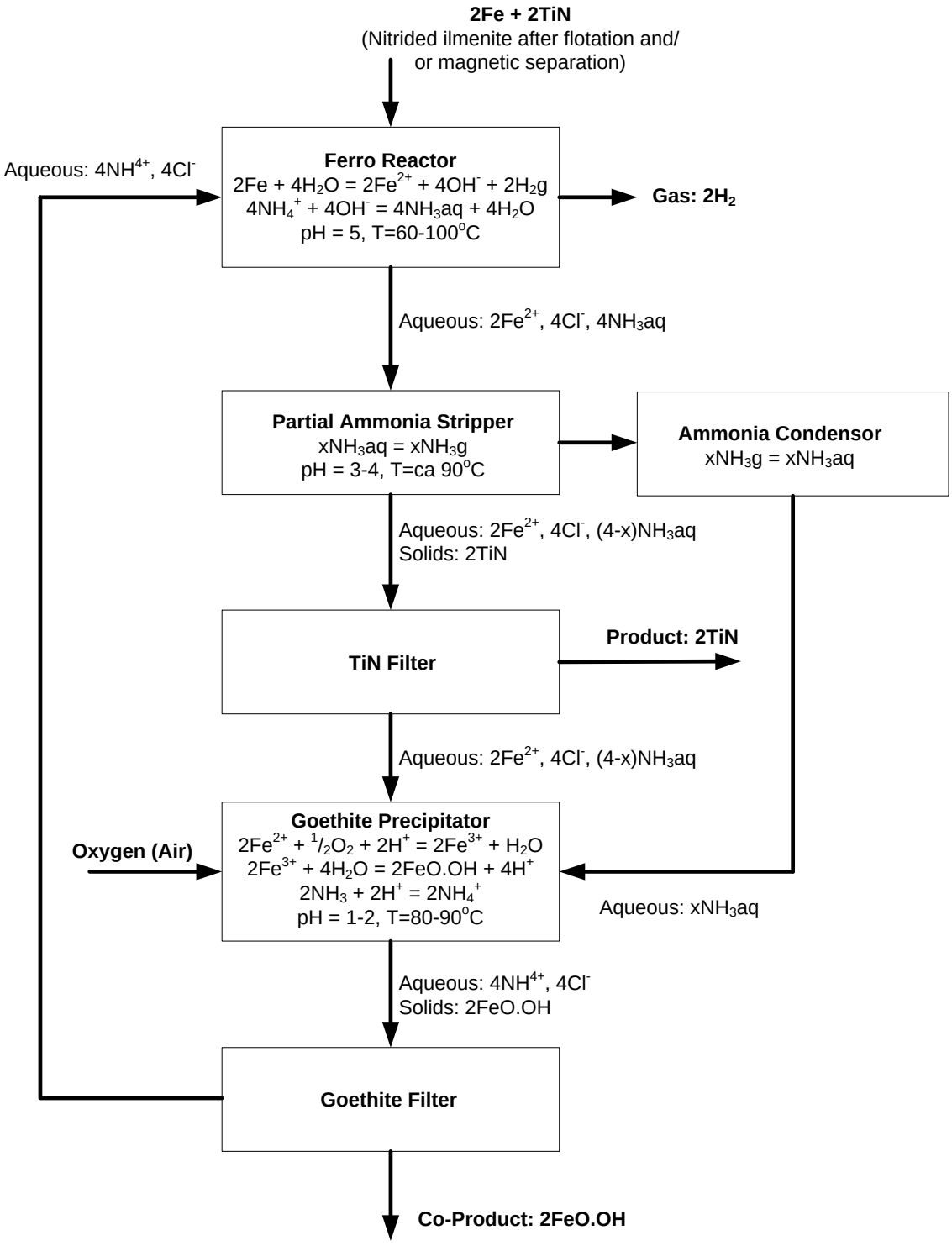


**Figure 4.6: Proposed process for the reaction between $NH_4Cl$ and iron in nitrided ilmenite**

### 4.4.1 – Materials, methods and equipment used

#### 4.4.1.1 – Sample characteristics

Refer to Chapter 3 for a detailed overview of the sample characteristics and the procedures used to obtain the sample.

#### 4.4.1.2 – Ferro Reactor procedure

The first step in the proposed process is the reaction between aqueous ammonium chloride and iron to form aqueous ferrous chloride.

A reaction solution was prepared by dissolving 50 g of $NH_4Cl$ in 150 ml of water. The reaction vessel was placed on a hot plate with a magnetic stirrer and heated to 60°C. The solution was mixed with 65 g of nitrided ilmenite to result in a 30 wt % slurry with approximately 30% excess ammonium chloride available.

The reaction vessel was closed to the atmosphere with a lid containing only one outlet. This outlet was connected to a scrubbing vessel to capture the ammonia gas that evolved during the reactions inside the Ferro Reactor. The outlet from the scrubbing vessel was connected to another vessel submerged in water to capture evolved hydrogen gas.

The reaction in the Ferro Reactor was left to continue for 16 hours. After this time, the reaction solution was separated from the unreacted feed material. The unreacted feed material was dried in air for 30 minutes at 90 ˚C.

#### 4.4.1.3 – Goethite Precipitator procedure

The second step in the proposed process is to oxidise the ferrous chloride solution so that goethite can precipitate. This was attempted by keeping the solution at 50 ˚C and then blowing air through the solution. Air was blown through the solution with a diffuser connected to a KNF-Neuberger diaphragm pump. The diaphragm pump supplied approximately 8 $l.min^{-1}$ of air to the solution.

### 4.4.2 – Results and conclusion

The results obtained from this investigation were only visually evaluated. Two key points identified are as follows.

- The unreacted feed material removed from the reaction vessel was still completely magnetic.

- The solution inside the Goethite Precipitator changed colour from black to green, from green to yellow, and then from yellow to orange in the first 10 minutes of oxidation. This indicated that goethite precipitation (yellow product) would require precise solution conditions. The pH of the solution is especially important. Only ~2 g of iron oxides precipitated. This indicates that a very low oxidation or iron dissolution was achieved.

These results indicated that a quantitative analysis for the proposed process was unnecessary. It is concluded that the proposed process is not a viable option for removing iron from nitrided ilmenite.

## 4.5 – The Austpac ERMS SR process

The Austpac ERMS SR process uses hydrochloric acid as lixiviant to remove iron oxide, and other impurities, from thermally pretreated ilmenite.

Thermal pretreatment in the Austpac ERMS SR process entails a two-step oxidation-partial reduction of ilmenite. The result of this thermal pretreatment is an ilmenite ore with a high FeO-to-$Fe_2O_3$ ratio (Winter, 2008).

Thermal pretreatment (during the nitriding reaction, Reaction 1.1) in the CSIR's proposed process produces metallic iron instead of iron oxide in the nitrided ilmenite. The objective of this section is therefore to evaluate the dissolution reaction of metallic iron (in nitrided ilmenite) in hydrochloric acid.

The Austpac ERMS SR process uses a 25 wt % hydrochloric acid solution in its leach section (Walpole & Winter, 2002). The evaluation conducted in this section, however, uses an 18% hydrochloric acid solution because this is more commonly used in industry (Metsep International, 2007).

### 4.5.1 – Materials, methods and equipment used

#### 4.5.1.1 - Sample characteristics

The sample described in Chapter 3 was used in this experiment. Refer to Chapter 3 for a detailed overview of the sample characteristics and the procedures used to obtain the sample.

Analytical-grade HCl was used in the leaching test.

#### 4.5.1.2 – Experimental procedure

Acid leaching of nitrided ilmenite was carried out using a 750 ml three-necked glass reactor. The reaction vessel was equipped with two condensers in series and an overhead stirrer fitted with a PTFE-coated shaft and impeller. A temperature-controlled heating mantle regulated the temperature inside the reaction vessel. A schematic diagram of this experimental set-up is illustrated in Figure 4.7.

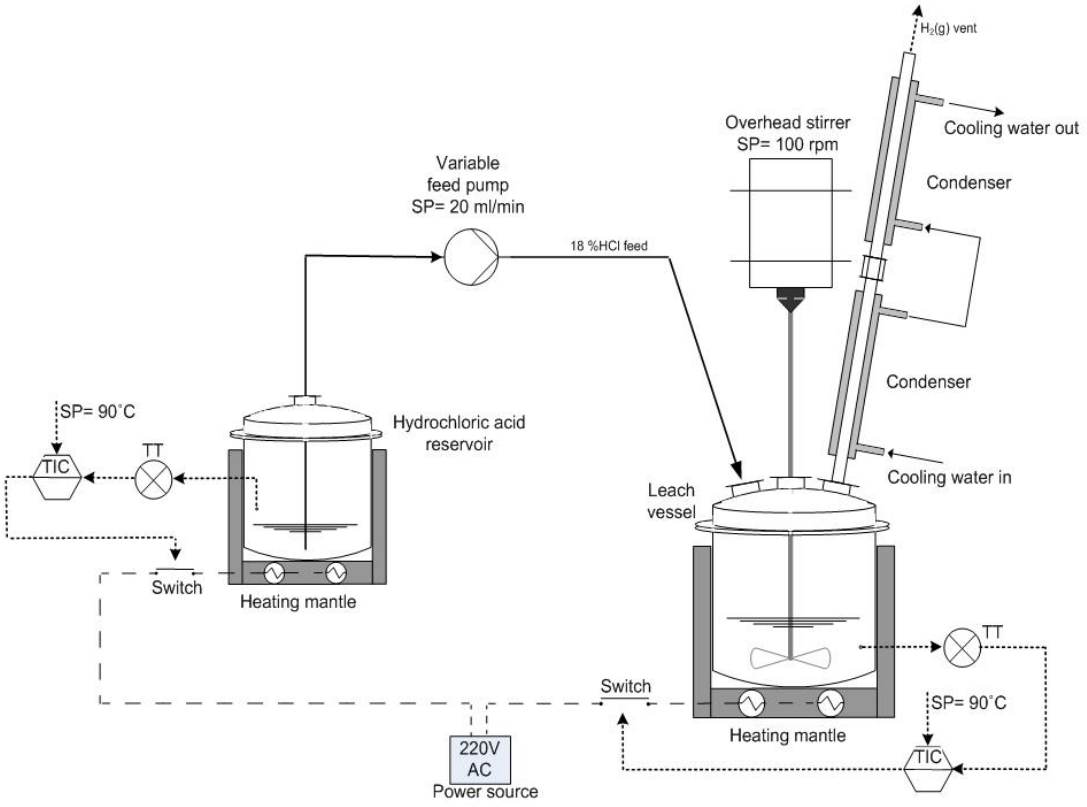


**Figure 4.7: Diagram of experimental set-up for hydrochloric acid-leaching test**

The required mass of nitrided ilmenite ($d_{50}$ = 185 µm) was first loaded into the reaction vessel. Once the reactor and solids had reached the temperature set-point (90 ˚C), 18 wt %

of hydrochloric acid (also at the temperature set-point) was added to the reactor at a rate of 20 ml/min from a second heated vessel. The 500 ml of hydrochloric acid was added over 25 minutes. This was done to prevent any foaming caused by excessive hydrogen gas evolution. A stirring speed of 100 r/min was applied to keep the slurry suspended during the leaching experiment.

After the required reaction period (150 minutes), the slurry was filtered off and the leach liquor sent for analysis by redox titration to determine the total iron(II) in solution. Refer to Appendix 3 for the redox titration procedure.

### 4.5.2 – Results

An excessive reaction occurs between hot hydrochloric acid and metallic iron in nitrided ilmenite. The evolution of hydrogen gas during the reaction required a slow addition of hydrochloric acid to the reaction vessel to prevent foaming.

The results indicated that approximately 98.6% of the metallic iron in nitrided ilmenite can be dissolved within 150 minutes in hot 18% hydrochloric acid.

### 4.5.3 – Conclusions

The results obtained from this preliminary evaluation indicated that hydrochloric acid can effectively remove metallic iron from nitrided ilmenite. The dissolution of metallic iron in 18% hydrochloric acid reached approximately 98.6% after 150 minutes.

## 4.6 – Conclusion: Selected process for further development

The following is a brief summary of findings from the preliminary experimental evaluation:

- Oxidative passivation of metallic iron in nitrided ilmenite against chlorination is not viable (Section 4.2).
- Approximately 27% metallic iron was removed from nitrided ilmenite after 19 hours with the aerated water-leaching step as used in the Becher process (Section 4.3).
- Using $NH_4Cl$ as stoichiometric reactant instead of catalyst is not a viable method for removing metallic iron from nitrided ilmenite (Section 4.4).

- Approximately 98.6% metallic iron was removed from nitrided ilmenite after 150 minutes when using hydrochloric acid as lixiviant.

The results summarised above indicate that hydrochloric acid leaching proved to be the most practical method for removing iron from nitrided ilmenite. The aerated water-leaching step, as used in the Becher process, could be further investigated to find its optimum operating conditions but it has been preliminarily discarded as a possible process option because it requires an added acid-leaching step to “polish” the final upgraded product.

Hydrochloric acid leaching was therefore selected as the process route to remove iron from nitrided ilmenite.

# CHAPTER 5 – AUSTPAC ERMS SR PROCESS REVIEW

## 5.1 – Overview

Hydrochloric acid leaching of thermally treated ilmenite, as used in the Austpac ERMS SR process, was identified in Chapter 4 as the most likely option to successfully remove iron from nitrided ilmenite. Hydrochloric acid leaching is, however, only one unit in a larger process. The aim of this chapter is to review the Austpac ERMS SR process to understand the overall process required to remove iron from ilmenite with hydrochloric acid.

The Austpac ERMS SR process was developed in Australia by a company called Austpac Resources N.L., which is a minerals technology company that develops new commercial processes for the titanium, steel and iron industries (Austpac Resources N.L., 2010).

The development of the Austpac ERMS SR process started in the early 1990s (Walpole, 1993). In 2008, the Austpac ERMS SR process technology was proven in a 3 000 t/a demonstration plant on Kooragang Island in Newcastle New South Wales (Austpac Resources N.L., 2010). The data obtained from the operation of the 3 000 t/a demonstration plant will be used for detailed engineering design and a feasibility study of a 60 000 t/a commercial ERMS SR synthetic rutile plant. In September 2008, Austpac Resources N.L. won the Australian Mining Industry Award for the “Applied Technology of the Year”, signifying the company’s achievement in technology development for the titanium and steel industries (ABN newswire, 2008; Austpac Resources N.L., 2010).

The overall Austpac ERMS SR process consists of four different proprietary processes or units. These are:

- The Enhanced Roasting and Magnetic Separation (ERMS) process (Walpole & Winter, 2002; Austpac Resources N.L., 2010)
- The continuous leaching unit (Winter, 2008)
- The Enhanced Acid Regeneration System (EARS) (Winter, 2009)
- The Direct Reduced Iron process (DRI) (Winter, 2009).

The Austpac ERMS SR process is shown in Figure 5.1 as a simplified block flow diagram to illustrate the different units in the process and how they connect with each other. Only the main process streams are shown.

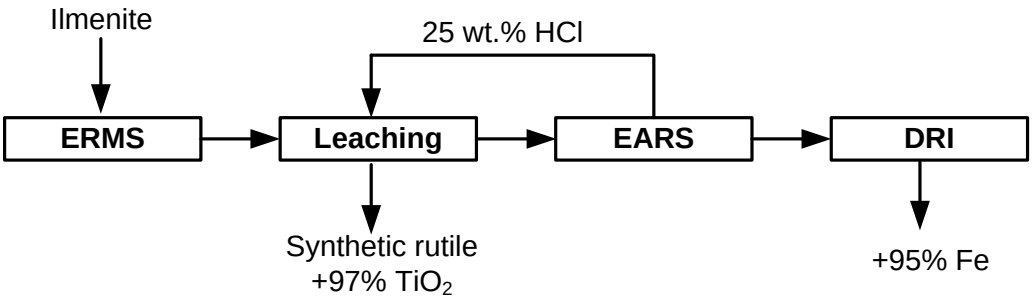


**Figure 5.1: Simplified block flow diagram of the Austpac ERMS SR process**

The units illustrated in Figure 5.1 are further discussed in Section 5.2. The leaching, EARS and DRI units are evaluated in Section 5.3 by determining the materials and energy balance over these units. This chapter closes in Section 5.4 with conclusions and recommendations on whether or not the Austpac ERMS SR process can be used on nitrided ilmenite as it is currently operated or whether further development work is required to adapt the process to use the alternative feed material.

## 5.2 – Process description

Figure 5.2 is an expanded block flow diagram for the Austpac ERMS SR process. The description below is based on this diagram.

### 5.2.1 –The ERMS process

The Enhanced Roasting and Magnetic Separation process is the first unit in the overall Austpac ERMS SR process. The function of this unit is to upgrade a heavy mineral feed material into a stream containing mostly ilmenite. The ilmenite produced has enhanced magnetic properties to improve downstream separation of gangue material from the upgraded product (see Section 5.2.2). Iron and other non-silica impurities in the ilmenite produced are also more selective for dissolution in hydrochloric acid (Walpole & Winter, 2002: 4; Walpole, 1997).

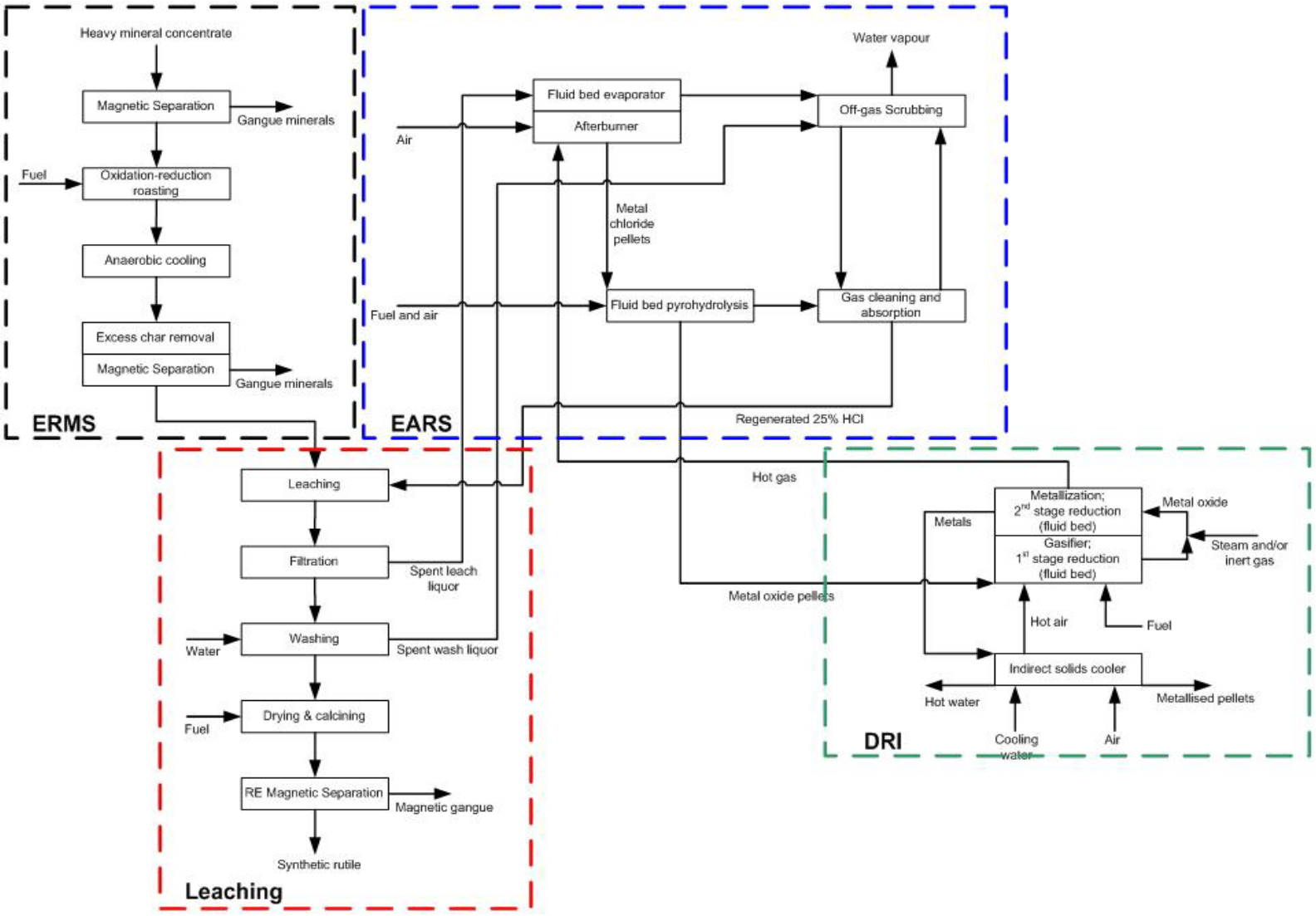


**Figure 5.2: Block flow diagram of the Austpac ERMS SR process**

The heavy mineral feed material used in the ERMS process is first upgraded with conventional wet gravity and dry mill separation methods to produce a heavy mineral concentrate (Walpole, 1997). This heavy mineral concentrate stream is then sent to a wet high-intensity magnetic separation (WHIMS) train, followed by drying and further upgrading of the dried magnetic fraction in a train of rare-earth magnetic separators (Walpole & Winter, 2002: 4). These processing steps remove the bulk of gangue materials and result in an upgraded ilmenite concentrate.

The ilmenite concentrate is then sent to a roasting section (Walpole, 1997). Roasting is carried out in two separate fluid bed stages. The first roast stage is operated under oxidising conditions to convert most of the iron species present in the ilmenite to the trivalent state, Fe(III) (Reaction 5.1).

$$FeO(s) + ½\ O_2(g) = Fe_2O_3(s) \qquad \text{Reaction 5.1}$$

Reaction 5.1 is normally carried out using air as the source for oxygen (Winter, 2008).

In the second roast stage, the trivalent iron is partially reduced back to its divalent state, Fe(II), (Walpole & Winter, 2002:4). Carbon monoxide (Reaction 5.2) and/or hydrogen (Reaction 5.3) can be used to operate the second roast stage under reducing conditions (Winter, 2008).

$$Fe_2O_3(s) + CO(g) = 2\ FeO(s) + CO_2(g) \qquad \text{Reaction 5.2}$$

$$Fe_2O_3(s) + H_2(g) = 2\ FeO(s) + H_2O(g) \qquad \text{Reaction 5.3}$$

The oxidation-reduction roast stages are operated at temperatures of 950 to 1 000 ˚C, with a total mean residence time of 2 hours (Austpac Resources N.L., 2010). The ilmenite product obtained from the second roast stage is anaerobically cooled below 200 ˚C to prevent re-oxidation of iron(II) (Winter, 2008).

Unreacted char (if coal is used as reductant) and the bulk of any ash are separated from the cooled product on a vibrating screen. A portion of the unreacted char is recycled to the roaster and the remainder is burnt as fuel (Walpole & Winter, 2002: 5).

The final processing step in the ERMS process is another magnetic separation unit with the objective of removing any remaining gangue minerals and fine char particles (Walpole, 1997).

### 5.2.2 – The leaching unit

The ilmenite product produced in the ERMS process is used as feed material in the Austpac ERMS SR process's patented leach unit. The dissolution of iron oxide in hydrochloric acid can be described with the chemical formula given in Reaction 5.4. Any other metal oxides will also be removed by similar reactions (Winter, 2008).

$$FeO.TiO_2(s) + 2\ HCl(aq) = FeCl_2(aq) + H_2O(l) + TiO_2(s) \quad \text{Reaction 5.4}$$

The patented leach unit consists of a number of vertical reactors or tubes that are connected in series to form a leach train (Winter, 2008). These vertical reactors are arranged in combinations of down-comers and risers. The ilmenite and acid solution flow co-currently with each other under plug flow conditions through these reactors. The reactor is called a "down-comer" if the slurry moves downwards and a "riser" if it moves upwards. Figure 5.3 is a simplified illustration of the leach train.

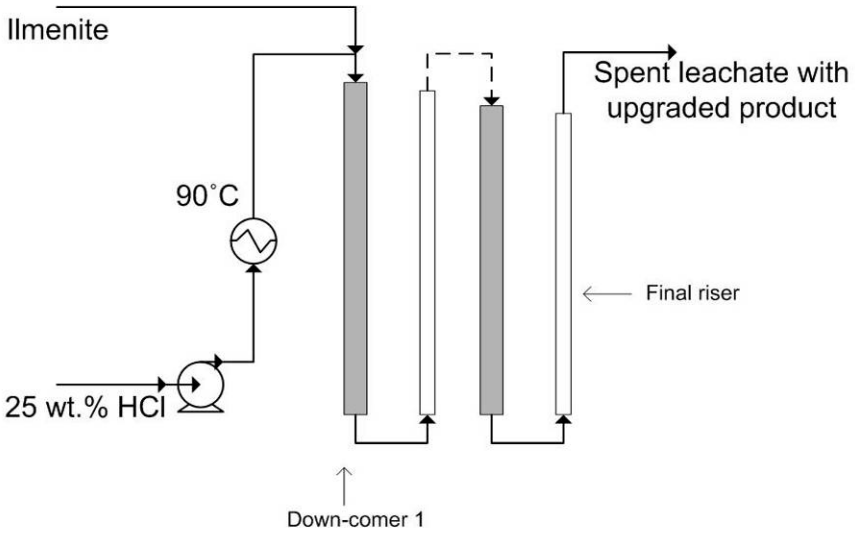


**Figure 5.3: Simplified illustration of Austpac ERMS SR's patented leach train**

In Figure 5.3, fresh hydrochloric acid (25 wt %) is heated to approximately 90 ˚C, after which it is mixed with ilmenite obtained from the ERMS unit. This slurry is pumped to the first

down-comer leach reactor, which fills up both itself and the adjacent riser leach reactor. The height of the adjacent riser leach reactor is just below that of the former down-comer leach reactor. The slurry then overflows from the riser leach reactor into the next down-comer leach reactor. This cycle repeats until the required residence time is obtained. A residence time of approximately 5 hours is required (Winter, 2008).

The hydrochloric acid is typically supplied in at least 10% excess to what is required for the reaction (Winter, 2008). The rate of hydrochloric acid addition is such that the fluid velocity inside the vertical leach reactor is just above the terminal settling velocity of the ilmenite particles in the slurry mixture. This in turn ensures that the particles will move with the fluid upwards. The diameter of each vertical leach reactor can be varied to ensure the fluid moves at the required velocity (Winter, 2008). This approach of fluid particle transport through the leach train is to reduce unnecessary agitation and attrition of product particles (Walpole & Winter, 2002: 6). Excessive agitation can also lead to foaming.

The reader is referred to the original patent for a more detailed description of the leach train (Winter, 2008).

The leachate solution obtained from the leach train is then sent to a four-stage vacuum belt filter for solid-liquid separation. The first stage separates the spent leach liquor from the solids and the remaining three stages are used for cake washing. The amount of wash water used determines the acid concentration that can theoretically be reached during acid regeneration (Walpole & Winter, 2002: 8). The spent leach liquor is sent to the fluid bed evaporator in the EARS process and the spent wash liquor is used as liquid absorbent in the off-gas scrubbing absorber, which is also in the EARS process (Austpac Resources N.L., 2010).

The washed product is dried and calcined at around 800 ˚C for 20 minutes in a fluid bed system to remove residual and chemically combined hydrochloric acid and water (Austpac Resources N.L., 2010).

The final step required in the Austpac ERMS SR's leach unit is to use a high-intensity magnetic separation procedure to remove any residual magnetic material from the final synthetic rutile product. This is usually a small fraction (2–3%) and comprises under-leached material and any residual gangue minerals (Austpac Resources N.L., 2010).

### 5.2.3 – The EARS process

The spent leach liquor produced in the leach unit is sent for complete evaporation in a fluid bed evaporator, which is operated at approximately 140 ˚C to produce hydrated metal chloride pellets. These pellets range in size from 1 to 3 mm and are sent to the pyrohydrolysis reactor (Walpole & Winter, 2002: 11). A portion of the thermal energy required for the fluid bed evaporator is obtained from combustion of unreacted carbon monoxide and hydrogen gas exiting the second reduction stage in the DRI process.

Evaporator off-gas is sent for adiabatic absorption in a packed column ("off-gas scrubbing" in Figure 5.2) with spent wash liquor from the washing step in the leach unit as liquid absorbent (Walpole & Winter, 2002:11). The weak acid liquor produced in this absorber is used as liquid absorbent in the gas-cleaning and absorption column (Austpac Resources N.L., 2010).

The metal chloride pellets produced in the fluid bed evaporator are fed to the air-fluidised pyrohydrolysis reactor. The predominant reaction in the pyrohydrolysis reactor is oxidation of iron(II) chloride and can be written as the chemical formula given by Reaction 5.5. Most of the other metal chlorides are also converted to oxides, except calcium (Walpole & Winter, 2002: 9).

$$2FeCl_2(s) + 2H_2O(g) + ½O_2(g) = Fe_2O_3(s) + 4HCl(g) \qquad \text{Reaction 5.5}$$

The water required for Reaction 5.5 is obtained from the dehydration of the hydrated iron(II) chloride pellet (Winter, 2009). Iron(II) chloride can have a dihydrate or tetrahydrate form. The pyrohydrolysis reactor is operated at a bed temperature of approximately 940 ˚C (Austpac Resources N.L., 2010). The metal oxide (mostly $Fe_2O_3$) pellets produced in the pyrohydrolysis reactor are in the size range of 0.5 to 2 mm (Walpole & Winter, 2002: 11). These pellets are then sent to the DRI process for reduction to produce metal pellets.

The off-gas produced in the pyrohydrolysis reactor is sent to the gas-cleaning and absorption column to recover hydrochloric acid. The weak acid liquor produced in the off-gas scrubbing absorber is used as liquid absorbent in this absorber to produce a super azeotropic acid with a concentration of 25 wt % (Austpac Resources N.L., 2010).

### 5.2.4 – The DRI process

The hot metal oxide pellets produced in the pyrohydrolysis reactor are sent to a two-stage fluid bed metallisation section. Strong reducing conditions are created in the first reduction stage by sub-stoichiometric combustion of a hydrocarbon fuel source (Austpac Resources N.L., 2010).

The metal oxides are reduced from $Fe_2O_3$ to FeO in the first reduction stage (Reactions 5.6 and 5.7) and from FeO to metallic iron (Reaction 5.8) in the second reduction stage (Winter, 2009). Reactions 5.6, 5.7 and 5.8 are for the case if coal is used as the hydrocarbon fuel source.

$$3\ Fe_2O_3(s) + CO(g) = 2\ Fe_3O_4(s) + CO_2(g) \qquad \text{Reaction 5.6}$$

$$Fe_3O_4(s) + CO(g) = 3\ FeO(s) + CO_2(g) \qquad \text{Reaction 5.7}$$

$$FeO(s) + CO(g) = Fe(s) + CO_2(g) \qquad \text{Reaction 5.8}$$

The temperature and residence time for these two reduction stages are approximately 950 ˚C, 30 minutes and 930 ˚C, 150 minutes respectively (Winter, 2009).

The hot metallised pellets are then anaerobically cooled to prevent re-oxidation.

## 5.3 – Leach, EARS and DRI process evaluation

Ilmenite nitriding, as discussed in Section 1.1, is a key step in the proposed low-temperature chlorination process. The thermal treatment unit (ERMS) in the Austpac ERMS SR process is therefore not required in a process that removes iron from nitrided ilmenite. The three remaining units in the Austpac ERMS SR process (leaching, EARS and DRI) are, however, still of importance and can possibly be used to remove iron from nitrided ilmenite.

A process flow diagram for these three units is proposed in this section. The material and energy balances and a brief discussion of these results are also reported.

### 5.3.1 – HSC 7.0 process model

The leach, EARS and DRI units in the Austpac ERMS SR process were modelled using the Flowsheet Simulation module in the HSC Chemistry 7.0© software package.

#### 5.3.1.1 – Assumptions

The assumptions made to compile the process model are listed below.

*Ilmenite feed stream from the ERMS unit (U01-ST01)*

Assume that 20 000 metric tons of titanium metal is required each year and assume there are 8 000 production hours per year. This translates into a required titanium metal production rate of 2.5 tons of titanium metal per hour.

To estimate the required ilmenite mass flow rate to the process, assume that all the titanium present in the ilmenite will be used to produce the final titanium metal. The titanium in ilmenite exists as titanium dioxide. The required titanium dioxide mass flow rate is therefore equal to 4.173 tons of $TiO_2$ per hour.

The chemical compositions summarised in Table 5.2 indicate a 50.4 wt % $TiO_2$ content in the leach train feed stream (Walpole & Winter, 2002: 8). The total ilmenite mass flow rate is therefore equal to 8.278 tons of ilmenite per hour. The mass flow rate for the other components is then obtained by multiplying the component wt % by the total mass flow rate.

*The leach train (U01-RC01)*

- Assume that a 25 wt % hydrochloric acid solution is used in the leach train.
- Assume that the hydrochloric acid solution is 10% in excess of the amount required to dissolve all iron(II)- and iron(III)-oxides in the feed stream.
- Assume that the following reactions can occur in the leach train:

$$FeO(s) + 2\ HCl(aq) = FeCl_2(aq) + H_2O \quad \text{Reaction 5.9}$$

$$Fe_2O_3(s) + 6\ HCl(aq) = 2\ FeCl_3(aq) + 3\ H_2O \quad \text{Reaction 5.10}$$

$$Al_2O_3(s) + 6\ HCl(aq) = 2\ AlCl_3(aq) + 3\ H_2O \quad \text{Reaction 5.11}$$

$$MgO(s) + 2\ HCl(aq) = MgCl_2(aq) + H_2O \quad \text{Reaction 5.12}$$

$$MnO(s) + 2\ HCl(aq) = MnCl_2(aq) + H_2O \quad \text{Reaction 5.13}$$

$$CaO(s) + 2\ HCl(aq) = CaCl_2(aq) + H_2O \quad \text{Reaction 5.14}$$

$$V_2O_5(s) + 2\ HCl(aq) = 2\ VO_2Cl(aq) + H_2O \quad \text{Reaction 5.15}$$

$$TiO_2(s) + 2\ HCl(aq) = TiOCl_2(aq) + H_2O \quad \text{Reaction 5.16}$$

$$Cr_2O_3(s) + 6\ HCl(aq) = 2\ CrCl_3(aq) + 3\ H_2O \quad \text{Reaction 5.17}$$

- Assume that Reaction 5.9 has a conversion of 98.5%.
- The model varies the conversions for Reactions 5.11 to 5.17 until the stream composition of stream U02-ST08 (solids product produced by the pyrohydrolysis reactor, U02-FR01) is equal to that of the Austpac ERMS SR process (third column in Table 5.2).
- The model varies the conversion for Reaction 5.10 until the mass of stream U01-ST12, the stream split with under-leached magnetic material, reaches 3% of the solids stream before magnetic separation (U01-SM01). This stream size can vary between 2 and 3% (Walpole & Winter, 2002: 9). The final conversions for Reactions 5.9 to 5.17 are summarised in Table 5.3.
- Assume that the following species do not react in the leach train:

  $SiO_2$, $P_2O_5$, $Nb_2O_5$, $ZrO_2$ and other gangue materials
- The chemical compositions obtained from Winter (2009) for the pyrohydrolysis solids product (U02-ST06) and the DRI metallised product (U03-ST07) are normalised to include the above assumption that these species will not dissolve. The chemical compositions for these two product streams before and after normalisation are given in Table 5.1.

**Table 5.1: Normalised chemical compositions for pyrohydrolysis and DRI solid products**

| | Pyrohydrolysis product | | DRI product | |
|---|---|---|---|---|
| **Constituent** | **Before assumption** | **With assumption** | **Before assumption** | **With assumption** |
| $TiO_2$ | 0.11 | 0.11 | 0.16 | 0.16 |
| FeO | 0.00 | 0.00 | 5.94 | 5.95 |
| Fe | 0.00 | 0.00 | 88.81 | 88.97 |
| $Fe_2O_3$ | 96.19 | 96.32 | 0.00 | 0.00 |
| $Al_2O_3$ | 0.38 | 0.38 | 0.53 | 0.54 |
| $SiO_2$ | 0.13 | 0.00 | 0.18 | 0.00 |
| MgO | 0.85 | 0.85 | 1.17 | 1.17 |
| MnO | 1.65 | 1.65 | 2.27 | 2.27 |
| $P_2O_5$ | 0.00 | 0.00 | 0.00 | 0.00 |
| $CaCl_2$ | 0.02 | 0.02 | 0.03 | 0.03 |
| $Nb_2O_5$ | 0.00 | 0.00 | 0.00 | 0.00 |
| $V_2O_5$ | 0.60 | 0.61 | 0.83 | 0.83 |
| $Cr_2O_3$ | 0.06 | 0.06 | 0.08 | 0.08 |

*Liquid filtration (U01-SF01), solids wash (U01-SF02) and solids drying (U01-FK01)*

Assume 100% solid-liquid separation in U01-SF01. There will therefore not be any components present in the spent wash water stream (U02-ST11) other than water. Also assume that no water or chlorine species will be contained within the solid product.

*High-intensity magnetic separation (U01-SM01)*

In this equipment the model varies the split of each component between the product stream (U01-ST09) and the stream with under-leached magnetic material (U01-ST12) until a product stream is obtained with a chemical composition as reported in the literature (Walpole & Winter, 2002: 9) and as summarised in the second column of Table 5.2. The product composition obtained in this process model is summarised in the last column of Table 5.2.

The percentage split for components in the high-intensity magnetic separator towards the magnetic under-leached stream (U01-ST12) is summarised in Table 5.4.

*The fluid bed evaporator (U02-SM01)*

- Assume 100% conversion for all reactions in the fluid bed evaporator.
- Assume that the following reactions will occur in the fluid bed evaporator:

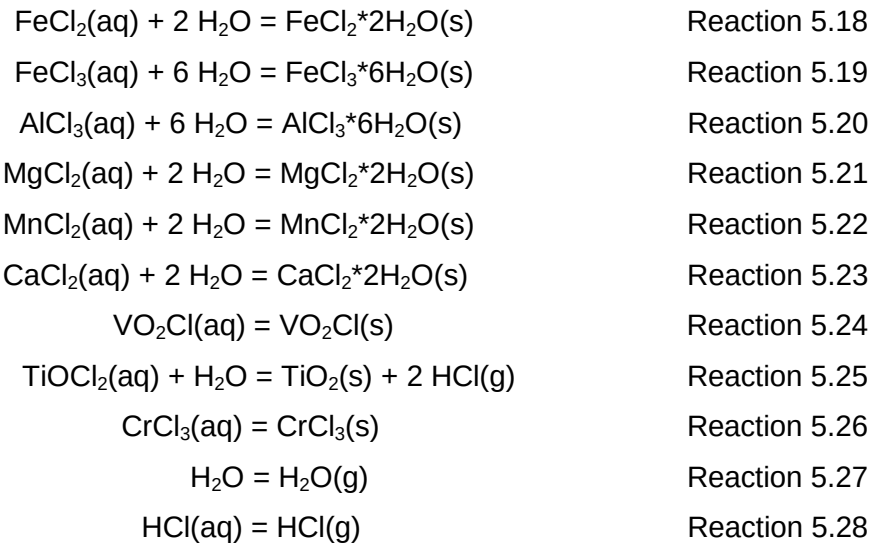


*The pyrohydrolysis reactor (U02-FR01)*

- Assume that $CaCl_2(s)$ does not react.
- Assume 100% conversion for all reactions in the pyrohydrolysis reactor.
- Assume that the following reactions will occur in the pyrohydrolysis reactor:

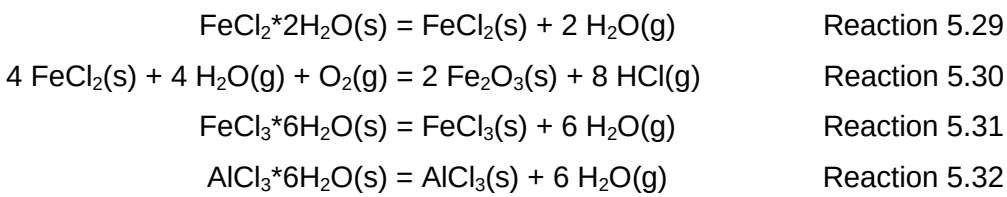

$$MgCl_2*2H_2O(s) = MgCl_2(s) + 2\ H_2O(g) \quad \text{Reaction 5.33}$$

$$MnCl_2*2H2O(s) = MnCl2(s) + 2\ H_2O(g) \quad \text{Reaction 5.34}$$

$$CaCl_2*2H_2O(s) = CaCl_2(s) + 2\ H_2O(g) \quad \text{Reaction 5.35}$$

$$2\ FeCl_3(s) + 3\ H_2O(g) = Fe_2O_3(s) + 6\ HCl(g) \quad \text{Reaction 5.36}$$

$$2\ AlCl_3(s) + 3\ H_2O(g) = Al_2O_3(s) + 6\ HCl(g) \quad \text{Reaction 5.37}$$

$$MgCl_2(s) + H_2O(g) = MgO(s) + 2\ HCl(g) \quad \text{Reaction 5.38}$$

$$MnCl_2 + H_2O(g) = MnO(s) + 2\ HCl(g) \quad \text{Reaction 5.39}$$

$$2\ VO_2Cl(s) + H_2O(g) = V_2O_5(s) + 2\ HCl(g) \quad \text{Reaction 5.40}$$

$$2\ CrCl_3(s) + 3\ H_2O(g) = Cr_2O_3(s) + 6\ HCl(g) \quad \text{Reaction 5.41}$$

*DRI Stage 1 (U03-FR01)*

- Assume that only CO(g) forms during the partial combustion of carbon (Reaction 5.42):

$$C(s) + O_2(g) = CO(g) \quad \text{Reaction 5.42}$$

- In this equipment, the model varies the amount of CO(g) produced so that it would be enough for both DRI stages and the off-gas afterburner (U02-FM01). The off-gas afterburner supplies thermal energy to the fluid bed evaporator (U02-SM01). See the paragraph on the off-gas afterburner on the next page for further discussion on how it works.
- Assume 100% conversion for the two reduction reactions (Reactions 5.6 and 5.7) in the first DRI stage.
- Assume that only the following reduction reactions will occur in the first DRI stage:

$$3\ Fe_2O_3(s) + CO(g) = 2\ Fe_3O_4(s) + CO_2(g) \quad \text{Reaction 5.6}$$

$$Fe_3O_4(s) + CO(g) = 3\ FeO(s) + CO_2(g) \quad \text{Reaction 5.7}$$

*DRI Stage 2 (U03-FR02)*

- Assume 100% conversion for the reduction reaction (Reactions 5.8) in the second DRI stage.
- Assume that only the following reduction reaction will occur in the second DRI stage:

$$FeO(s) + CO(g) = Fe(s) + CO_2(g) \quad \text{Reaction 5.8}$$

*Absorbers (U02-AB01 and U02-AB02)*

- The heat of solution for hydrochloric acid gas absorption into water is not taken into account for this process model. Adiabatic absorbers are used to produce the 25 wt % hydrochloric acid solution and therefore the inter-stage heat exchangers are also not shown.
- The heat of hydrochloric acid condensation is taken into account.

The heat removed from these absorbers in this process model will therefore be only the bare minimum. The heat of solution can increase this amount significantly.

*Off-gas evaporative quenching (U02-HX01 and U02-HX02)*

The off-gas streams from the fluid bed evaporator (U02-SM01) and pyrohydrolysis reactor (U02-FR01) are cooled by means of evaporative quenching with the spent leachate solution before the spent leachate stream enters the fluid bed evaporator (Austpac Resources N.L., 2010). The heat that must be removed in these heat exchangers is therefore subtracted from the heat requirement in the fluid bed evaporator.

*Indirect solids cooler (U03-EC01)*

This heat exchanger is operated with both air and water. The air used in the pyrohydrolysis reactor (U02-FR01) is first preheated to approximately 200 ˚C in this heat exchanger. The excess heat is then removed with cooling water.

*Off-gas afterburner (U02-FM01)*

- Assume that 100% of all CO(g) is burned with air in the off-gas afterburner (according to Reaction 5.43).

$$0.5\ O_2(g) + CO(g) = CO_2(g) \qquad \text{Reaction 5.43}$$

- The amount of CO(g) supplied (and varied by the process model) to the off-gas afterburner is such that the heat produced by the combustion reaction (Reaction 5.43) would be sufficient to reduce the heat requirement in the fluid bed evaporator to zero.
- A fraction of the afterburner off-gas stream (U02-ST16) can also be passed through the fluid bed evaporator, but this is not included in the process model.

*Hydrochloric acid feed stream (U01-ST04)*

The amount of hydrochloric acid lost due to $CaCl_2$(s) production and other possible losses are made up with this stream. The process model automatically determines this amount.

### 5.3.2 – Summary of results

Table 5.2 summarises the chemical compositions of the feed and product streams for both the Austpac ERMS SR process (as reported in the literature) and this process model.

These results indicate significant agreement with reported stream compositions. Only the DRI product differs, because 100% metallisation was assumed in the process model.

**Table 5.2: Compositions for the Austpac ERMS SR process and the process model**

| | Austpac ERMS SR process | | | | Process model | | |
|---|---|---|---|---|---|---|---|
| **Constituent** | **Feed**[1] | **U02-FR01**[2] | **DRI product**[2] | **SR product**[1] | **U02-FR01** | **DRI product** | **SR product** |
| $TiO_2$ | 50.40 | 0.11 | 0.16 | 97.30 | 0.11 | 0.16 | 97.30 |
| Fe | 0.00 | 0.00 | 88.97 | 0.00 | 0.00 | 95.54 | 0.00 |
| FeO | 34.10 | 0.00 | 5.95 | 0.00 | 0.00 | 0.00 | 0.00 |
| $Fe_2O_3$ | 12.10 | 96.32 | 0.00 | 1.08 | 96.83 | 0.00 | 1.08 |
| $Al_2O_3$ | 0.55 | 0.38 | 0.54 | 0.13 | 0.38 | 0.54 | 0.13 |
| $SiO_2$ | 0.76 | 0.00 | 0.00 | 0.79 | 0.00 | 0.00 | 0.79 |
| MgO | 0.67 | 0.85 | 1.17 | 0.02 | 0.85 | 1.19 | 0.02 |
| MnO | 0.61 | 1.65 | 2.27 | 0.01 | 1.21 | 1.71 | 0.01 |
| $P_2O_5$ | 0.01 | 0.00 | 0.00 | 0.02 | 0.00 | 0.00 | 0.02 |
| CaO | 0.04 | 0.00 | 0.00 | 0.01 | 0.00 | 0.00 | 0.01 |
| $CaCl_2$ | 0.00 | 0.02 | 0.03 | 0.00 | 0.02 | 0.03 | 0.00 |
| $Nb_2O_5$ | 0.11 | 0.00 | 0.00 | 0.23 | 0.00 | 0.00 | 0.21 |
| $V_2O_5$ | 0.28 | 0.60 | 0.83 | 0.02 | 0.53 | 0.75 | 0.02 |
| $ZrO_2$ | 0.04 | 0.00 | 0.00 | 0.01 | 0.00 | 0.00 | 0.01 |
| $Cr_2O_3$ | 0.09 | 0.06 | 0.08 | 0.02 | 0.06 | 0.09 | 0.02 |
| Other | 0.23 | 0.00 | 0.00 | 0.38 | 0.00 | 0.00 | 0.38 |

The conversions for Reactions 5.10 to 5.17 are summarised in Table 5.3.

[1] (Walpole & Winter, 2002)
[2] (Winter, 2009) These are normalised compositions; see assumptions for U01-RC01.

**Table 5.3: Conversions for Reactions 5.10 to 5.17**

| Reaction # | Conversion (%) |
|---|---|
| 5.10 | 94.80 |
| 5.11 | 34.70 |
| 5.12 | 64.30 |
| 5.13 | 99.10 |
| 5.14 | 14.00 |
| 5.15 | 96.00 |
| 5.16 | 0.11 |
| 5.17 | 36.36 |

The percentage split of components in the high-intensity magnetic separator (U01-SM01) towards the magnetic under-leached stream (U01-ST12) is summarised in Table 5.4.

**Table 5.4: Component split in high-intensity magnetic separator**

| Constituent | Split (%) |
|---|---|
| $TiO_2$ | 0.00 |
| FeO | 100.00 |
| $Fe_2O_3$ | 11.20 |
| $Al_2O_3$ | 81.50 |
| $SiO_2$ | 46.30 |
| MgO | 95.60 |
| MnO | 6.74 |
| $P_2O_5$ | 14.40 |
| CaO | 83.40 |
| $Nb_2O_5$ | 0.00 |
| $V_2O_5$ | 6.90 |
| $ZrO_2$ | 85.70 |
| $Cr_2O_3$ | 80.80 |
| Other | 14.30 |

The resulting process model is illustrated in Figure 5.4 as a simplified process flow diagram. This diagram contains a stream table to illustrate the stream compositions of the main components in the process (e.g. Fe and Ti). A complete stream table for all components is given in Appendix 4.

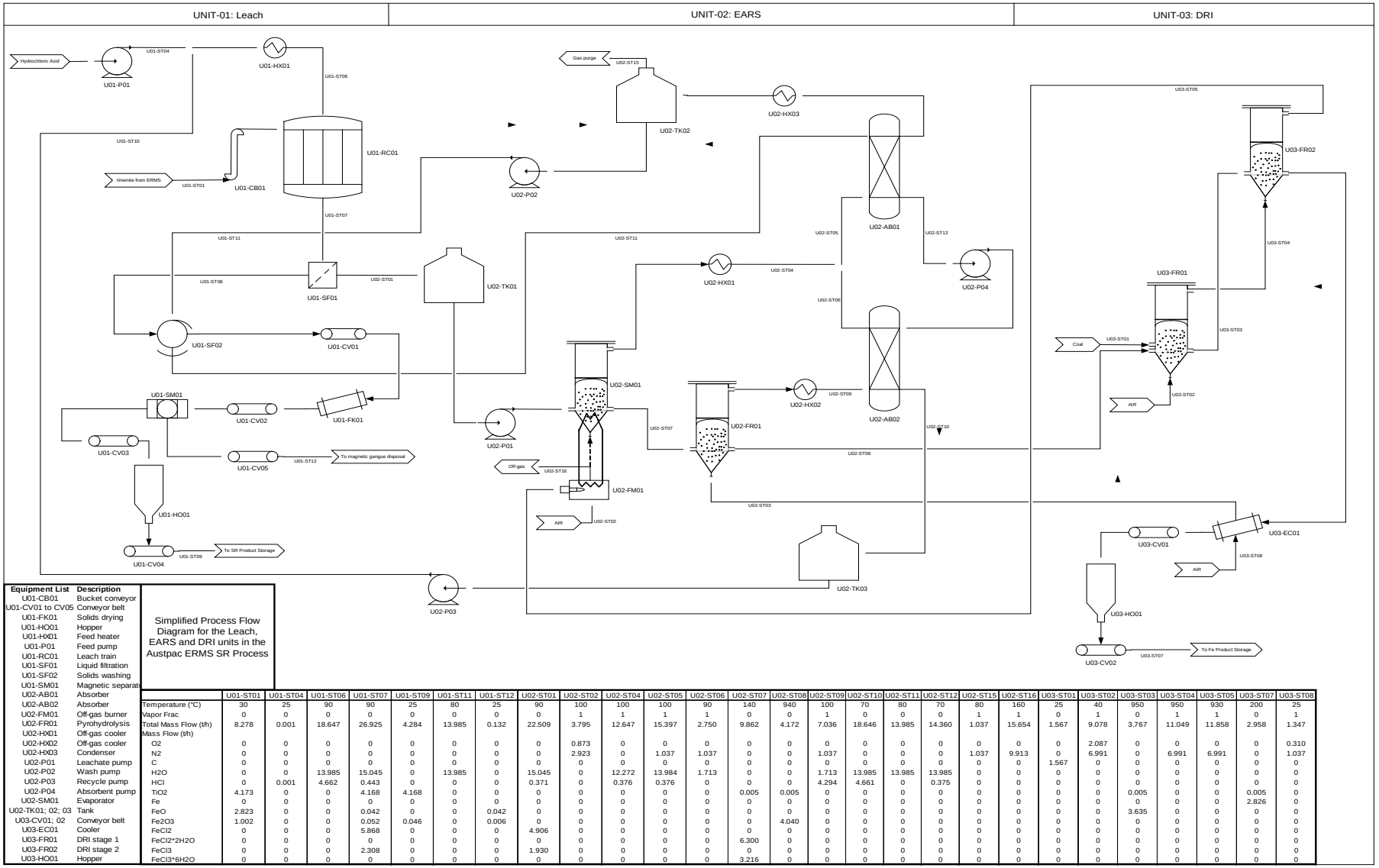


| Equipment List | Description |
|---|---|
| U01-CB01 | Bucket conveyor |
| U01-CV01 to CV05 | Conveyor belt |
| U01-FK01 | Solids drying |
| U01-HO01 | Hopper |
| U01-HX01 | Feed heater |
| U01-P01 | Feed pump |
| U01-RC01 | Leach train |
| U01-SF01 | Liquid filtration |
| U01-SF02 | Solids washing |
| U01-SM01 | Magnetic separator |
| U02-AB01 | Absorber |
| U02-AB02 | Absorber |
| U02-FM01 | Off-gas burner |
| U02-FR01 | Pyrohydrolysis |
| U02-HX01 | Off-gas cooler |
| U02-HX02 | Off-gas cooler |
| U02-HX03 | Condenser |
| U02-P01 | Leachate pump |
| U02-P02 | Wash pump |
| U02-P03 | Recycle pump |
| U02-P04 | Absorbent pump |
| U02-SM01 | Evaporator |
| U02-TK01; 02; 03 | Tank |
| U03-CV01; 02 | Conveyor belt |
| U03-EC01 | Cooler |
| U03-FR01 | DRI stage 1 |
| U03-FR02 | DRI stage 2 |
| U03-HO01 | Hopper |

Simplified Process Flow Diagram for the Leach, EARS and DRI units in the Austpac ERMS SR Process

| | U01-ST01 | U01-ST04 | U01-ST06 | U01-ST07 | U01-ST09 | U01-ST11 | U01-ST12 | U02-ST01 | U02-ST02 | U02-ST04 | U02-ST05 | U02-ST06 | U02-ST07 | U02-ST08 | U02-ST09 | U02-ST10 | U02-ST11 | U02-ST12 | U02-ST15 | U02-ST16 | U03-ST01 | U03-ST02 | U03-ST03 | U03-ST04 | U03-ST05 | U03-ST07 | U03-ST08 |
|---|---|---|---|---|---|---|---|---|---|---|---|---|---|---|---|---|---|---|---|---|---|---|---|---|---|---|---|
| Temperature (°C) | 30 | 25 | 90 | 90 | 25 | 80 | 25 | 90 | 100 | 100 | 100 | 90 | 140 | 940 | 100 | 70 | 80 | 70 | 80 | 160 | 25 | 40 | 950 | 950 | 930 | 200 | 25 |
| Vapor Frac | 0 | 0 | 0 | 0 | 0 | 0 | 0 | 0 | 1 | 1 | 1 | 1 | 0 | 0 | 1 | 0 | 0 | 0 | 1 | 1 | 0 | 1 | 0 | 1 | 1 | 0 | 1 |
| Total Mass Flow (t/h) | 8.278 | 0.001 | 18.647 | 26.925 | 4.284 | 13.985 | 0.132 | 22.509 | 3.795 | 12.647 | 15.397 | 2.750 | 9.862 | 4.172 | 7.036 | 18.646 | 13.985 | 14.360 | 1.037 | 15.654 | 1.567 | 9.078 | 3.767 | 11.049 | 11.858 | 2.958 | 1.347 |
| Mass Flow (t/h) | | | | | | | | | | | | | | | | | | | | | | | | | | | |
| O2 | 0 | 0 | 0 | 0 | 0 | 0 | 0 | 0 | 0.873 | 0 | 0 | 0 | 0 | 0 | 0 | 0 | 0 | 0 | 0 | 0 | 0 | 2.087 | 0 | 0 | 0 | 0 | 0.310 |
| N2 | 0 | 0 | 0 | 0 | 0 | 0 | 0 | 0 | 2.923 | 0 | 1.037 | 1.037 | 0 | 0 | 1.037 | 0 | 0 | 0 | 1.037 | 9.913 | 0 | 6.991 | 0 | 6.991 | 6.991 | 0 | 1.037 |
| C | 0 | 0 | 0 | 0 | 0 | 0 | 0 | 0 | 0 | 0 | 0 | 0 | 0 | 0 | 0 | 0 | 0 | 0 | 0 | 0 | 1.567 | 0 | 0 | 0 | 0 | 0 | 0 |
| H2O | 0 | 0 | 13.985 | 15.045 | 0 | 13.985 | 0 | 15.045 | 0 | 12.272 | 13.984 | 1.713 | 0 | 0 | 1.713 | 13.985 | 13.985 | 13.985 | 0 | 0 | 0 | 0 | 0 | 0 | 0 | 0 | 0 |
| HCl | 0 | 0.001 | 4.662 | 0.443 | 0 | 0 | 0 | 0.371 | 0 | 0.376 | 0.376 | 0 | 0 | 0 | 4.294 | 4.661 | 0 | 0.375 | 0 | 0 | 0 | 0 | 0 | 0 | 0 | 0 | 0 |
| TiO2 | 4.173 | 0 | 0 | 4.168 | 4.168 | 0 | 0 | 0 | 0 | 0 | 0 | 0 | 0.005 | 0.005 | 0 | 0 | 0 | 0 | 0 | 0 | 0 | 0 | 0.005 | 0 | 0 | 0.005 | 0 |
| Fe | 0 | 0 | 0 | 0 | 0 | 0 | 0 | 0 | 0 | 0 | 0 | 0 | 0 | 0 | 0 | 0 | 0 | 0 | 0 | 0 | 0 | 0 | 0 | 0 | 2.826 | 0 | 0 |
| FeO | 2.823 | 0 | 0 | 0.042 | 0 | 0 | 0.042 | 0 | 0 | 0 | 0 | 0 | 0 | 0 | 0 | 0 | 0 | 0 | 0 | 0 | 0 | 0 | 3.635 | 0 | 0 | 0 | 0 |
| Fe2O3 | 1.002 | 0 | 0 | 0.052 | 0.046 | 0 | 0.006 | 0 | 0 | 0 | 0 | 0 | 0 | 4.040 | 0 | 0 | 0 | 0 | 0 | 0 | 0 | 0 | 0 | 0 | 0 | 0 | 0 |
| FeCl2 | 0 | 0 | 0 | 5.868 | 0 | 0 | 0 | 4.906 | 0 | 0 | 0 | 0 | 0 | 0 | 0 | 0 | 0 | 0 | 0 | 0 | 0 | 0 | 0 | 0 | 0 | 0 | 0 |
| FeCl2*2H2O | 0 | 0 | 0 | 0 | 0 | 0 | 0 | 0 | 0 | 0 | 0 | 0 | 6.300 | 0 | 0 | 0 | 0 | 0 | 0 | 0 | 0 | 0 | 0 | 0 | 0 | 0 | 0 |
| FeCl3 | 0 | 0 | 0 | 2.308 | 0 | 0 | 0 | 1.930 | 0 | 0 | 0 | 0 | 0 | 0 | 0 | 0 | 0 | 0 | 0 | 0 | 0 | 0 | 0 | 0 | 0 | 0 | 0 |
| FeCl3*6H2O | 0 | 0 | 0 | 0 | 0 | 0 | 0 | 0 | 0 | 0 | 0 | 0 | 3.216 | 0 | 0 | 0 | 0 | 0 | 0 | 0 | 0 | 0 | 0 | 0 | 0 | 0 | 0 |

**Figure 5.4: Leach, EARS and DRI process flow diagram**

### 5.3.3 – Material and energy balances

The HSC Chemistry 7.0© process model developed for the leach, EARS and DRI units in the Austpac ERMS SR process was used to determine the material and energy balances for the proposed process flowsheet.

Table 5.5 lists the material and energy balances for the main equipment used in the process model.

**Table 5.5: Material and energy balances for main equipment in the process model**

| Equipment | Description | Mass balance (t/h) | Energy balance (kW) |
|---|---|---|---|
| U01-HX01 | Feed heater | 0.000 | 246 |
| U01-RC01 | Leach train | 0.000 | -1 413 |
| U02-AB01 | Absorber | 0.000 | -474 |
| U02-AB02 | Absorber | 0.000 | -2 689 |
| U02-FM01 | Off-gas burner | 0.000 | -7 115 |
| U02-FR01 | Pyrohydrolysis | 0.000 | 5 625 |
| U02-HX01 | Off-gas cooler | 0.000 | -250 |
| U02-HX02 | Off-gas cooler | 0.000 | -1 974 |
| U02-HX03 | Condenser | 0.000 | -9 070 |
| U02-SM01 | Evaporator | 0.000 | 9 350 |
| U03-EC01 | Cooler | 0.000 | -391 |
| U03-FR01 | DRI stage 1 | 0.000 | -1 049 |
| U03-FR02 | DRI stage 2 | 0.000 | -241 |
| | **Total:** | 0.000 | -9 443 |

Table 5.6 summarises the input-output material and energy balances for the process model as a whole. The input and output streams in the process model can be seen in Figure 5.4.

**Table 5.6: Overall input-output material and energy balances for the process model**

| Constituent | Input streams (t/h) | | | | | | Output streams (t/h) | | | | | BALANCE: |
|---|---|---|---|---|---|---|---|---|---|---|---|---|
| | U03-ST08 | U03-ST02 | U03-ST01 | U01-ST01 | U01-ST04 | U02-ST02 | U01-ST09 | U01-ST12 | U02-ST15 | U02-ST16 | U03-ST07 | |
| $N_2$(g) | 1.037 | 6.991 | | | | 2.923 | | | 1.037 | 9.913 | | |
| $CO_2$(g) | | | | | | | | | | 5.740 | | **2.471** |
| $O_2$(g) | 0.310 | 2.087 | | | | 0.873 | | | | | | |
| HCl(aq) | | | | | 0.001 | | | | | | | **-0.001** |
| C | | | 1.567 | | | | | | | | | |
| $TiO_2$ | | | | 4.173 | | | 4.168 | | | | 0.005 | |
| FeO | | | | 2.823 | | | | 0.042 | | | | |
| Fe | | | | | | | | | | | 2.826 | |
| $Fe_2O_3$ | | | | 1.002 | | | 0.046 | 0.006 | | | | |
| $Al_2O_3$ | | | | 0.046 | | | 0.006 | 0.024 | | | 0.016 | |
| MgO | | | | 0.055 | | | 0.001 | 0.019 | | | 0.035 | |
| MnO | | | | 0.051 | | | 0.000 | 0.000 | | | 0.051 | |
| CaO | | | | 0.003 | | | 0.000 | 0.002 | | | | **-2.471** |
| $V_2O_5$ | | | | 0.023 | | | 0.001 | 0.000 | | | 0.022 | |
| SiO2 | | | | 0.063 | | | 0.034 | 0.029 | | | | |
| $P_2O_5$ | | | | 0.001 | | | 0.001 | 0.000 | | | | |
| $Nb_2O_5$ | | | | 0.009 | | | 0.009 | | | | | |
| $ZrO_2$ | | | | 0.003 | | | 0.000 | 0.003 | | | | |
| $Cr_2O_3$ | | | | 0.007 | | | 0.001 | 0.004 | | | 0.003 | |
| Other | | | | 0.019 | | | 0.016 | 0.003 | | | | |
| $CaCl_2$ | | | | | | | | | | | 0.001 | |
| **TOTAL MASS** (t/h) | 1.347 | 9.077 | 1.567 | 8.278 | 0.001 | 3.795 | 4.284 | 0.132 | 1.037 | 15.654 | 2.958 | **0.000** |
| **ENTHALPY** (kWh) | | 38 | | -18 996 | -1 | 80 | -13 976 | -387 | 16 | -13 674 | -299 | **-9 442** |

### 5.3.4 – Discussion of results

The stream compositions obtained from this process model correlate well with the reported chemical compositions for the Austpac ERMS SR process, as can be seen in Table 5.2. This correlation suggests that the process model can be used in a techno-economic study as a rough estimate to evaluate equipment and process flow within the leach, EARS, and DRI process units in the Austpac ERMS SR process.

In this study the process model is, however, used only to identify important aspects within the Austpac ERMS SR process that can be useful in a process for removing iron from nitrided ilmenite. These observations are briefly discussed below.

The importance of increasing the magnetic properties of the ilmenite ore in the ERMS process unit is the first significant feature identified in the Austpac ERMS SR process. In Section 5.2.1 it was stated that the magnetic properties of the ore are enhanced in the ERMS process unit for downstream separation of gangue material from the upgraded product. The extent of this enhancement is clear from the results obtained in the process model. Table 5.7 reports the product composition before and after the high-intensity magnetic separation (U01-SM01) step.

**Table 5.7: Effect of magnetic separation on product quality**

| Constituent | Before magnetic separation (wt %) | After magnetic separation (wt %) |
|---|---|---|
| $TiO_2$ | 94.39 | 97.30 |
| FeO | 0.96 | 0.00 |
| $Fe_2O_3$ | 1.18 | 1.08 |
| $Al_2O_3$ | 0.68 | 0.13 |
| $SiO_2$ | 1.43 | 0.79 |
| MgO | 0.45 | 0.02 |
| MnO | 0.01 | 0.01 |
| $P_2O_5$ | 0.02 | 0.02 |
| CaO | 0.06 | 0.01 |
| $Nb_2O_5$ | 0.20 | 0.21 |
| $V_2O_5$ | 0.02 | 0.02 |
| $ZrO_2$ | 0.07 | 0.01 |
| $Cr_2O_3$ | 0.10 | 0.02 |
| Other | 0.43 | 0.38 |

The results given in Table 5.7 indicate that a significant improvement in final product quality is obtained with the use of the high-intensity magnetic separator. Approximately 3 wt % of

the leached solids are removed during the magnetic separation step, which consists mostly of gangue materials. This gangue material would have resulted in chlorine consumption in a high-temperature carbo-thermal chlorination reactor. A considerable saving in chlorine is therefore achieved. The gangue material and its composition are discussed later in this section.

The results from the process model indicate that hydrochloric acid recovery in the EARS process unit can reach levels of 99.99% when no hydrochloric acid vapour is lost in the absorbers. A 100% recovery is, however, not possible because calcium chloride ($CaCl_2$) does not hydrolyse in the pyrohydrolysis reactor (Winter, 2008). In the process model it was found that 0.835 kg of $CaCl_2$ is produced per hour in the leach train. Assuming that a 100% recovery of HCl(g) can be reached in the absorbers results in a required hydrochloric acid make-up stream (U01-ST04) of 0.548 kg of HCl per hour. This equates to a requirement of 11.85 ton of 37 wt % of hydrochloric acid per year. This is an acceptable acid consumption for a process that produces approximately 60 000 tons of synthetic rutile annually.

Another feature of the Austpac ERMS SR process, and perhaps the most significant one, is process integration (both mass and energy) within the process. It is the author's opinion that innovative process integration is the key attribute of the Austpac ERMS SR process.

Innovative mass integration was applied in the arrangement of the two absorbers to produce a super-azeotropic (25 wt %) hydrochloric acid solution (Section 5.2.3). This hydrochloric acid is then used in the leach train. Hydrochloric acid with an 18 wt % concentration is produced from conventional spent pickle liquor acid-recovery systems (Metsep International, 2007). The amount of water circulating through the process is significantly reduced when a 25 wt % solution is used instead of an 18 wt % hydrochloric acid solution. This results in a large reduction in energy requirements (less water to evaporate). The size of all equipment is also reduced.

The fluid bed evaporator (U02-SM01) has the highest energy requirement (~9.3 MWh) in the entire Austpac ERMS SR process (Section 5.3.2). Two process integration steps are used to reduce this energy requirement:

- The first process integration method is evaporative quenching of the off-gas streams from the pyrohydrolysis reactor (~950 °C) and fluid bed evaporator (~140 °C) with the spent leachate solution before these streams enter the fluid bed evaporator. This

reduces the energy requirement in the fluid bed evaporator by approximately 20% (~1.9 MWh).

- The second process integration method is the recovery of energy from the off-gas stream of the second DRI stage (~930 °C). This is achieved by sending the hot off-gas stream through an internal or external heat exchanger (U02-FM01), coupled to the fluid bed evaporator. An off-gas stream split from this unit can be sent directly through the fluid bed evaporator to fluidise the bed. The fluid bed evaporator's energy requirement is further reduced by approximately 1.8 MWh when it is assumed that the off-gas stream is cooled to 160 °C (ΔT = 20 °C).

In total, the fluid bed evaporator's energy requirement can be reduced by approximately 40% from ~9.3 MWh to ~5.3 MWh using the above-described process integration methods.

Another process integration method entails the means in which the remaining (~5.3 MWh) thermal energy is supplied to the fluid bed evaporator. This is done by the combustion (in U02-FM01) of the excess carbon monoxide produced in the DRI process unit. Excess carbon monoxide is required in the DRI stages to ensure sufficient reduction of iron oxides.

Stoichiometric reduction of iron oxide with carbon monoxide requires partial combustion of approximately 912 kg of coal per hour. The partial combustion of an extra 655 kg of coal per hour is required to obtain the required ~5.2 MWh from the combustion reaction of carbon monoxide with air. This value was determined by the process model. The carbon monoxide is therefore more than 50% in excess of the required stoichiometric amount.

A negative aspect in the Austpac ERMS SR process is, however, the amount of carbon dioxide produced. A total of 1.567 tons of coal is consumed per hour in the process model. This equates to approximately 5.74 tons of carbon dioxide produced per hour. In other words, each ton of titanium dioxide produced will result in approximately 1.3 tons of carbon dioxide. It is therefore crucial that an effective carbon-capturing or minimisation system is included with the process.

It can be seen in the process model that the Austpac ERMS SR process has the potential to be a zero-liquid-effluent process (Austpac Resources N.L., 2010).

Aside from the synthetic rutile and metallised iron products, another solid material is also produced. This is the 3% magnetic stream split (U01-ST12) produced in the high-intensity magnetic separation step. The chemical composition for this material, as determined in the process model, is given in Table 5.8.

**Table 5.8: Composition of material in stream U01-ST12**

| Constituent | Mass% |
|---|---|
| $TiO_2$ | 0.00 |
| FeO | 32.11 |
| $Fe_2O_3$ | 4.43 |
| $Al_2O_3$ | 18.54 |
| $SiO_2$ | 22.11 |
| MgO | 14.26 |
| MnO | 0.02 |
| $P_2O_5$ | 0.11 |
| CaO | 1.63 |
| $Nb_2O_5$ | 0.00 |
| $V_2O_5$ | 0.05 |
| $ZrO_2$ | 1.95 |
| $Cr_2O_3$ | 2.73 |
| Other | 2.06 |

According to the process model, a total of 1 055 tons per year of this material is produced. An advantage of the Austpac ERMS SR process is that none of the solid material produced will have to be treated as a hazardous waste.

## 5.4 – Conclusions and recommendations

In the opening section of this chapter, it was mentioned that Austpac Resources N.L. had received an “Applied Technology of the Year” award for their work in technology development for the titanium and steel industries. After a detailed review of the Austpac ERMS SR process, it can be seen that in fact they redeveloped existing technology – through innovative process integration and optimisation – into a process that will be hard to improve on.

Only two of the four process units in the Austpac ERMS SR process can, however, be used when iron is removed from nitrided ilmenite. These are the EARS and the DRI process units. The EARS process unit is of particular interest, but the applicability of the DRI unit must first be determined by establishing whether the metallised iron pellets can be sold as a by-product.

The reason why the leaching unit cannot be used is due to the presence of metallic iron in nitrided ilmenite and not iron oxide as in the product from the ERMS process unit. A leach unit will therefore have to be developed to accommodate the production of hydrogen gas during the dissolution reaction.

It is therefore necessary to evaluate whether hydrochloric acid can be used as a lixiviant to remove iron form nitrided ilmenite. This is the objective of Chapter 6.

# CHAPTER 6 – EXPERIMENTAL EVALUATION: DISSOLUTION OF NITRIDED ILMENITE IN HCl

## 6.1 – Overview

Hydrochloric acid leaching was identified and evaluated (Chapters 2 and 4) as a possible process route to remove metallic iron from nitrided ilmenite. Commercially, hydrochloric acid is used to remove iron oxides and most other metal oxides from thermally pretreated ilmenite (Lanyon *et al.*, 1999). The overall dissolution reaction for iron oxide is given in Reaction 6.1.

$$FeO.TiO_2(s) + 2HCl(aq) = FeCl_2(aq) + H_2O(l) + TiO_2(s) \qquad \text{Reaction 6.1}$$

The solid product obtained is known as “synthetic rutile” and contains at least 92% $TiO_2$.

However, the iron in nitrided ilmenite is reduced to metallic iron during the nitriding reaction. The dissolution reaction of nitrided ilmenite is therefore different from that in commercial processes in that the hydrochloric acid will react with metallic iron to produce hydrogen gas, (Reaction 6.2), instead of reacting with iron oxide to produce water (Reaction 6.1).

$$Fe(s) + 2HCl(aq) = FeCl_2(aq) + H_2(g) \qquad \text{Reaction 6.2}$$

The aim of this chapter is therefore to evaluate whether hydrochloric acid can be used as lixiviant to remove iron from nitrided ilmenite without excessive product (TiN) dissolution and dissolution of species that could lead to acid consumption (e.g. CaO forming $CaCl_2$).

The dissolution of metallic iron is evaluated at different temperatures (Section 6.3.1) and hydrochloric acid concentrations (Section 6.3.2). The rate data obtained from Sections 6.3.1 and 6.3.2 are analysed in Section 6.3.3 to propose a possible rate law that could describe the dissolution reaction of metallic iron in nitrided ilmenite in a hydrochloric acid solution. The dissolution of other species (aluminium, calcium, magnesium and titanium) is evaluated in Section 6.3.4 at different acid concentrations, initial acid-to-iron mole ratios and solid-to-liquid mass ratios after a fixed period during which iron dissolution is virtually complete.

This chapter concludes (Section 6.4) by evaluating whether or not hydrochloric acid can be used as a viable lixiviant to remove metallic iron from nitrided ilmenite.

## 6.2 – Experimental

### 6.2.1 – Sample characteristics

The sample described in Chapter 3 was used in the experiments of this chapter. Refer to Chapter 3 for a detailed overview of the sample characteristics and the procedures used to obtain the sample. Analytical-grade HCl was used in all leach experiments.

### 6.2.2 – Experimental planning

The variables manipulated were selected with the aim of evaluating the viability of using hydrochloric acid as lixiviant to remove metallic iron from nitrided ilmenite.

The variables investigated during the leach study are listed in Table 6.1.

**Table 6.1: Variables investigated during the leach study**

| Variable | Conditions |
|---|---|
| Hydrochloric acid concentration (wt %) | 11%; 18%; 25% |
| Temperature (˚C) | 11; 18; 25 |
| Dissolution of other species | Refer to Section 6.3.4 |

The conditions for each variable were selected so as to simulate conditions that can be found in a commercial plant. This is also the reason why particle size and agitation speed were not varied. The sample used contained particles with an average particle diameter of 185 µm and the agitation speed was such that all particles were kept in suspension.

### 6.2.3 – Experimental procedure

Metallic iron reacts violently with hydrochloric acid (Reaction 6.2) to produce hydrogen gas. Two experimental set-ups were required because of this.

- The first experimental set-up was used to evaluate the dissolution reaction after 25 minutes and longer. This was the case because it took approximately 10 minutes to add the required amount of hydrochloric acid to the nitrided ilmenite sample without loss of reaction solution due to excessive hydrogen gas evolution and foaming.

- The second experimental set-up was used to evaluate the dissolution for the first 10 minutes of reaction. This set-up could not, however, be used for periods longer than 10 minutes.

### 6.2.3.1 – Experimental set-up #1

Acid leaching of nitrided ilmenite was carried out using a 500 ml three-necked glass reactor. The reaction vessel was equipped with two condensers in series and an overhead stirrer fitted with a PTFE-coated shaft and impeller. A temperature-controlled heating mantle regulated temperature inside the reaction vessel. A schematic diagram of this experimental set-up is illustrated in Figure 6.1.

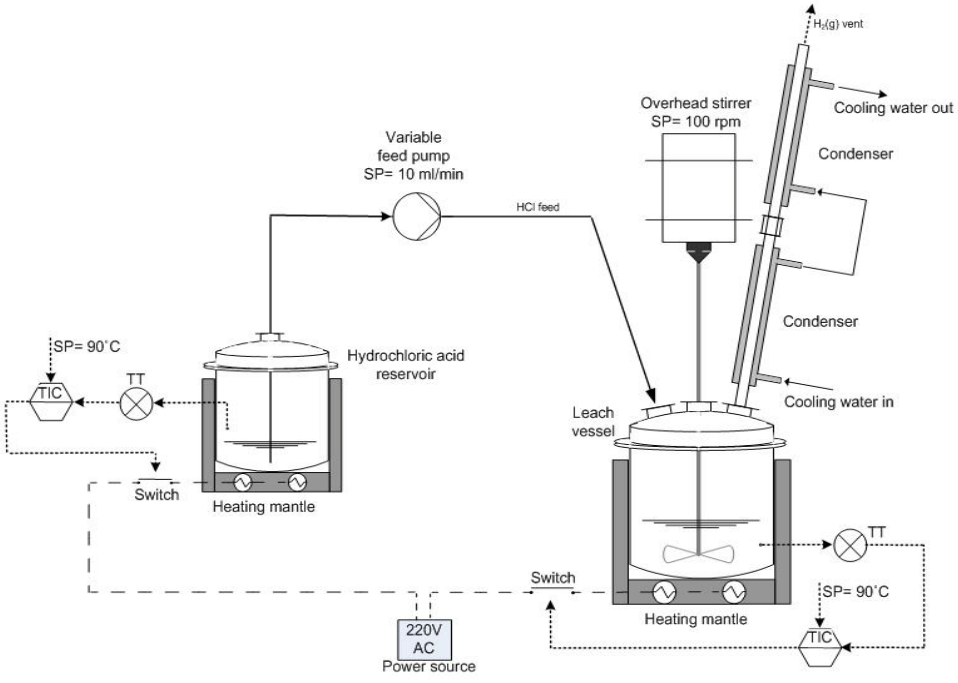


**Figure 6.1: Overview of leach experimental set-up #1**

The required mass of nitrided ilmenite sample ($d_{50}$ = 185 µm) was first loaded into the reaction vessel. Once the reactor and solids had reached the temperature set-point, hydrochloric acid (also at temperature set-point) at the required concentration (11, 18 or

25%) was added to the reactor at a rate of 10 ml/min from a second heated vessel. The 100 ml of hydrochloric acid was thus added over 10 minutes. The slow addition was done to prevent foaming caused by excessive hydrogen gas evolution. A stirring speed of 100 r/min was applied to keep the slurry suspended during the leaching experiment.

After the required reaction period, the slurry was filtered off and the solid residue thoroughly washed with hot water. The washed solids were then dried in air for 60 minutes at 80 ˚C. The dried solids were sent for chemical analysis (ICP-OES, when required) and the leach liquor for analysis by redox titration to determine the total iron(II) in solution. Refer to Appendix 3 for the redox titration procedure.

#### 6.2.3.2 – Experimental set-up #2

Acid leach data for the first 10 minutes of reaction between nitrided ilmenite and hydrochloric acid were obtained using a “filter bed-reactor” experimental set-up. A negative pressure gradient below the filter bed removed evolved hydrogen gas, which in turn prevented foaming and loss of reaction solution. The hydrochloric acid solution was repeatedly recycled through the particles at a rate of 25 ml/min to ensure that the solids were in contact with the entire hydrochloric acid solution at least 2.5 times within the first 5 minutes of reaction.

The hydrochloric acid inventory was limited to the solid load in the filter bed-reactor which could contain only up to 20 g of nitrided ilmenite sample per run. The hydrochloric acid solution was held constant at 50 ml for all runs. The required mass of nitrided ilmenite sample was calculated from the available hydrochloric acid in solution. A schematic diagram of this experimental set-up is illustrated in Figure 6.2.

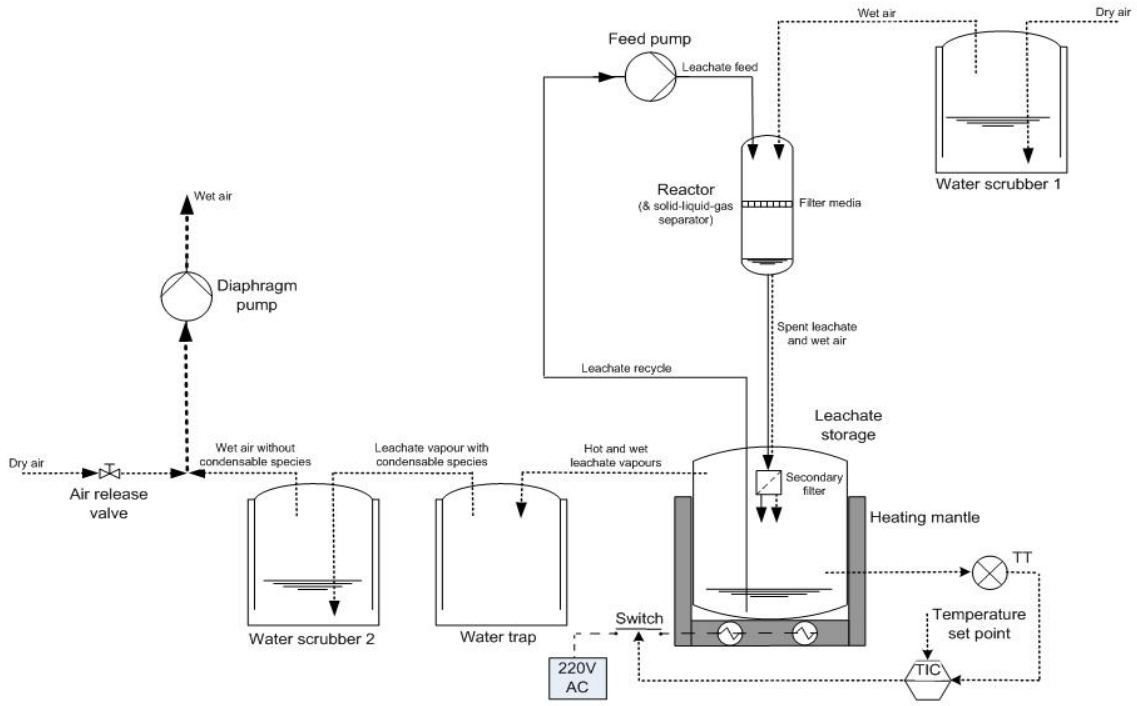


**Figure 6.2: Overview of leach experimental set-up #2**

The required mass of nitrided ilmenite ($d_{50}$ = 185 µm) was first loaded into the filter bed-reactor. The 50 ml of hydrochloric acid solution was then added to the "leachate storage" vessel and heated to reach the required temperature set-point. A temperature-controlled heating mantle controlled the temperature inside the leachate storage vessel.

The diaphragm pump was switched on once the hydrochloric acid solution had reached its temperature set-point. The diaphragm pump sucked air through the first water scrubber, the filter bed-reactor, the leachate storage vessel, the water trap and then finally through the second water scrubber. The first water scrubber was used to prevent dry air from flowing through the system, which in turn prevented excessive evaporation and losses of liquid solution. The second water scrubber washed the extracted air clean of possible hydrochloric acid vapours. An air-release valve was used to control the amount of air passing through the filter bed-reactor. The air flow was manually controlled to ensure that only evolved hydrogen gas was removed from the reactor and, if possible, no air. The hydrochloric acid feed pump was switched on once the air-release valve had been correctly positioned.

After the required reaction period, the slurry was filtered off and the solid residue thoroughly washed with hot water. The washed solids were then dried in air for 60 minutes at 80 ˚C. The dried solids were sent for chemical analysis (when required) and the leach liquor for analysis by redox titration to determine the total iron(II) in solution.

### 6.2.4 – Experimental error

Both experimental set-ups described above have intrinsic experimental errors that cause the results to vary. The experimental error for both set-ups is reported in this section. These experimental errors were calculated with a 95% confidence level and the assumption that the data fitted a normal distribution. Appendix A6.1 gives an example of how the experimental error was determined.

It is considered conventional to indicate the experimental errors on figures illustrating the results. To prevent unnecessary cluttering of the graphs used in this chapter, this has, however, not been done.

#### 6.2.4.1 – Experimental error for set-up #1

The experimental error for this set-up was determined by repeating an experiment three times. The following conditions were held constant:

- Hydrochloric acid concentration of 18 wt %
- Temperature set-point equal to 90 ˚C
- Average particle diameter of 185 µm
- Mixing speed equal to 100 r/min
- Acid-to-iron mole ratio of 2.5:1
- Leach duration of 35 minutes.

Iron conversion was used as response variable.

The experimental error for this set-up was found to be equal to 5%.

#### 6.2.4.2 – Experimental error for set-up #2

The experimental error for this set-up was determined by repeating an experiment four times. The following conditions were held constant:

- Hydrochloric acid concentration of 11 wt %
- Temperature set-point equal to 25 ˚C
- Average particle diameter of 185 µm
- Feed pump recycle rate equal to 25 ml/min
- Acid-to-iron mole ratio of 2.5:1
- Leach duration of 5 minutes.

Iron conversion was also used as response variable to calculate the experimental error.

The experimental error for this set-up was found to be equal to 8%.

## 6.3 – Results and discussion

### 6.3.1 – Effect of temperature

Three experiments were conducted at 25, 60 and 90 °C to study the effect of temperature on metallic iron dissolution in hydrochloric acid. A relatively low hydrochloric acid concentration (11%) was used in an attempt to reduce the rate of reaction between metallic iron and hydrochloric acid. The results are illustrated in Figure 6.3.

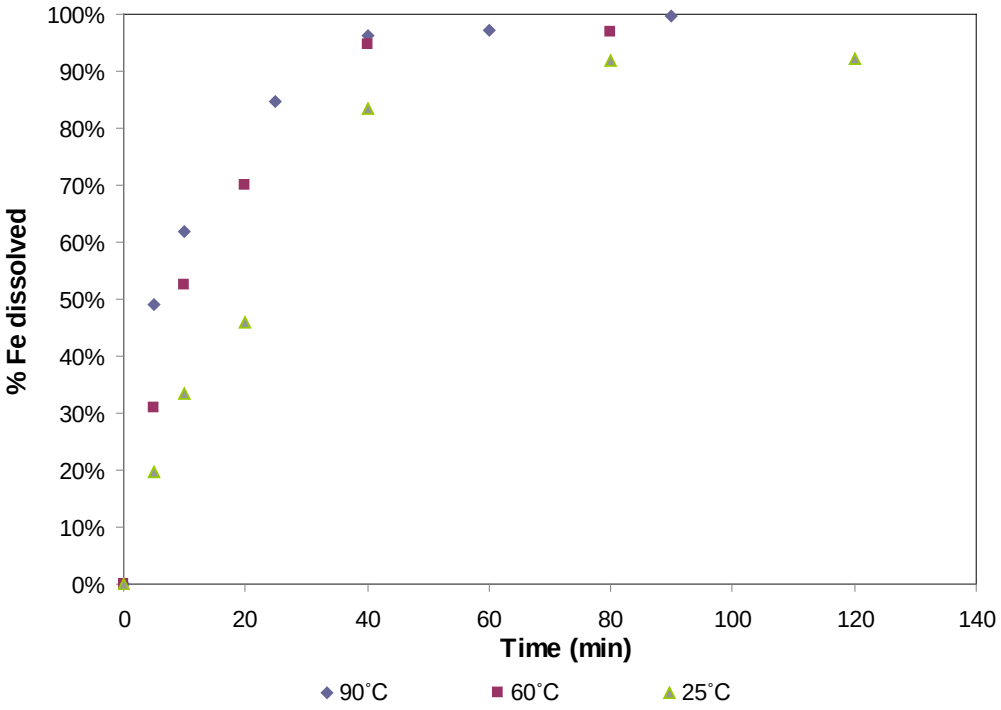


**Figure 6.3: Effect of temperature on iron dissolution**
(11 wt % HCl, $d_{50}$ = 185 µm, 100 r/min, 2.5 initial HCl/Fe mole ratio)

The results in Figure 6.3 show that iron dissolution increases with temperature. The temperature has a noticeable effect on the dissolution rate of iron below 60 °C, but to a lesser extent above 60 °C. This might be an indication that there is a change in the rate-limiting step somewhere between 25 °C and 90 °C (Fogler, 2006: 97).

### 6.3.2 – Effect of hydrochloric acid concentration

To study the effect of hydrochloric acid concentration, three dissolution experiments were conducted using 11, 18 and 25% (wt %) hydrochloric acid concentrations. The temperature (90 °C), time duration (90 minutes) and initial acid-to-iron mole ratio (2.5:1) were held constant. The results obtained are illustrated in Figure 6.4.

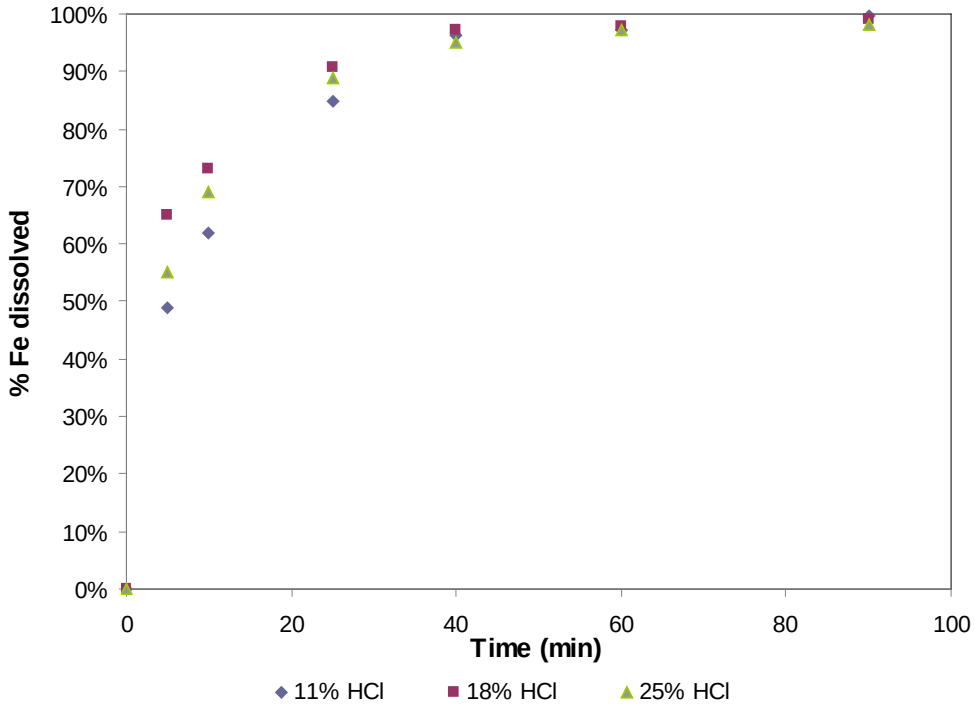


**Figure 6.4: Effect of acid concentration on iron dissolution (as % Fe dissolved)**
(90 ˚C, $d_{50}$ = 185 µm, 100 r/min, 2.5 initial HCl/Fe mole ratio)

From the results illustrated in Figure 6.4, it seems that the dissolution of iron is not strongly dependent on the hydrochloric acid concentration. Referring to Figure 6.4, after 25 minutes the conversions are all relatively close to each other. The dissolution seems to be virtually complete after 60 minutes, with a +96% conversion in hydrochloric acid at 90 °C.

The time required to obtain the same FeO dissolution in Reaction 6.1 is approximately 3-5 hours (Wang, Xue, Wang & Jiang, 2009: 840; Walpole & Winter, 2002: 7; Winter, 2008: 7–8). The residence time required for metallic iron dissolution is therefore significantly less than that required for partially reduced iron (i.e. iron as FeO).

Figure 6.5 illustrates the iron(II) load in solution for each hydrochloric acid concentration used. There is a significant difference in the iron (II) load for the different acid concentrations evaluated, but the dissolution profiles seem to correlate well.

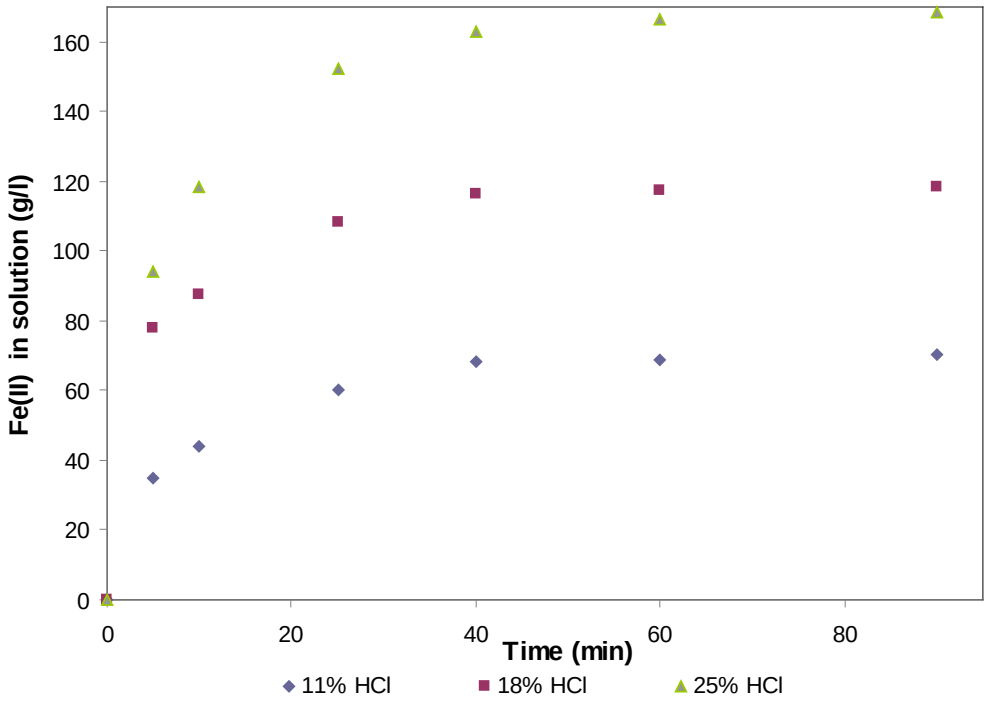


**Figure 6.5: Effect of acid concentration on iron dissolution (as g/l Fe(II) in solution)**
(90 ˚C, $d_{50}$ = 185 µm, 100 r/min, 2.5 initial HCl/Fe mole ratio)

### 6.3.3 – Analysis of rate data

The data obtained from the reaction between hydrochloric acid and metallic iron are analysed in this section to deduce a rate law. The objective of this analysis is to suggest a rate law that could be used as a starting point for future detailed kinetic studies.

The Shrinking-Core model can be used to describe the dissolution of a solid particle in a heterogeneous liquid-solid reaction (Seader & Henley, 2006: 639). The constant particle size variation of this model is applicable to the Fe(s)/HCl(l) system. This is due to the formation of a “shell” or “product layer” (Levenspiel, 1999: 569). This product layer consists of a unreacting species, which is mainly titanium nitride.

Five steps in a typical reaction are considered in the Shrinking-Core model. These are (Seader & Henley, 2006: 639):

1. Mass transfer of the hydrochloric acid from the bulk liquid to the outer surface of the nitrided ilmenite particle
2. Pore diffusion of hydrochloric acid through the leached shell or product layer
3. Chemical reaction at the interface between the leached shell and the unleached core

4. Pore diffusion of the reaction products ($FeCl_2$(aq) and $H_2$(g)) back through the leached shell
5. Mass transfer of the reaction products back into the bulk liquid surrounding the particle.

Any one or more of these steps can control the rate of the reaction. The following equations are used to describe (for spherical particles with unchanging size) the reaction in terms of each limiting step:

- Diffusion through the liquid film controls – Steps 1 and 5 combined, (Levenspiel, 1999: 571–573):

$$f(X_{Fe}) = X_{Fe}$$

$$\text{and } f(X_{Fe}) = k_{1,5} \cdot t \qquad \text{Equation 6.1}$$

$$\text{with } k_{1,5} = \frac{3 \cdot b \cdot k_g \cdot C_{HCl,bulk}}{\rho_{Fe} \cdot R_0}$$

*where*

$k_{1,5}$ = apparent rate constant ($\text{min}^{-1}$)
t = time (min)
b = stoichiometric coefficient for Fe = 0.5
(when stoichiometric coefficient for HCl = 1)
$k_g$ = mass transfer coefficient between liquid and particle ($\text{m} \cdot \text{min}^{-1}$)
$C_{HCl,bulk}$ = *HCl* concentration in the bulk liquid ($\text{mol} \cdot \text{m}^3$)
$\rho_{Fe}$ = *molar density* of Fe in the solid ($\text{mol Fe} \cdot \text{m}^3 \text{ solid}^{-1}$)
$R_0$ = radius of the particle with unchanging size (m)

- Diffusion through the product layer controls – Steps 2 and 4 combined (Levenspiel, 1999: 573–575):

$$f(X_{Fe}) = 1 - 3 \cdot (1 - X_{Fe})^{2/3} + 2 \cdot (1 - X_{Fe})$$

Equation 6.2

$$\text{and } f(X_{Fe}) = k_{2,4} \cdot t$$

$$with\ k_{2,4} = \frac{6 \cdot b \cdot D_e \cdot C_{HCl,bulk}}{\rho_{Fe} \cdot R_0{}^2}$$

*where*

$k_{2,4}$ = apparent rate constant ($\text{min}^{-1}$)

$D_e$ = the effective diffusion coefficient of HCl in product layer ($\text{m}^3 \cdot m\ solid^{-1} \cdot \text{min}^{-1}$)

- Chemical reaction controls – Step 3, (Levenspiel, 1999: 575–576):

$$f(X_{Fe}) = 1 - (1 - X_{Fe})^{1/3}$$

$$and\ f(X_{Fe}) = k_3 \cdot t \qquad \text{Equation 6.3}$$

$$with\ k_3 = \frac{b \cdot k'' \cdot C_{HCl,bulk}}{\rho_{Fe} \cdot R_0}$$

*where*

$k_3$ = apparent rate constant ($\text{min}^{-1}$)

$k''$ = first - order rate constant for the surface reaction ($\text{m} \cdot \text{min}^{-1}$)

Equation 6.2 is valid for a liquid-solid system only if the rate at which the reaction interface (between the unreacted core and the product layer) moves is small with respect to the diffusion rate of hydrochloric acid through the product layer. In other words, it is assumed that no hydrochloric acid will accumulate in the product layer as the thickness of that layer increases. This is referred to as the “pseudo-steady-state approximation” (Seader & Henley, 2006: 640). This assumption enables the formulation of the model as an ordinary differential equation rather than as a partial differential equation (Liddell, 2005: 63). The pseudo-steady-state approximation is assumed valid for the Fe(s)/HCl(l) system.

The experimental data (illustrated in Figure 6.3) were plotted for each model described by Equations 6.1 to 6.3. The time limit in these graphs was taken as 40 minutes, because at that stage the reaction was to all intents and purposes complete, with an iron conversion of at least 95%. The apparent rate constants (slope of graphs) with their correlation coefficient values ($R^2$) obtained from the resulting graphs are summarised in Table 6.2.

**Table 6.2: Apparent rate constants and correlation coefficients for three rate-controlling models at different temperatures**

| | Apparent rate constant ($min^{-1}$) | | | Correlation coefficient ($R^2$) | | |
|---|---|---|---|---|---|---|
| **Temperature** | **$k_3$** | **$k_{2,4}$** | **$k_{1,5}$** | **$k_3$** | **$k_{2,4}$** | **$k_{1,5}$** |
| 25 ˚C | 0.0110 | 0.0091 | 0.0221 | 0.985 | 0.878 | 0.940 |
| 60 ˚C | 0.0162 | 0.0160 | 0.0276 | 0.978 | 0.970 | 0.740 |
| 90 ˚C | 0.0179 | 0.0184 | 0.0290 | 0.908 | 0.999 | 0.504 |

The results in Table 6.2 indicate that both the diffusion through the product layer and the reaction control limiting models fit the experimental data in different temperature regions.

The Arrhenius plot for both these models is illustrated in Figure 6.6.

The correlation coefficients in Table 6.2 indicate that reaction control is dominant at lower temperatures and diffusion control through the product layer at higher temperatures. The data with the highest correlation coefficients is emphasized on Figure 6.6 to illustrate the change in the rate-limiting step.

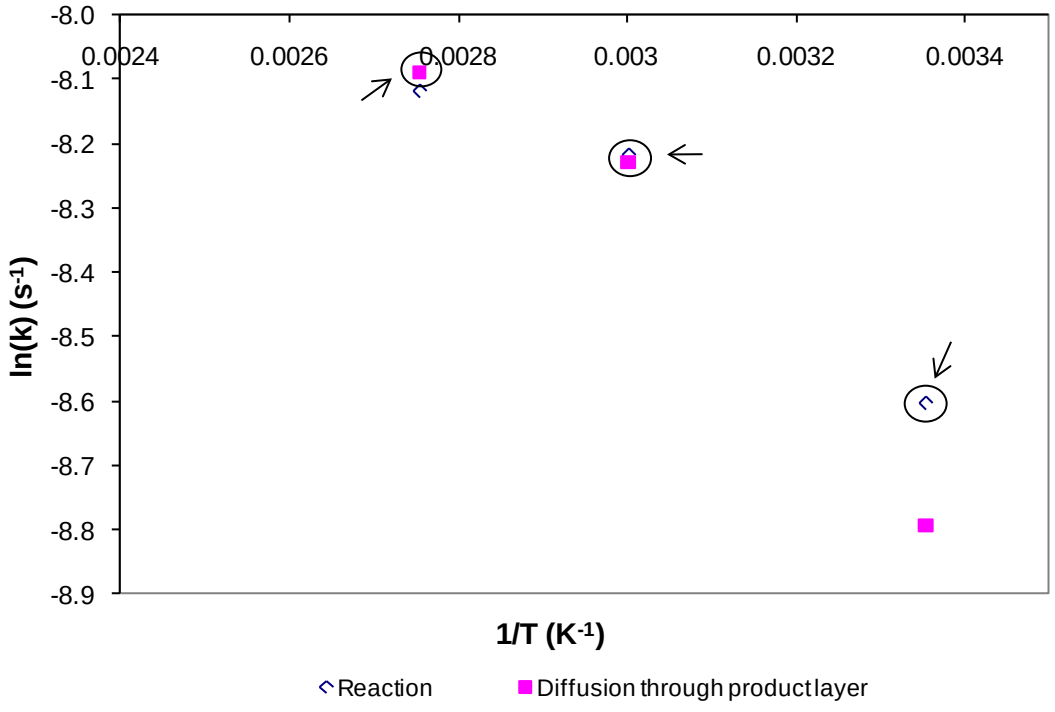


**Figure 6.6: Arrhenius plot of apparent rate constant ($s^{-1}$) against reciprocal of temperature for two different controlling steps**
(11 wt % HCl, $d_{50}$ = 185 µm, 100 r/min, 2.5 initial HCl/Fe mole ratio)

Levenspiel (1999: 31) stated that a shift in the observed activation energy (slope of Arrhenius plot) indicates a shift in the controlling mechanism of reaction. Levenspiel (1999:

31) also stated that if the observed activation energy increased for a decrease in temperature, this is an indication of reaction steps taking place in series with each other. The results illustrated in Figure 6.6, together with the correlation coefficients summarised in Table 6.2, therefore suggest that there is a shift in the dominant rate-controlling step and also that these steps occur in series with each other.

In order to analyse this reaction accurately, many more data points are required on the Arrhenius plot to describe the two different rate-limiting regimes. Keep in mind that each data point on the Arrhenius plot is the result of at least three experimental runs. The amount of experimental work still required is therefore substantial. However, the objective for this dissertation's rate data analysis section is not to conduct a detailed kinetic study but to serve as a starting point for a future detailed kinetic study. The data obtained from this study was still used to derive a simplified model that can be used for initial leach tank sizing. This simplified model is therefore not academically correct, but rather a "down and dirty" way to describe the experimental results.

To account for the combined effect of different rate-limiting steps in series, assume a first-order reaction with respect to the hydrochloric acid concentration in the bulk solution. The following equation can then be used to account for the disappearance of hydrochloric acid at any particular stage of conversion (Levenspiel, 1999: 581):

$$-r''_{HCl} = \frac{-1}{S_{ex}} \cdot \frac{dN_{HCl}}{dt} = \bar{k}''_{combined} \cdot C_{HCl,bulk} \qquad \text{Equation 6.4}$$

where

$-r''_{HCl}$ $= \dfrac{moles\ HCl\ \text{consumed}}{(\text{unit surface of solid}) \cdot (\text{time})}$, $(\text{mol} \cdot \text{m}^{-2} \cdot \text{min}^{-1})$

$S_{ex}$ $= unchanging\ external\ \text{surface area of particle}, (\text{m}^2)$

$N_{HCl}$ $= mole\ HCl\ \text{in solution (mol)}$

$\bar{k}''_{combined}$ $=$ average *combined* - resistance rate constant $(\text{m} \cdot \text{min}^{-1})$

The combined-resistance rate constant is obtained from the approximation that the time required for complete conversion ($\tau_{total}$) is equal to the sum of all the times needed if each resistance acted alone (Levenspiel, 1999: 579). This is illustrated in Equation 6.5.

$$\tau_{total} = \tau_{iquid\ film} + \tau_{Pr\,oduct\ layer} + \tau_{reaction} \qquad \text{Equation 6.5}$$

The time for complete conversion can be related to the rate constant for each rate-limiting step by the following equation (Levenspiel, 1999: 571–576):

$$\tau_i = \frac{1}{k_i''} \qquad \text{Equation 6.6}$$

with

$$i = \text{liquid film; product layer; reaction}$$

The combined-resistance rate constant can then be obtained by substituting Equation 6.5 with the relation written in Equation 6.6. The resulting equation is given in Equation 6.7:

$$k''_{combined} = \frac{1}{\frac{1}{k''_{1,5}} + \frac{1}{k''_{3}} + \frac{1}{k''_{2,4}}} \qquad \text{Equation 6.7}$$

Levenspiel (1999: 581) found that the relative roles of each resistance can, on average, be related for the whole progression from fresh to completely converted particle by the average combined-resistance rate coefficient ($\bar{k}''_{combined}$) given in Equation 6.8:

$$\bar{k}''_{combined} = \frac{1}{\frac{1}{k_g} + \frac{R_0}{2 \cdot D_e} + \frac{3}{k''}} \qquad \text{Equation 6.8}$$

Using the integral method of rate data analysis (Fogler, 2006: 267) and assuming a batch system with negligible reaction volume loss (i.e. the $H_2$(g) produced has a negligible effect on the reaction volume), Equation 6.4 can be rewritten as an equation with two terms: one is a function of mol Fe not yet reacted ($f(N_{Fe})$) and the other of the product between a constant and reaction time. This equation is given by Equation 6.9 and its derivation is reported in Appendix A6.2.

$$f(N_{Fe}) = -\ln\left(1 - \frac{N_{HCL,0} - N_{Fe}/b}{N_{HCL,0}}\right)$$

$$and \quad f(N_{Fe}) = \alpha \cdot t \qquad \text{Equation 6.9}$$

$$with\ \alpha = \frac{S_{ex} \cdot \bar{k}''_{combined}}{V_0} \qquad \text{Equation 6.10}$$

*where*

$V_0 = \text{Initial reaction volume } (m^3)$

A plot of $f(N_{Fe})$ against time gives a linear graph through the origin with a slope ($\alpha$) given by Equation 6.10. This equation can be rewritten (into Equation 6.11) and used to calculate the average combined-resistance rate coefficient ($\bar{k}''_{combined}$) for each rate data set.

$$\bar{k}''_{combined} = \frac{V_0 \cdot \alpha}{S_{ex}} = \frac{V_0 \cdot \alpha}{4 \cdot \pi \cdot R_0^{\,2}} \qquad \text{Equation 6.11}$$

Figure 6.7 is the graph obtained after the rate data from Figure 6.3 had been substituted into Equation 6.9. The numerical results used to compile this graph are summarised in Appendix 7.

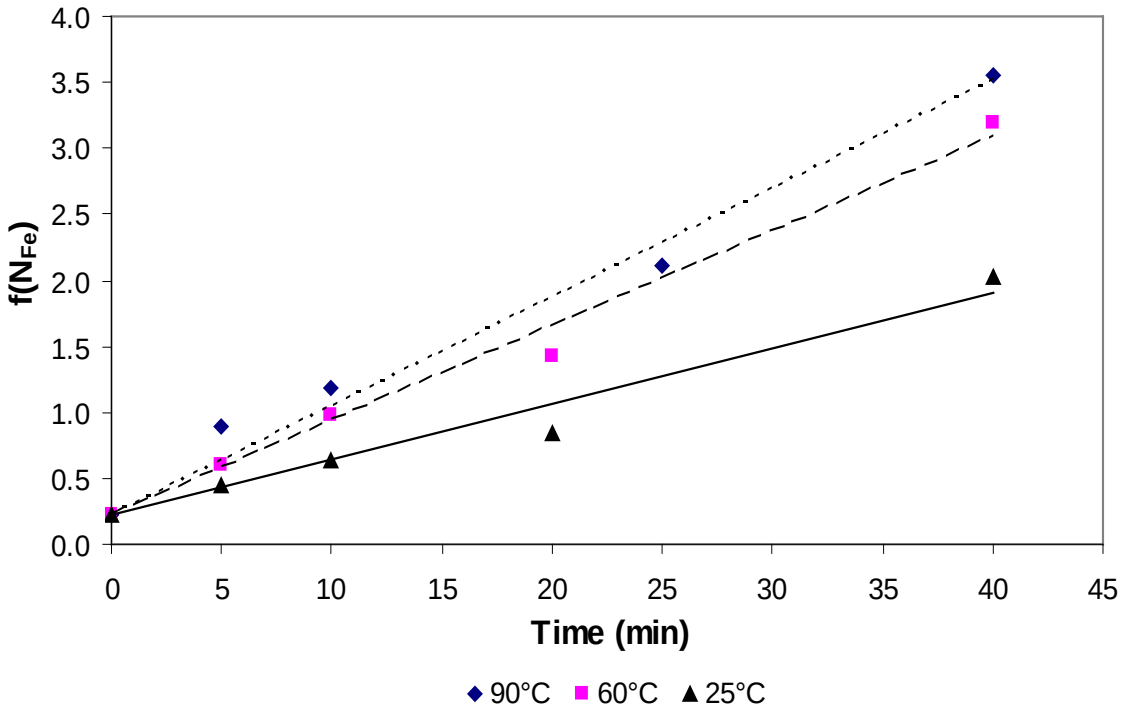


**Figure 6.7: $f(N_{Fe})$ vs. time for 11 wt % HCl at three different temperatures**

($d_{50}$ = 185 µm, 100 r/min, 2.5 initial HCl/Fe mole ratio)

It is important to note that the y-axis intercept for the graphs in Figure 6.7 does not start at the origin of the plot. The reason for this is the 20% excess hydrochloric acid ($N_{HCL,0}$) present in the reaction solution. The y-axis intercept will be equal to zero if the hydrochloric acid is supplied in stoichiometric ratio with iron. Refer to function $f(N_{Fe})$ in Equation 6.9 to evaluate this remark.

Table 6.3 summarises important parameters and the resulting $\bar{k}''_{combined}$ value obtained for each leach profile.

**Table 6.3: Important parameters for the combined-resistance rate law**

| Temperature | Correlation coefficient ($R^2$) | Slope ($\alpha$, $min^{-1}$) | Av. combined-resistance rate coeff. ($\bar{k}''_{combined}$, $m.s^{-1}$) |
|---|---|---|---|
| 25 ˚C | 0.967 | 0.0422 | 0.654 |
| 60 ˚C | 0.988 | 0.0717 | 1.111 |
| 90 ˚C | 0.982 | 0.0822 | 1.274 |

The correlation coefficient values ($R^2$) summarised in Table 6.3 indicate that the first-order rate assumption (Equation 6.4) used to derive Equation 6.9 is valid. The average combined-resistance rate coefficient values ($\overline{k}''_{combined}$) summarised in Table 6.3 were then used to construct the Arrhenius plot for this model. This plot is illustrated in Figure 6.8.

It is important to note that the change between different rate-controlling steps is still visible in Figure 6.8 (i.e. different slopes between points). Due to the limited data available, it is not possible to describe each regime accurately. It was therefore assumed that the reaction could be sufficiently described with a linear equation forced through all three data points. This assumption was necessary in order to estimate the averaged observed activation energy and pre-exponential factors with the available data. The resulting reaction model that uses these "averaged" constants will not give the correct answer, but will give an estimated prediction. Even though this model is not academically correct, it is assumed sufficient for initial leach tank sizing if it can estimate good conversions.

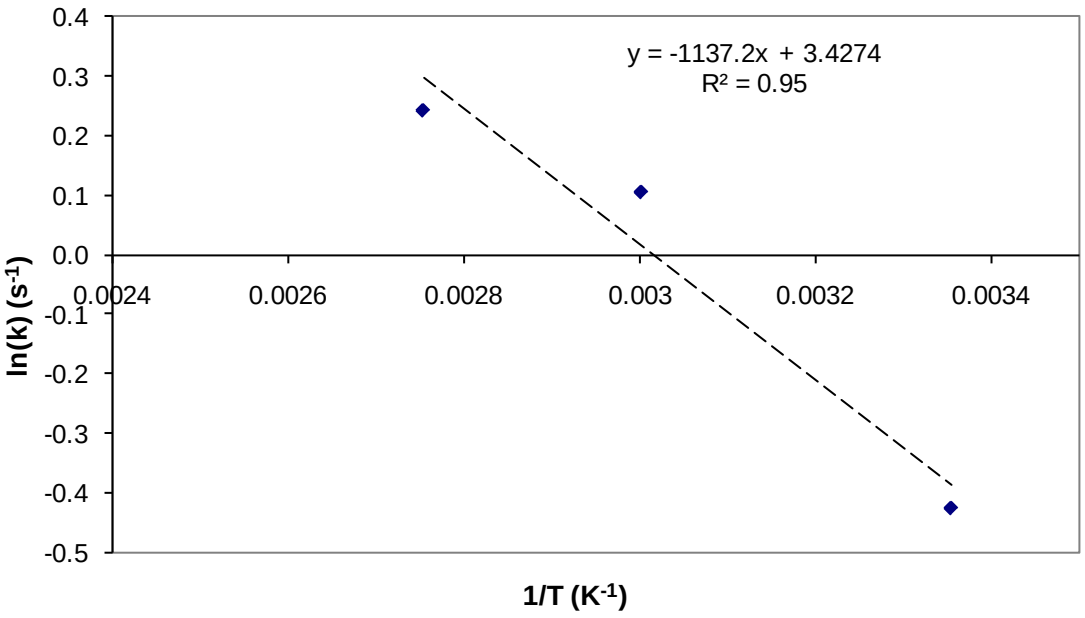


**Figure 6.8: Arrhenius plot of average combined-resistance rate constant against reciprocal of temperature**
(11 wt % HCl, $d_{50}$ = 185 µm, 100 r/min, 2.5 initial HCl/Fe mole ratio)

The equation giving the best fit of the data ($R^2$ equal to 0.95) in Figure 6.8 was then used to calculate the constants in the Arrhenius equation. The observed activation energy (slope of plot multiplied by the gas constant) and the pre-exponential factor (antilog of y-intercept) were found to be equal to 9.45 kJ.mol$^{-1}$ and 30.8 s$^{-1}$ respectively (Fogler, 2006: 95–97). A

low value for the activation energy was suspected in Section 6.3.1 due to the limited effect that temperature had on the rate of dissolution. The calculated value of 9.45 kJ.mol$^{-1}$ confirms the suspicion. The Arrhenius equation for this model can therefore be written as:

$$\bar{k}''_{combined}(T) = A \cdot \exp\left(\frac{-E}{R \cdot T}\right) = 30.8 \cdot \exp\left(\frac{-1137.2}{T}\right) \qquad \text{Equation 6.12}$$

with T in kelvin and $\bar{k}''_{combined}$ in $m \cdot sec^{-1}$

Equation 6.12 can then be used to rewrite Equation 6.4 and Equation 6.9 to include the effect of temperature on the rate of iron dissolution. The rewritten form of Equation 6.9 is given below as Equation 6.13. This equation is manipulated to give the expected iron conversion as the answer, but as a function of temperature, time, radius of particle and reaction volume. The derivation of Equation 6.13 is given in Appendix A6.3.

$$X_{Fe} = 1 - \frac{N_{HCL,0} \cdot b}{N_{Fe,0}} \cdot \exp(\beta \cdot \phi) \qquad \text{Equation 6.13}$$

$$\text{with } \beta = \frac{-23222.6 \cdot R_0^{\,2} \cdot t}{V} \qquad (t, \text{minutes})$$

$$\phi = \exp\left(\frac{-1137.2}{T}\right) \qquad (T, \text{Kelvin})$$

A limitation of Equation 6.13 is that it is only valid when the hydrochloric acid is supplied stoichiometrically to iron. With excess hydrochloric acid, Equation 6.13 results in a negative iron conversion at the start of the leach. This results in Equation 6.13 being effectively independent of the concentrations of both these species. This is a serious limitation for the model, but is not considered terminal as the hydrochloric acid concentration does not have a significant effect on the rate of metallic iron dissolution (Figure 6.4).

The iron conversion ($X_{Fe}$) predicted by Equation 6.13 was compared with the rate data given in Figures 6.3 and 6.4. The results are illustrated in Figures 6.9 and 6.10 and the numerical results are summarised in Appendix 7.

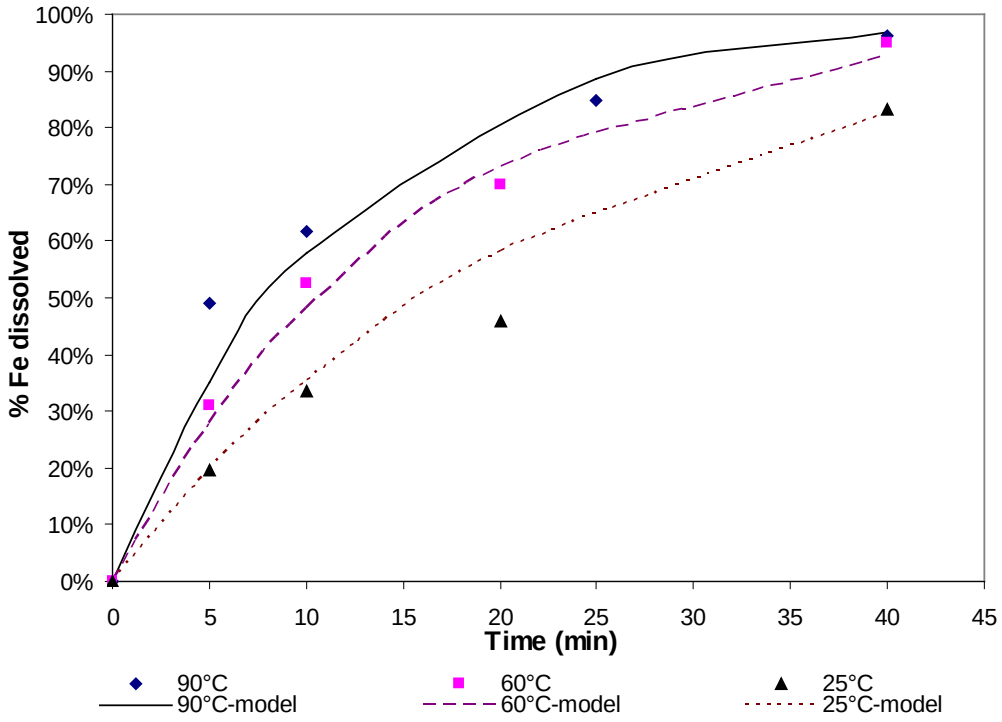


**Figure 6.9: Model fit for predicted iron conversion as a function of time**
(11 wt % HCl, $d_{50}$ = 185 µm, 100 r/min, 2.5 initial HCl/Fe mole ratio)

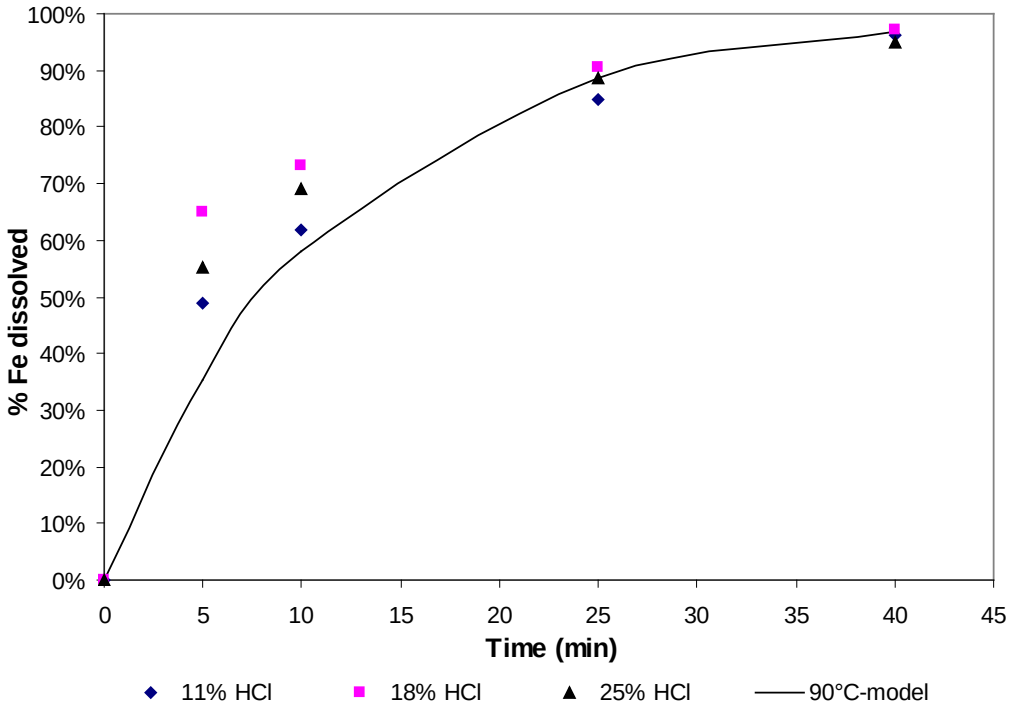


**Figure 6.10: Model fit for predicted iron conversion as a function of acid concentration**
(90 °C, d50 = 185 µm, 100 r/min, 2.5 initial HCl/Fe mole ratio)

Equation 6.13 gives a good fit for the results illustrated in Figure 6.9. The iron conversion for the first 10 minutes in Figure 6.10 was, however, underpredicted, but the conversion for 25 minutes and later was more accurate. It should be noted that the predicted conversion at 40 minutes compared well with the actual conversion for all levels of hydrochloric acid concentrations and temperatures.

The underprediction for the first 10 minutes in Figure 6.10 could possibly be attributed to the range of particle sizes available during the reaction. The particles used in this experimental campaign had a mass mean diameter of 185 µm and therefore consist of both small and large particles. Equation 6.13 is a function of the square of the particle radius and therefore has a large influence on the predicted iron conversion. The applicability of Equation 6.13 could be verified in future work in which particle size would be a manipulated variable.

It was mentioned in the Section 6.3.3 that the objective of the rate data analysis in this study is for it to serve as a starting point for future detailed kinetic studies. The model derived in this section (Equation 6.13) is, however, sufficient for initial sizing of a leach tank.

### 6.3.4 – Dissolution of other species

Unrecoverable acid consumption in a typical hydrochloric acid leach plant can be attributed mostly to the dissolution of calcium oxide (Winter, 2008). The optimum conditions for hydrochloric acid to be viable as a lixiviant for nitrided ilmenite would be if it could dissolve most of the iron but without excessive dissolution of other species, especially TiN (product) and CaO (unrecoverable acid consumption). It is therefore necessary to evaluate the dissolution of other species, such as Al, Ca, Ti and Mg, in hydrochloric acid.

The nitrided ilmenite sample and the experimental set-up with the procedure described in Sections 6.2.1 and 6.2.3.1 respectively was used to evaluate the dissolution of other species in hydrochloric acid. The results illustrated in Figure 6.4 indicate that the dissolution of metallic iron can reach levels of at least 96% after 60 minutes in 90 °C hydrochloric acid. A leach duration of 60 minutes is therefore assumed to be sufficient to evaluate the dissolution of other constituents in hydrochloric acid.

The variables investigated during this study are listed in Table 6.4.

**Table 6.4: Variables investigated during the study of the dissolution of other species**

| Variable | Conditions |
|---|---|
| Hydrochloric acid concentration (wt %) | 11%; 18%; 25% |
| Initial $N_{HCl}/N_{Fe}$ mole ratio (mol/mol) | 2.0:1; 2.5:1; 3.3:1 |
| Initial solid-to-liquid mass ratio (g/g) | 0.12 to 0.47 |

The washed and dried solids obtained from each experiment were sent for chemical analysis (ICP-OES) and the leach liquor for analysis (ICP-AES) to determine the total Ti, Ca, Mg and Al species in solution.

### 6.3.4.1 – Effect of HCl concentration on dissolution of other species

Figure 6.11 illustrates the effect of hydrochloric acid concentration on the dissolution of Al, Ti, Ca and Mg. An increase in hydrochloric acid concentration results in an increase in Al and Ti dissolution but a decrease in the dissolution of Ca and Mg. The increase in Ti dissolution with an increase in acid concentration agrees with the findings of El-Hazek, Lasheen, El-Sheikh & Zaki (2007: 46) and Wang *et al.* (2009: 837).

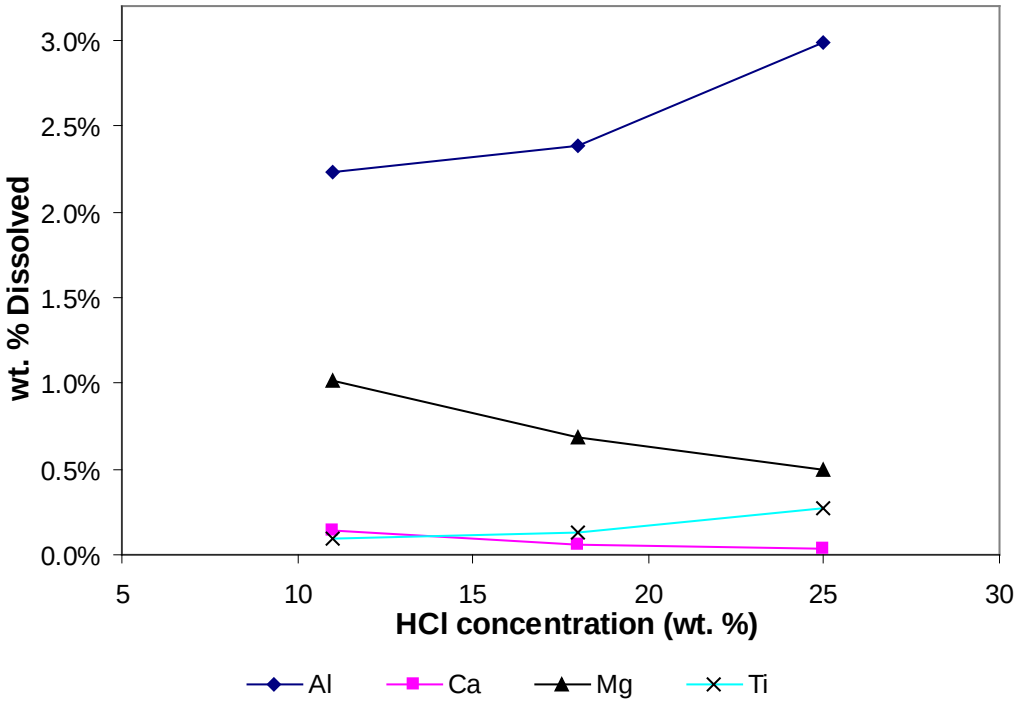


**Figure 6.11: Effect of hydrochloric acid concentration on dissolution**

(90 ˚C, $d_{50}$ = 185 µm, 100 r/min, 2.5 mol HCl/mol Fe)

The dissolution of components illustrated in Figure 6.11 is relatively low. These components will therefore still be present in the upgraded nitrided ilmenite. This is acceptable for the low-temperature chlorination process as these species will not react with $Cl_2$ (as discussed in Section 1.1). The dissolution of these species (excluding Ti), and other impurities, is almost complete in existing FeO-leach practices (Walpole & Winter, 2002: 8; Winter, 2008: 5).

### 6.3.4.2 – Effect of initial HCl/Fe mole ratio on dissolution of other species

Table 6.5 summarises the results obtained from the evaluation of different hydrochloric acid-to-iron mole ratios on the dissolution of Al, Ti, Ca and Mg in 25 wt % hydrochloric acid. The wt % dissolved is based on the results of the leach liquor analysis.

**Table 6.5: Effect of initial HCl/Fe mole ratios on dissolution in 25% HCl**

| **Excess acid** (mol %) | | **0** | **20** | **40** |
|---|---|---|---|---|
| **$N_{HCl}$/ $N_{Fe}$** (mol/mol) | | **2.0** | **2.5** | **3.3** |
| wt % dissolved | Al | 2.14 | 2.99 | 3.57 |
| | Ca | 0.01 | 0.03 | 0.05 |
| | Mg | 0.17 | 0.49 | 0.84 |
| | Ti | 0.11 | 0.27 | 0.44 |

The tendency for Ti dissolution to increase with an increase in the acid-to-iron mole ratio, as reported in Table 6.5, is similar to findings from previous work (Van Dyk, Vegter & Pistorius, 2002: 32; Mahmoud, *et al.*, 2004: 105–106; El-Hazek *et al.*, 2007: 46). The extent of Ti dissolution is, however, significantly lower due to the high acid-to-ilmenite ratios evaluated in these previous works. For example, after 8 hours in a 105 ˚C 6M hydrochloric acid solution, Van Dyk *et al.* (2002: 34) found that 45% Ti had dissolved in a 60:1 acid-to-ilmenite ratio, and approximately 5% in a 4:1 acid-to-ilmenite ratio.

The dissolution of all species given in Table 6.5 increased significantly with an increase in the acid-to-iron mole ratio. The dissolution of Al increased by 67% when the acid-to-iron ratio was increased from the stoichiometric level of 2:1 to 3.3:1. The dissolution of Ti, Ca and Mg increased significantly more, by at least four times. The dissolution of these species is therefore dependent on the quantity of excess acid available for reaction. The optimum mole ratio of acid-to-iron would be at levels equal to or very close to the stoichiometric ratio.

### 6.3.4.3 – Effect of solid-to-liquid mass ratio on dissolution of other species

Figures 6.12 and 6.13 illustrate the effect of solid-to-liquid mass ratio on the dissolution of Ca and Ti respectively. Magnesium presents the same dissolution profile as illustrated in Figure 6.12, and Al the same dissolution profile as illustrated in Figure 6.13.

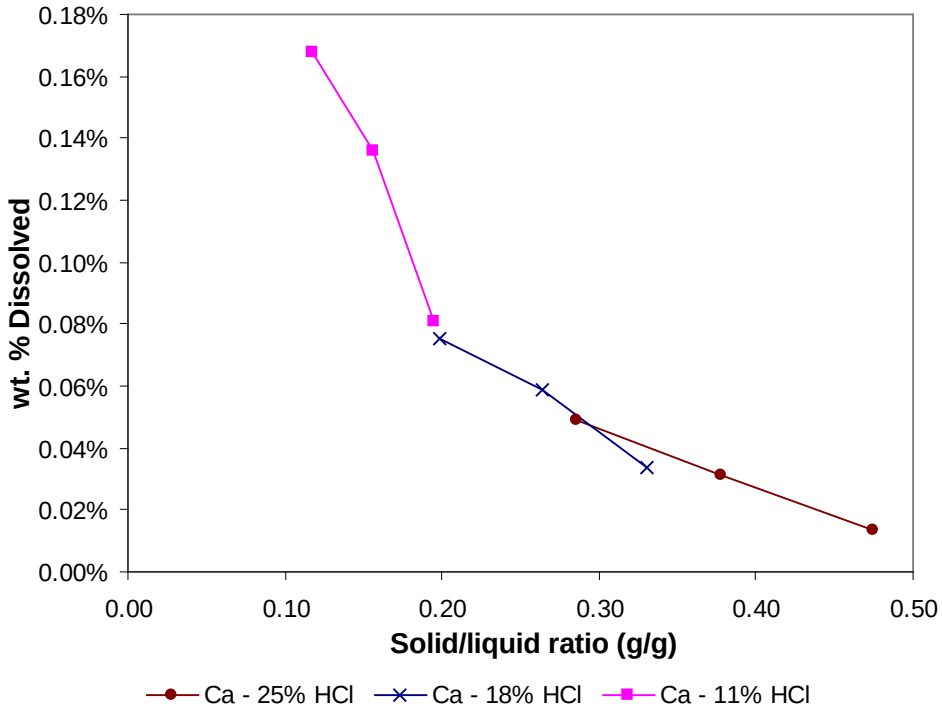


**Figure 6.12: Effect of solid/liquid mass ratio on calcium dissolution**

(90 ˚C, $d_{50}$ = 185 µm, 100 r/min)

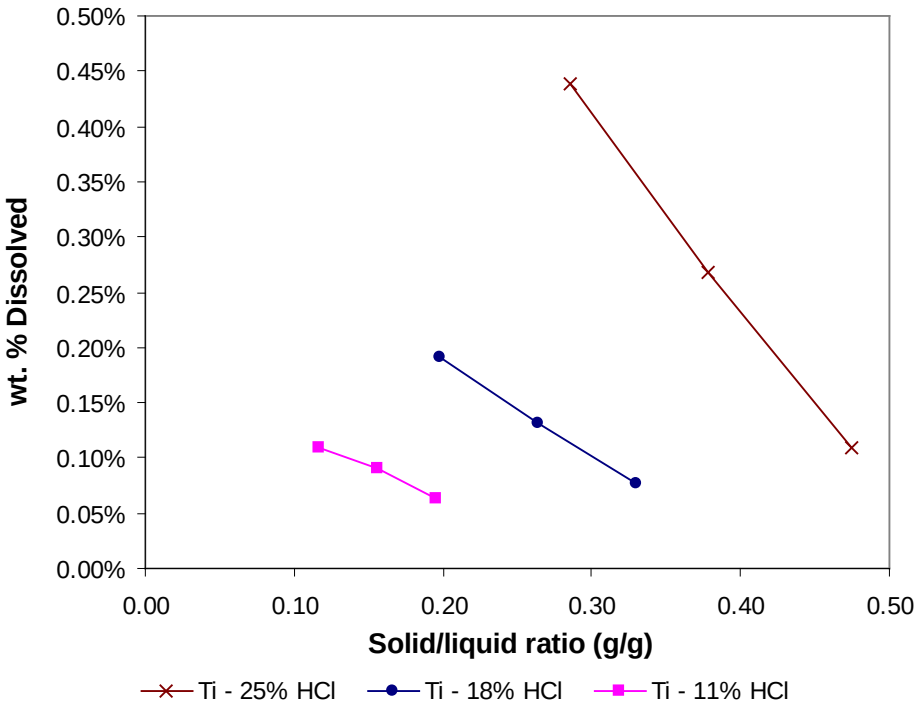


**Figure 6.13: Effect of solid/liquid mass ratio on titanium dissolution**

(90 ˚C, $d_{50}$ = 185 µm, 100 r/min)

The results illustrated in Figure 6.12 indicate that the dissolution of Ca (and Mg) is significantly more favourable at lower solid/liquid mass ratios than at higher ratios. This suggests that the dissolution of Ca and Mg is dependent on the solid/liquid mass ratio of the reaction solution.

The dissolution of Ti and Al seems not to be strongly dependent on the solid/liquid mass ratio in Figure 6.13. The results do, however, suggest that the acid-to-iron mole ratio has a dominant effect on the dissolution of Ti and Al.

#### 6.3.4.4 – Optimum HCl leach conditions regarding dissolution of other species

Further evaluation of the findings indicates that a 25 wt % HCl acid with an initial acid-to-iron mole ratio close to 2:1 at 90 °C would produce a favourable upgraded nitrided ilmenite product.

The normalised composition of a nitrided ilmenite sample leached with 25 wt % HCl acid for 60 minutes (at ca 90 °C) is given in Table 6.6 for an acid-to-Fe mole ratio of 2:1.

**Table 6.6: Composition of leached nitrided ilmenite**

| Component | Mass % |
|---|---|
| $SiO_2$ | 6.06 |
| $Al_2O_3$ | 3.56 |
| Fe(metal) | 2.15 |
| $TiO_2$ | 10.00 |
| TiN | 69.90 |
| CaO | 0.12 |
| MgO | 1.29 |
| $K_2O$ | 0.07 |
| MnO | 1.10 |
| $P_2O_5$ | 0.03 |
| $V_2O_5$ | 0.56 |
| C(total) | 5.16 |
| S(total) | 0.27 |

The limited dissolution of CaO, as illustrated in Table 6.6, will lead to reduced acid consumption compared with that of FeO leach units where most of the CaO is dissolved (Walpole & Winter, 2002).

## 6.4 – Conclusions

The results obtained in this chapter indicate that hydrochloric acid can be successfully used as lixiviant to remove iron from nitrided ilmenite.

The following is a summary of the findings of this study:

- Temperature has a relatively small effect on the rate of metallic iron dissolution (i.e. low observed activation energy).
- Hydrochloric acid concentration does not have a significant effect on the rate of metallic iron dissolution (Figure 6.4).
- Metallic iron dissolution from nitrided ilmenite reached levels of at least 96% after 60 minutes in 90 °C HCl acid. This is applicable to all hydrochloric acid concentrations (11, 18 and 25%) evaluated in this study. An average combined-resistance rate law (Equation 6.13) can be used to estimate the dissolution of metallic iron in nitrided ilmenite in a hydrochloric acid solution.
- The average observed activation energy and Arrhenius pre-exponential factor were found to be equal to 9.45 $kJ.mol^{-1}$ and 30.8 $s^{-1}$ respectively.

- An increase in hydrochloric acid concentration results in an increase in titanium and aluminium dissolution, but a decrease in calcium and magnesium dissolution.
- The dissolution of all four species (Al, Ca, Mg and Ti) increased with an increase in excess acid available for reaction (or acid-to-iron mole ratio). This had the largest effect on the dissolution of aluminium and titanium.
- The dissolution of calcium and magnesium reduced with an increase in the solid/liquid mass ratio of the reaction solution, but the dissolution of aluminium and titanium was independent of the solid/liquid mass ratio. The solid/liquid ratio of the reaction solution had the largest effect on the dissolution of calcium and magnesium.

# CHAPTER 7 – PROPOSED PROCESS TO REMOVE IRON FROM NITRIDED ILMENITE

## 7.1 – Overview

Chapter 5 concluded that hydrochloric acid leaching of nitrided ilmenite in combination with the Enhanced Acid Regeneration System (EARS) and Direct Reduced Iron (DRI) process units, both developed by Austpac Resources N.L., would result in an effective process for the removal of iron from nitrided ilmenite. It was, however, necessary to evaluate whether hydrochloric acid can be used as lixiviant to remove iron from nitrided ilmenite without excessive dissolution of titanium nitride. The experimental work reported in Chapter 6 found that hydrochloric acid leaching was both a viable and an efficient method of removing iron from nitrided ilmenite.

The outcome of this chapter is a proposed process for removing iron from nitrided ilmenite. This proposed process is developed by combining the results of the experimental work (Chapter 6) with existing process technology (Chapter 5).

A brief process description, with the resulting process flow diagram for the proposed process, is given in Section 7.2. Section 7.3 discusses the results obtained from modelling the proposed process. Finally, Section 7.4 gives conclusions and recommendations for the proposed process.

## 7.2 – Process description of proposed process

Hydrochloric acid leaching as used in the Austpac ERMS SR process was found in Chapters 4 and 5 to be a viable process route for removing iron from nitrided ilmenite. The process proposed here for the removal of iron from nitrided ilmenite is therefore based on the Austpac ERMS SR process, even to the extent that two process units in the Austpac ERMS SR process are used in the proposed process, namely the EARS and DRI process units. Only an additional hydrogen off-gas burner and a small modification to the fluid bed evaporator are required in the EARS process unit.

It was, however, found that a different leach train is required from that used in the Austpac ERMS SR process if nitrided ilmenite is used as feed material. The remaining process flow in the leach unit, as described in Section 5.2.2, stays the same.

The reader is therefore referred to Section 5.2 for a description of these process units to prevent repetition. Only the modifications to the EARS process unit will be described in this section.

The process flow diagram for the proposed process is illustrated in Figure 7.1.

### 7.2.1 – The leach unit

Nitrided ilmenite is used as feed material in the leach train. Table 7.1 summarises the normalised composition of the nitrided ilmenite. Refer to Chapter 3 for a detailed characterisation of the nitrided ilmenite.

The optimum leach train design still needs to be determined, but the basic idea is to use a continuous stirred-tank reactor (CSTR) fitted with a hydrogen-extraction fan (U11-KB01). A one-hour residence time is required for complete iron dissolution in a 25 wt % hydrochloric acid solution at 90 ˚C with 10% excess acid available for reaction.

The leachate solution obtained from the leach train is further treated by the same process route as described in Section 5.2.2. Refer to that section for a description.

### 7.2.2 – The EARS process

An extra hydrogen off-gas burner (U12-FM02) is the only addition to the EARS process unit.

The hydrogen gas produced in the leach train (U11-RC01) is extracted with a blower fan (U12-KB01) and fed to a hydrogen off-gas burner (U12-FM02). The hydrogen gas is burned in air to produce water vapour. The off-gas produced by the hydrogen off-gas burner is sent to the fluid bed evaporator (U12-SM01) where any hydrochloric acid (produced in the leach train) and water vapour are recovered. This prevents hydrochloric acid or water inventory losses from the process.

The heat produced by the combustion reaction is used as an extra heat source to reduce energy requirements in the fluid bed evaporator.

The remaining EARS process stays the same as described in Section 5.2.3. The reader is referred to that section for a description.

### 7.2.3 – The DRI process

This unit stays precisely the same as described in Section 5.2.4. Refer to that section for a description.

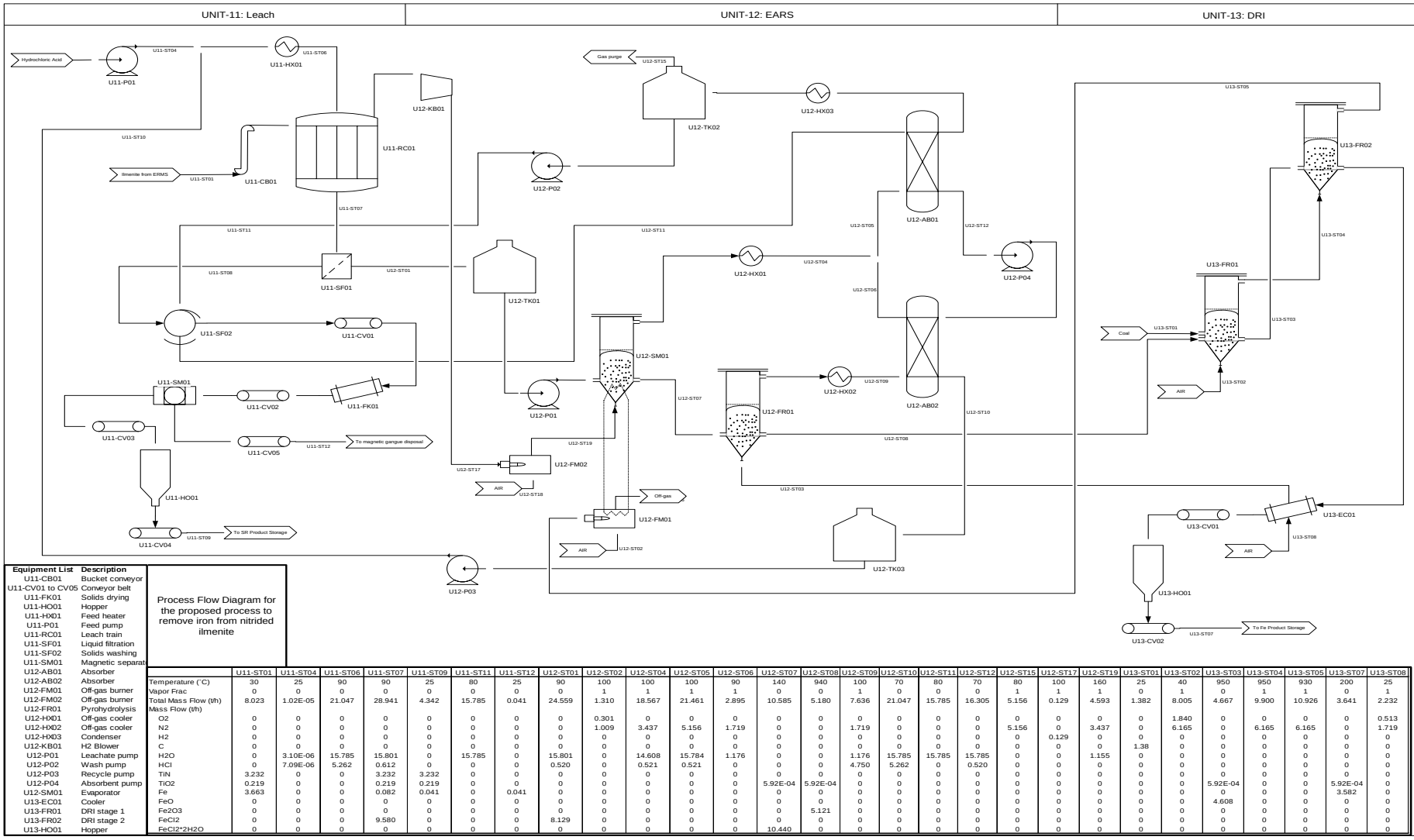


| Equipment List | Description |
|---|---|
| U11-CB01 | Bucket conveyor |
| U11-CV01 to CV05 | Conveyor belt |
| U11-FK01 | Solids drying |
| U11-HO01 | Hopper |
| U11-HX01 | Feed heater |
| U11-P01 | Feed pump |
| U11-RC01 | Leach train |
| U11-SF01 | Liquid filtration |
| U11-SF02 | Solids washing |
| U11-SM01 | Magnetic separat |
| U12-AB01 | Absorber |
| U12-AB02 | Absorber |
| U12-FM01 | Off-gas burner |
| U12-FM02 | Off-gas burner |
| U12-FR01 | Pyrohydrolysis |
| U12-HX01 | Off-gas cooler |
| U12-HX02 | Off-gas cooler |
| U12-HX03 | Condenser |
| U12-KB01 | H2 Blower |
| U12-P01 | Leachate pump |
| U12-P02 | Wash pump |
| U12-P03 | Recycle pump |
| U12-P04 | Absorbent pump |
| U12-SM01 | Evaporator |
| U13-EC01 | Cooler |
| U13-FR01 | DRI stage 1 |
| U13-FR02 | DRI stage 2 |
| U13-HO01 | Hopper |

Process Flow Diagram for the proposed process to remove iron from nitrided ilmenite

| | U11-ST01 | U11-ST04 | U11-ST06 | U11-ST07 | U11-ST09 | U11-ST11 | U11-ST12 | U12-ST01 | U12-ST02 | U12-ST04 | U12-ST05 | U12-ST06 | U12-ST07 | U12-ST08 | U12-ST09 | U12-ST10 | U12-ST11 | U12-ST12 | U12-ST15 | U12-ST17 | U12-ST19 | U13-ST01 | U13-ST02 | U13-ST03 | U13-ST04 | U13-ST05 | U13-ST07 | U13-ST08 |
|---|---|---|---|---|---|---|---|---|---|---|---|---|---|---|---|---|---|---|---|---|---|---|---|---|---|---|---|---|
| Temperature (°C) | 30 | 25 | 90 | 90 | 25 | 80 | 25 | 90 | 100 | 100 | 100 | 90 | 140 | 940 | 100 | 70 | 80 | 70 | 80 | 100 | 160 | 25 | 40 | 950 | 950 | 930 | 200 | 25 |
| Vapor Frac | 0 | 0 | 0 | 0 | 0 | 0 | 0 | 0 | 1 | 1 | 1 | 1 | 0 | 0 | 1 | 0 | 0 | 0 | 1 | 1 | 1 | 0 | 1 | 0 | 1 | 1 | 0 | 1 |
| Total Mass Flow (t/h) | 8.023 | 1.02E-05 | 21.047 | 28.941 | 4.342 | 15.785 | 0.041 | 24.559 | 1.310 | 18.567 | 21.461 | 2.895 | 10.585 | 5.180 | 7.636 | 21.047 | 15.785 | 16.305 | 5.156 | 0.129 | 4.593 | 1.382 | 8.005 | 4.667 | 9.900 | 10.926 | 3.641 | 2.232 |
| Mass Flow (t/h) | | | | | | | | | | | | | | | | | | | | | | | | | | | | |
| O2 | 0 | 0 | 0 | 0 | 0 | 0 | 0 | 0 | 0.301 | 0 | 0 | 0 | 0 | 0 | 0 | 0 | 0 | 0 | 0 | 0 | 0 | 0 | 1.840 | 0 | 0 | 0 | 0 | 0.513 |
| N2 | 0 | 0 | 0 | 0 | 0 | 0 | 0 | 0 | 1.009 | 3.437 | 5.156 | 1.719 | 0 | 0 | 1.719 | 0 | 0 | 0 | 5.156 | 0 | 3.437 | 0 | 6.165 | 0 | 6.165 | 6.165 | 0 | 1.719 |
| H2 | 0 | 0 | 0 | 0 | 0 | 0 | 0 | 0 | 0 | 0 | 0 | 0 | 0 | 0 | 0 | 0 | 0 | 0 | 0 | 0.129 | 0 | 0 | 0 | 0 | 0 | 0 | 0 | 0 |
| C | 0 | 0 | 0 | 0 | 0 | 0 | 0 | 0 | 0 | 0 | 0 | 0 | 0 | 0 | 0 | 0 | 0 | 0 | 0 | 0 | 0 | 1.38 | 0 | 0 | 0 | 0 | 0 | 0 |
| H2O | 0 | 3.10E-06 | 15.785 | 15.801 | 0 | 15.785 | 0 | 15.801 | 0 | 14.608 | 15.784 | 1.176 | 0 | 0 | 1.176 | 15.785 | 15.785 | 15.785 | 0 | 0 | 1.155 | 0 | 0 | 0 | 0 | 0 | 0 | 0 |
| HCl | 0 | 7.09E-06 | 5.262 | 0.612 | 0 | 0 | 0 | 0.520 | 0 | 0.521 | 0.521 | 0 | 0 | 0 | 4.750 | 5.262 | 0 | 0.520 | 0 | 0 | 0 | 0 | 0 | 0 | 0 | 0 | 0 | 0 |
| TiN | 3.232 | 0 | 0 | 3.232 | 3.232 | 0 | 0 | 0 | 0 | 0 | 0 | 0 | 0 | 0 | 0 | 0 | 0 | 0 | 0 | 0 | 0 | 0 | 0 | 0 | 0 | 0 | 0 | 0 |
| TiO2 | 0.219 | 0 | 0 | 0.219 | 0.219 | 0 | 0 | 0 | 0 | 0 | 0 | 0 | 5.92E-04 | 5.92E-04 | 0 | 0 | 0 | 0 | 0 | 0 | 0 | 0 | 0 | 5.92E-04 | 0 | 0 | 5.92E-04 | 0 |
| Fe | 3.663 | 0 | 0 | 0.082 | 0.041 | 0 | 0.041 | 0 | 0 | 0 | 0 | 0 | 0 | 0 | 0 | 0 | 0 | 0 | 0 | 0 | 0 | 0 | 0 | 0 | 0 | 0 | 3.582 | 0 |
| FeO | 0 | 0 | 0 | 0 | 0 | 0 | 0 | 0 | 0 | 0 | 0 | 0 | 0 | 0 | 0 | 0 | 0 | 0 | 0 | 0 | 0 | 0 | 0 | 4.608 | 0 | 0 | 0 | 0 |
| Fe2O3 | 0 | 0 | 0 | 0 | 0 | 0 | 0 | 0 | 0 | 0 | 0 | 0 | 0 | 5.121 | 0 | 0 | 0 | 0 | 0 | 0 | 0 | 0 | 0 | 0 | 0 | 0 | 0 | 0 |
| FeCl2 | 0 | 0 | 0 | 9.580 | 0 | 0 | 0 | 8.129 | 0 | 0 | 0 | 0 | 0 | 0 | 0 | 0 | 0 | 0 | 0 | 0 | 0 | 0 | 0 | 0 | 0 | 0 | 0 | 0 |
| FeCl2*2H2O | 0 | 0 | 0 | 0 | 0 | 0 | 0 | 0 | 0 | 0 | 0 | 0 | 10.440 | 0 | 0 | 0 | 0 | 0 | 0 | 0 | 0 | 0 | 0 | 0 | 0 | 0 | 0 | 0 |

**Figure 7.1: Process flow diagram of proposed process for removing iron from nitrided ilmenite**

## 7.3 – Process model for proposed process

The proposed process, illustrated in Figure 7.1, was modelled using the Flowsheet Simulation module in the HSC Chemistry 7.0© software package.

### 7.3.1 – Assumptions

The assumptions made to are listed below.

*Nitrided ilmenite feed stream (U11-ST01)*

Table 7.1 gives the normalised chemical composition of the nitrided feed stream used in the process model. Species assumed not to react during the dissolution reaction are grouped together under "other". These are C, S, $P_2O_5$ and $K_2O$. Silicon dioxide is also assumed to be inert but is shown in Table 7.1 to illustrate that ilmenite high in impurities can be used in the low-temperature chlorination process. Refer to Chapter 3 for a characterisation of the nitrided ilmenite.

**Table 7.1: Composition of nitrided ilmenite used in the process model**

| Constituent | Mass % |
|---|---|
| $TiO_2$ | 2.73 |
| TiN | 40.26 |
| Fe | 45.64 |
| $Al_2O_3$ | 1.88 |
| $SiO_2$ | 3.54 |
| MgO | 0.62 |
| MnO | 1.27 |
| CaO | 0.14 |
| $V_2O_5$ | 0.19 |
| Other | 3.69 |

To evaluate the proposed process on the same basis as the Austpac ERMS SR process in Chapter 5, assume a required titanium production rate of 2.5 tons of titanium per hour.

Only titanium nitride in the low-temperature chlorination reactor will result in titanium tetrachloride. To estimate the required nitrided ilmenite mass flow rate, assume that all the titanium present in titanium nitride will result in titanium metal. The required titanium nitride mass flow rate is therefore equal to 3.231 tons of titanium nitride per hour. The mass fraction of titanium nitride present in the feed (Table 7.1) is equal to 40.26%; this equates to a required nitrided ilmenite mass flow rate of 8.028 tons of nitrided ilmenite per hour. The

mass flow rate of other components in the feed stream is then obtained by multiplying the component mass fraction by the total stream mass flow rate.

*The leach train (U11-RC01)*

- Assume that a 25 wt % hydrochloric acid solution is used in the leach train.
- Assume that the hydrochloric acid is 10% in excess of the amount required to dissolve all iron contained in the feed stream.
- Assume that Reactions 5.9 to 5.17 in Chapter 5 can also occur in this leach train, including the following (main) reaction:

$$Fe(s) + 2\ HCl(aq) = FeCl_2(aq) + H_2(g) \qquad \text{Reaction 7.1}$$

- Assume that $SiO_2$, $P_2O_5$ and any other gangue materials are inert in the leach train.
- Assume that leaching of $TiO_2$, CaO, MgO and $Al_2O_3$ reaches the same extent as experimentally determined in Section 6.3.
- The process model varies the conversions for other possible reactions until the composition is reached as experimentally determined in Section 6.3.
- The experiments in Section 6.3 were, however, based on either 0 or 20% excess acid being available for reaction. The chemical composition of a product leached with 10% excess acid is therefore interpolated from the results of these two known compositions. The resulting leached product composition is given in Table 7.2. Appendix 7 reports the chemical compositions of all the leached products obtained in Section 6.3.

**Table 7.2: Normalised composition of leached nitrided ilmenite product**

| Component | Mass % |
|---|---|
| $TiO_2$ | 5.10 |
| TiN | 75.00 |
| Fe | 1.86 |
| $Al_2O_3$ | 3.63 |
| $SiO_2$ | 6.13 |
| MgO | 1.31 |
| MnO | 1.13 |
| CaO | 0.12 |
| $V_2O_5$ | 0.32 |
| Other | 5.43 |

*High-intensity magnetic separation (U11-SM01)*

The magnetic properties of metallic iron in nitrided ilmenite are considerable. They have, however, not yet been quantified. Therefore, assume that approximately 50% of iron can be separated from the product stream with high-intensity magnetic separators. Other components will also separate with the magnetic fraction, but this is not included in the process model. The presence of these other components does not, however, degrade the final product. Iron is the only impurity that is important for the low-temperature chlorination process.

*Hydrogen off-gas burner (U12-FM02)*

- Assume 100% conversion for the following reaction

$$H_2(g) + ½O_2(g) = H_2O(g) \qquad \text{Reaction 7.2}$$

The same assumptions made in Chapter 5 were used to model the following process units:

- Liquid filtration (U11-SF010)
- Solids wash (U11-SF02) and solids drying (U11-FK01)
- Fluid bed evaporator (U12-SM01)
- Pyrohydrolysis reactor (U12-FR01)
- Both DRI stages (U13-FR01 and U13-FR02)
- Both absorbers (U12-AB01 and U12-AB02)
- Indirect solids cooler (U13-EC01)
- Off-gas afterburner (U12-FM01)
- Hydrochloric acid make-up stream (U11-ST04)

Refer to Section 5.3 to review these assumptions.

### 7.3.2 – Material and energy balances

Table 7.3 reports the material and energy balances for the main equipment used in the process model.

**Table 7.3: Material and energy balances for main equipment in the proposed process**

| Equipment | Description | Mass balance (t/h) | Energy balance (kW) |
|---|---|---|---|
| U11-HX01 | Feed heater | 0.000 | 278 |
| U11-RC01 | Leach train | 0.000 | -1 686 |
| U12-AB01 | Absorber | 0.000 | -607 |
| U12-AB02 | Absorber | 0.000 | -2 973 |
| U12-FM01 | Off-gas afterburner | 0.000 | -4 123 |
| U12-FM02 | Off-gas afterburner | 0.000 | -4 099 |
| U12-FR01 | Pyrohydrolysis | 0.000 | 4 895 |
| U12-HX01 | Off-gas cooler | 0.000 | -341 |
| U12-HX02 | Off-gas cooler | 0.000 | -1 971 |
| U12-HX03 | Condenser | 0.000 | -10 249 |
| U12-SM01 | Evaporator | 0.000 | 10 543 |
| U13-EC01 | Cooler | 0.000 | -443 |
| U13-FR01 | DRI stage 1 | 0.000 | -953 |
| U13-FR02 | DRI stage 2 | 0.000 | -277 |
| | **Total:** | 0.000 | -12 006 |

Table 7.4 summarises the input-output material and energy balances for the process model as a whole. The input and output streams in the process model are shown in Figure 7.1.

**Table 7.4: Overall input-output material and energy balances for the proposed process**

| Constituent | Input streams (t/h) | | | | | | | Output streams (t/h) | | | | | BALANCE: |
|---|---|---|---|---|---|---|---|---|---|---|---|---|---|
| | U13-ST02 | U11-ST01 | U13-ST01 | U11-ST04 | U12-ST02 | U13-ST08 | U12-ST18 | U11-ST09 | U11-ST12 | U12-ST15 | U12-ST16 | U13-ST07 | |
| $N_2$(g) | 6.165 | | | | 1.009 | 1.719 | 3.437 | | | 5.156 | 7.174 | | |
| $CO_2$(g) | | | | | | | | | | | 5.060 | | **1.382** |
| $O_2$(g) | 1.840 | | | | 0.301 | 0.513 | 1.026 | | | | | | |
| $H_2O$ | | | | 3.1E-6 | | | | | | | | | **1.02 x $10^{-5}$** |
| HCl(aq) | | | | 7.0E-6 | | | | | | | | | |
| C | | | 1.382 | | | | | | | | | | |
| TiN | | 3.232 | | | | | | 3.232 | | | | | |
| $TiO_2$ | | 0.219 | | | | | | 0.219 | | | | 0.001 | |
| Fe | | 3.663 | | | | | | 0.041 | 0.041 | | | 3.582 | |
| $Al_2O_3$ | | 0.151 | | | | | | 0.146 | | | | 0.005 | |
| MgO | | 0.050 | | | | | | 0.050 | | | | 2.4E-4 | **-1.382** |
| MnO | | 0.102 | | | | | | 0.049 | | | | 0.053 | |
| CaO | | 0.011 | | | | | | 0.011 | | | | | |
| $V_2O_5$ | | 0.015 | | | | | | 0.014 | | | | 0.001 | |
| $SiO_2$ | | 0.284 | | | | | | 0.284 | | | | | |
| Other | | 0.296 | | | | | | 0.296 | | | | | |
| $CaCl_2$ | | | | | | | | | | | | 1.1E-5 | |
| **TOTAL MASS** (t/h) | 8.005 | 8.023 | 1.382 | 1.0E-5 | 1.310 | 2.232 | 4.464 | 4.342 | 0.041 | 5.156 | 12.236 | 3.641 | **0.000** |
| **ENTHALPY** (kWh) | 34 | -7 930 | | | 28 | | -31 | -7 847 | | 82 | -12 121 | -20 | **-12 006** |

### 7.3.3 – Discussion

The composition of the upgraded nitrided ilmenite product is summarised in Table 7.5. These results indicate that a product with a very low iron content can be produced using the proposed process.

**Table 7.5: Composition of nitrided ilmenite product produced by proposed process**

| Constituent | After magnetic separation (wt %) |
|---|---|
| $TiO_2$ | 5.03 |
| TiN | 74.43 |
| Fe | 0.94 |
| $Al_2O_3$ | 3.37 |
| $SiO_2$ | 6.54 |
| MgO | 1.14 |
| MnO | 1.14 |
| CaO | 0.26 |
| $V_2O_5$ | 0.32 |
| Other | 6.82 |

The reader is, however, reminded that a 50% split for only iron was assumed in the high-intensity magnetic separation step. The results summarised in Table 7.5 are therefore only an indication of a possible product composition. The actual product composition is expected to have a much higher titanium nitride content than that reported in Table 7.5. This is because the high-intensity magnetic separation step used in the Austpac ERMS SR process (U01-SM01) significantly increased the titanium dioxide content in the final synthetic rutile product (Section 5.3.4).

The iron content can potentially be further reduced if all the metallic iron (magnetic) can be separated with the high-intensity magnetic separation step (U12-SM01). The magnetic stream split (U11-ST12) can be recycled to the leach train (U11-RC01) if a substantial amount of titanium nitride is still present.

The extent to which magnetic separation can be achieved in the high-intensity magnetic separation step (U11-SM01) will, however, have to be quantified through experimental work (Section 6.4).

Section 5.3.4 indicated that process integration reduces the fluid bed evaporator's (U01-SM01) energy requirements by approximately 40%. Energy savings can be increased further when using nitrided ilmenite as feed material.

The first reason for the achievement of energy savings is because hydrogen gas instead of water is produced during the dissolution reaction. This means that less water needs to be evaporated.

The second method for reducing the fluid bed evaporator's (U12-SM01) energy requirement is to utilise the heat of hydrogen combustion in air (produced in U12-FM02, the off-gas afterburner). Using this heat of combustion in the fluid bed evaporator can reduce its energy requirements by an extra ~35%. Combining existing process integration, as used in the EARS process unit, with this proposed hydrogen combustion reaction can result in a ~75% reduction in the fluid bed evaporator's energy requirements. Table 7.3 shows that approximately 4 MWh is produced by the hydrogen off-gas afterburner (U12-FM02).

The result of the above process integration is that the proposed process requires only one third (226 kg of coal per hour) of the coal used by the Austpac ERMS SR process (655 kg of coal per hour) to supply the remaining heat (~1.8 MWh) to the fluid bed evaporator (U12-SM01) by combustion of excess carbon monoxide gas from the DRI process unit.

Significantly less carbon dioxide is therefore produced in the proposed process. The iron content in the nitrided ilmenite used is, however, much higher than the ilmenite product produced in the ERMS process. An extra 756 kg of iron per hour is produced in the DRI process unit when this nitrided ilmenite is used instead of the ERMS process's ilmenite product. This extra iron requires an additional ~2.4 ton 25 wt % of hydrochloric acid in the leach train and 244 kg of coal per hour extra in the DRI process unit. The amount of water circulating in the process and the amount of carbon dioxide produced by the process are therefore significantly higher due to this excess iron. This will, however, only be the case if low-grade ilmenite is nitrided.

The reactivity of metallic iron with hydrochloric acid, together with the short residence time in the leach train, leads to reduced acid consumption (Section 6.3.4). Using the wt % of calcium dissolved, as experimentally determined, in the model of the proposed process reveals that a very low acid consumption is theoretically possible – possibly as low as 154 kg 37 wt % of hydrochloric acid per year. This is significantly less than the 11.85 tons 37 wt % of hydrochloric acid required per year by the Austpac ERMS SR process model (Section 5.3.4).

The limited dissolution of other species in the leach train results in a DRI product with a very high iron content. The composition of the predicted DRI product is reported in Table 7.6.

**Table 7.6: Composition of proposed process's DRI product**

| Constituent | Mass% |
|---|---|
| Fe | 98.37 |
| $Al_2O_3$ | 0.12 |
| MgO | 0.01 |
| MnO | 1.45 |
| $CaCl_2$ | ~ 0.00 |
| $V_2O_5$ | 0.03 |
| $TiO_2$ | 0.02 |

## 7.4 – Conclusions and recommendations

The result of this chapter is a proposed process flow diagram of a process that can remove iron from nitrided ilmenite and produce a high-quality metallised iron by-product.

*It is concluded that hydrochloric acid leaching of nitrided ilmenite, in combination with the Enhanced Acid Regeneration System (EARS) and the Direct Reduced Iron (DRI) process units as used in the Austpac ERMS SR process, is a viable process route for removing iron from nitrided ilmenite.* Licensing will have to be obtained from Austpac Resources N.L. before the EARS and DRI process units can be used. This is assumed to be possible as process technology is the core business of Austpac Resources N.L. (Austpac Resources N.L., 2010).

Future work recommended to further develop and evaluate the proposed process includes:

- Determine the extent to which a high-intensity magnetic separation step can remove iron from the leached product stream and whether it is necessary to leach the separated magnetic stream again.
- Develop an optimum leach train that can contain and extract the hydrogen gas produced during the dissolution reaction.
- Determine whether there is a market for the metallised iron product. If not, the DRI process unit should be removed from the proposed process.
- Upgrade process models for both the Austpac ERMS SR process and the proposed process to include both the ERMS and nitriding sections, as well as the high- and low-temperature chlorination processes. These models should then be used in a

techno-economic evaluation. The results will indicate whether the low-temperature chlorination route is comparable to the existing route and whether further development work should continue.

# REFERENCES

ABN NEWSWIRE, 9/18/2008, 2008-last update, 2008 National Mining Awards Recognise The Globally Competitive Australian mining sector. Available: http://www.abnnewswire.net/press/en/57130/Aquila_Resources_Limited.html [1/29/2010, 2010].

AUSTPAC RESOURCES N.L., 2010-last update, Austpac Resources. Available: http://www.austpacresources.com/ [1/29/2010, 2010].

BECHER, R.G. 1963. *An improved process for the beneficiation of ores containing contaminating iron.* Australian patent 247,110.

BRUCKARD, W.J., CALLE, C., CONSTANTI-CAREY, K., FLETCHER, S. & HORNE, M.D. 2003. Redox catalysts for Becher aeration. *Proceedings of the Heavy Minerals Conference, Current Challenges in Heavy Mineral Exploitation,* 6–8 October, Cape Town.

CSIR, 7/17/2009, 2009-last update, Metal and Metals Processes. Available: http://www.csir.co.za/msm/metals_and_metals_processes/index.html [9/25/2009, 2009].

CUNNINGHAM, G.L. 1958. *Electrolytic Process.* U.S. patent 2,852,452.

EL-HAZEK, N., LASHEEN, T.A., EL-SHEIKH, R. and ZAKI, S.A., 2007. Hydrometallurgical criteria for $TiO_2$ leaching from Rosetta ilmenite by hydrochloric acid. *Hydrometallurgy,* **87:** 45-50.

FOGLER, H.S., 2006. *Elements of Chemical Reaction Engineering,* 4th ed. UK: Pearson Education International.

GEETHA, K.S. and SURENDER, G.D., 1997. Modeling of ammoniacal oxygen leaching of metallic iron in a stirred slurry reactor. *Hydrometallurgy,* **44**(1–2): 213–230.

GEETHA, K.S. and SURENDER, G.D., 2000. Experimental and modeling studies on the aeration leaching process for metallic iron removal in the manufacture of synthetic rutile. *Hydrometallurgy,* **56**(1): 41–62.

LANYON, M.R., LWIN, T. and MERRITT, R.R., 1999. The dissolution of iron in the hydrochloric acid leach of an ilmenite concentrate. *Hydrometallurgy,* **51**(3): 299–323.

LEVENSPIEL, O., 1999. *Chemical Reaction Engineering*. 3rd ed. New York: Wiley.

LIDDELL, K.C., 2005. Shrinking core models in hydrometallurgy: What students are not being told about the pseudo-steady approximation. *Hydrometallurgy,* **79**(1–2): 62–68.

MAHMOUD, M.H.H., AFIFI, A.A.I. and IBRAHIM, I.A., 2004. Reductive leaching of ilmenite ore in hydrochloric acid for preparation of synthetic rutile. *Hydrometallurgy,* **73**(1-2): 99–109.

METSEP INTERNATIONAL, 2007-last update, our technology. Available: http://www.metsep.co.za/Technology.htm [7/26/2010, 2010].

MOTSIE, R., 2008. *An overview of South Africa's titanium mineral concentrate industry.* Report R71 /2008, Pretoria: Department Minerals and Energy.

NATIONAL METROLOGY INSTITUTE OF SOUTH AFRICA, 2008-last update, NMISA – services and NMISA laboratories. Available: http://www.nmisa.org/labs [10/21/2009, 2009].

NOUBACTEP, C., 2009. Metallic iron for environmental remediation: Learning from the Becher process. *Journal of Hazardous Materials,* **168**(2–3): 1609–1612.

SEADER, J.D. and HENLEY, E.J., 2006. *Separation Process Principles,* 2nd ed. New York: Wiley.

SHIAH, C.D. 1966. *Process for producing titanium dioxide concentrate and other useful products from ilmenite and similar ores.* U.S. patent 3,252,787.

SOLE, K.C., 1999a. Recovery of titanium from the leach liquors of titaniferous magnetites by solvent extraction: Part 1. Review of the literature and aqueous thermodynamics. *Hydrometallurgy,* **51**(2): 239–253.

SOLE, K.C., 1999b. Recovery of titanium from the leach liquors of titaniferous magnetites by solvent extraction: Part 2. Laboratory-scale studies. *Hydrometallurgy,* **51**(3): 263–274.

SOLE, K.C., FEATHER, A. and O'CONNELL, J.P., 1999. Recovery of titanium from the leach liquors of titaniferous magnetites by solvent extraction: Part 3. Continuous mini-plant trials. *Hydrometallurgy,* **51**(3): 275–284.

UIS ANALYTICAL SERVICES, 17 November 2009. Available: http://www.uis-as.co.za [12/3/2009, 2009].

VAN DYK, J.P. 1999. *Process development for the production of beneficiated titania slag.* PhD thesis, Pretoria: Faculty of Engineering, University of Pretoria.

VAN DYK, J.P., VEGTER, N.M. and PISTORIUS, P.C., 2002. Kinetics of ilmenite dissolution in hydrochloric acid. *Hydrometallurgy,* **65:** 31–36.

VAN VUUREN, D.S. and STONE, A.K., 2006. Selective recovery of titanium dioxide from low grade sources. *Proceedings of the South African Chemical Engineering Congress,* Durban, 20–22 September 2006.

VERRYN, S., 2009-last update, XRD Analytical & Consulting. Available: http://www.xrd.co.za/ [12/3/2009, 2009].

WALPOLE, E.A. 1993. *Acid regeneration.* International patent: WO 93/16000.

WALPOLE, E.A. 1997. *Process for separating ilmenite.* U.S. patent 5,595,347.

WALPOLE, E.A. and WINTER, J.D., 2002. The Austpac ERMS and EARS processes for the manufacture of high-grade synthetic rutile by the hydrochloric acid leaching of ilmenite. *Proceedings of Chloride Metallurgy 2002 – International Conference on the Practice and Theory of Chloride/Metal interaction,* Montreal, October 2002.

WANG, Z., XUE, J., WANG, H. and JIANG, X., 2009. Kinetic study of hydrochloric acid leaching process of ilmenite for rutile synthesis. *Proceedings of the EPD Congress 2009,* Minerals, Metals & Materials Society, pp. 837–843.

WARD, C.B. 1990. *The production of synthetic rutile and by-product iron oxide pigments from Ilmenite processing.* PhD thesis, Perth, Western Australia: School of Mathematical and Physical Sciences, Murdoch University.

WARD, J.M. 1999. *Catalysed aeration of reduced ilmenite.* PhD thesis, Perth, Western Australia: School of Applied Chemistry, Curtin University of Technology.

WINTER, J. 2008. *Production of synthetic rutile by continuous leaching.* U.S. patent 7,404,937.

WINTER, J.D. 2009. *Processing of metal chloride solutions and method and apparatus for producing direct reduced iron.* U.S. patent 2009/0095132.

ZHANG, S. and NICOL, M.J., 2009. An electrochemical study of the reduction and dissolution of ilmenite in sulphuric acid solutions. *Hydrometallurgy,* **97**(3–4): 146–152.

# APPENDICES

## Appendix 1 – Magnetic separation procedure for removing residual char from nitrided ilmenite

This appendix describes the dry magnetic separation procedure developed to remove residual char from nitrided ilmenite. This is a batch-wise operation and therefore only suitable for small (approximately 200 g) samples.

### A1.1 – Introduction

#### A1.1.1 – Background and motivation

The production of titanium tetrachloride in the CSIR's proposed process recovers titanium dioxide from feed materials such as ilmenite by first nitriding the feed and then chlorinating the titanium nitride contained in the nitrided feed.

The iron contained within the nitrided ilmenite must, however, first be removed before chlorination. Various process options have been considered for iron removal (Section 2.5) but experimental work is required to evaluate them. A standard nitrided ilmenite sample is required to evaluate all these process options on the same basis.

Three sequential steps are required to prepare a standardised nitrided ilmenite sample. These are:

Step1. Prepare a batch sample of nitrided ilmenite at fixed nitriding conditions.
Step 2. Remove residual char from the nitrided sample prepared in (1).
Step 3. Characterise the nitrided ilmenite sample prepared in (2).

Step 2 from the above sequence is described in this dissertation. The nitrided ilmenite obtained from Step 1 is illustrated in Figure A1.1 which is a photograph of a nitrided ilmenite sample with residual char still present. The larger particles are the residual char.

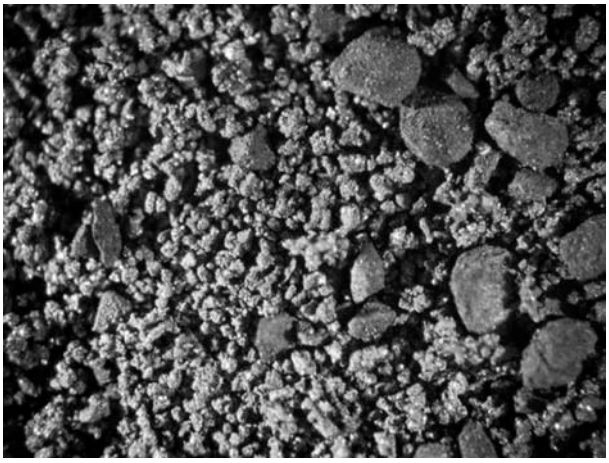

**Figure A1.1: Nitrided ilmenite sample before dry magnetic separation (Approx. x10 magnification)**

The residual char is separated from the nitrided ilmenite by using the difference in their magnetic properties. The nitrided ilmenite contains metallic iron in its complex form and is therefore magnetic. The char, however, is not magnetic.

## A1.2 – Materials, methods and equipment used

### A1.2.1 – Sample characteristics

The nitrided ilmenite described in Chapter 3 was used for this procedure. Refer to Chapter 3 for an overview of the sample characteristics and procedures used to obtain the sample. The nitrided ilmenite with residual char present is illustrated in Figure A1.1.

A sample was taken from a container with thoroughly mixed nitrided ilmenite. The nitrided ilmenite was mixed for 5 minutes in a Turbula mixer to ensure that a representative sample was taken.

### A1.2.2 – Magnetic separation procedure

Figures A1.2 and A1.3 illustrate the experimental apparatus used to separate magnetic from non-magnetic particles.

The experimental apparatus used for magnetic separation consisted of an AEG DR50 vibrating feeder fitted with a magnet on one of its outer-sides. The position of the magnet is

indicated in Figure A1.2 with an arrow. The side of the vibrating feeder fitted with the magnet is raised by approximately 1 cm to ensure that the unseparated feed does not come close to the magnet without some assistance (A-arrow in Figure A1.3) to guide the material towards the magnet. In other words, the natural path of the material is as far away from the magnet as possible.

A test tube is also fixed on the same side as the magnet with a position and angle to “catch” the magnetic fraction collected by the magnet.

**Figure A1.2: Apparatus used for magnetic separation**

Figure A1.3 is a close-up photograph of the magnetic separator at the point where magnetic separation occurs.

In Figure A1.3, the A-arrow points to an obstruction added in the path of the down-coming unseparated feed to “guide” the feed to the position of the magnet. The magnetic fraction in the unseparated feed is then attracted to the magnet and attaches itself to the side of the feeder to form a magnetic lump (B-arrow).

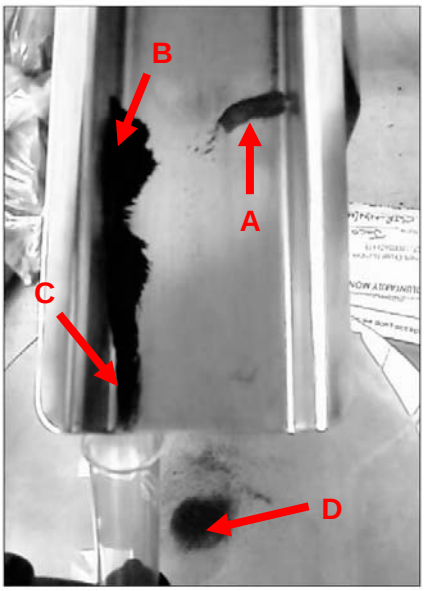


**Figure A1.3: Magnetic separation in progress**

Once this magnetic lump becomes large enough, the vibration effect of the feeder causes the magnetic fraction to separate from the bundle and it starts to form a “guided” magnetic stream (C-arrow). This magnetic stream is collected in the test tube.

The non-magnetic fraction falls back to the lower part of the vibrating feeder once it passes the obstacle (A-arrow) and becomes a non-magnetic stream, which is then collected once it falls off the vibrating feeder (D-arrow). In other words, the material returns to its natural flow path.

An Olympus SZ61 Stereo Microscope was used to qualitatively determine the separation efficiency.

### A1.2.3 – Particle size distribution

The particle size distribution of the residual char was measured with a HAVER EML 200 Test Sieve Shaker fitted with 800, 630, 500, 315, 250, 200, 180, 125, 90, 63 and 45 µm DIN 4 188 screens.

The residual char obtained from the magnetic separation procedure was added to the top screen of the sieve shaker and left for 15 minutes to shake on the “high” setting.

The screens were cleaned, weighed and the mass noted before the sample was added to the shaker. The mass of each screen was weighed and noted again after 15 minutes of shaking.

A Mettler-Toledo PM30 Electronic Balance was used to determine the mass of each screen.

## A1.3 – Results and discussion

### A1.3.1 – Magnetic separation procedure

The residual char separated from the nitrided ilmenite was on average 9% of the mass of the original sample. This average was obtained from three magnetic separation runs.

Figure A1.4 is a photograph of the residual char separated from the nitrided ilmenite.

**Figure A1.4: Residual char removed during magnetic separation (Approx. x10 magnification)**

Qualitative interpretation of the results suggested that the separation of residual char from nitrided ilmenite was approximately +98% successful.

### A1.3.2 – Particle size distribution

A frequency distribution for both the residual char and the carbon used in nitriding is given in Figure A1.5. The results illustrated in Figure A1.5 present the mass % of sample retained for each mean particle size.

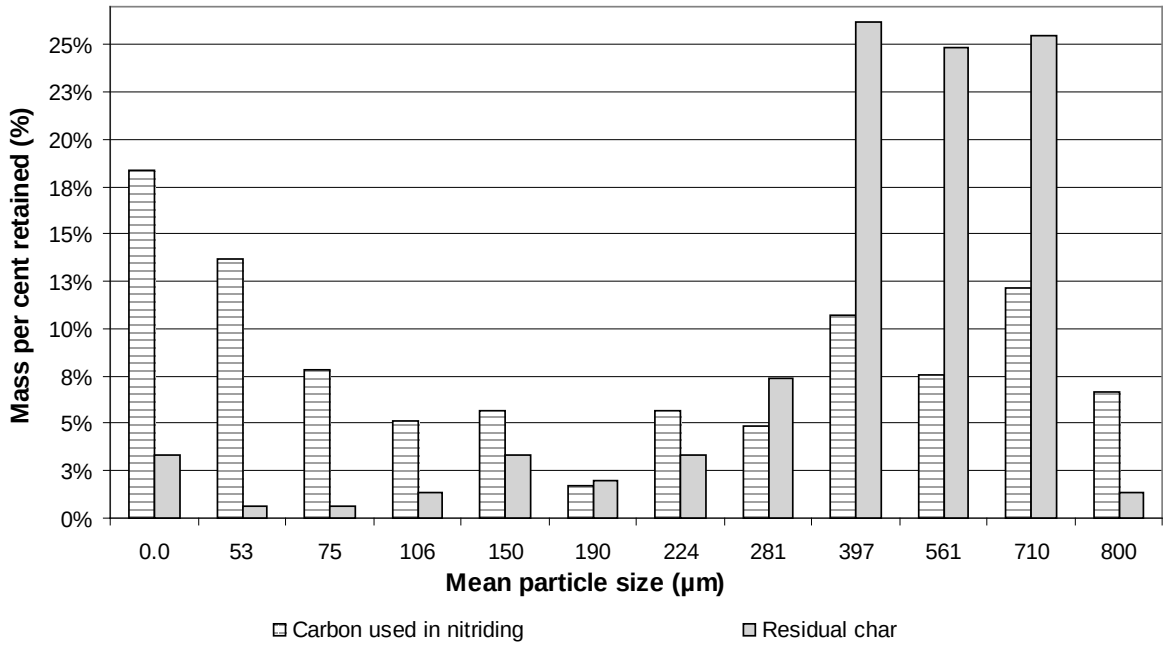


**Figure A1.5: Particle size distribution for both residual char and carbon used in nitriding**

Equation A1.1 gives the mean particle size of each size increment.

$$Mean\ \text{particle size} = \sqrt{(bottom\ screen\ \text{size} * top\ screen\ \text{size})} \qquad \text{Equation A1.1}$$

The average mass mean particle diameters for the residual char and carbon used in nitriding are 474 and 281 µm respectively. From this it is clear that the smaller carbon particles react first during nitriding and that the larger carbon particles are left behind as residual char.

Another observation from the particle size distribution is that 77% of the residual char is larger than 315 µm.

## A1.4 – Conclusions

A separation procedure was developed and described in this appendix. It has an estimated separation efficiency of approximately + 98%.

Evaluation of the results suggested that the original sample contained approximately 9% (mass) residual char and that 77% of this was larger than 315 µm.

The disadvantage of the proposed procedure is that it can only be used with small samples (approximately 200 g) in a semi-batch operation mode. It is also time-consuming and requires continuous supervision to obtain sufficient separation efficiency.

The proposed procedure is, however, more than adequate for laboratory-scale sample preparations and it will therefore be used as the standard method for removing residual char from nitrided ilmenite.

# Appendix 2 – Separation attempts to remove iron globules mechanically from nitrided ilmenite

The standard nitrided ilmenite sample used in experiments was characterised in Chapter 3 to determine its quantitative and qualitative properties. SEM photos with elemental mapping revealed that there were some iron globules on the outer surface of the nitrided ilmenite complex. It appeared as if these iron globules "sweat" out of the ilmenite complex during nitriding. Figure A2.1 shows a SEM photo with an iron globule indicated by the arrow.

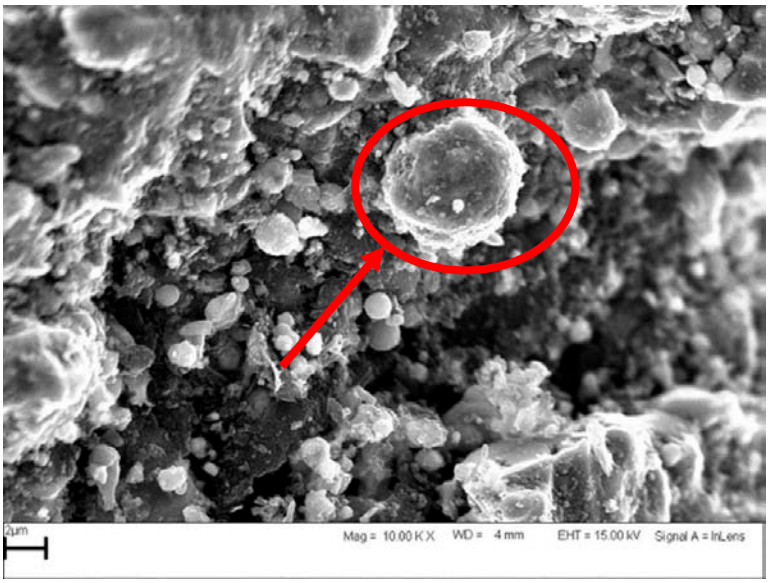


**Figure A2.1: SEM photo with iron globule illustrated**

The iron globule indicated in Figure A2.1 has a diameter of approximately 10 µm and is still attached to the surface of the nitrided ilmenite complex.

It was decided to test if these iron globules can be physically separated from the nitrided ilmenite complex. If they could be separated from the complex, the next step would then be to remove the separated iron globules from the nitrided ilmenite sample to produce two product streams, namely an upgraded nitrided ilmenite sample and iron powder.

The reduced iron content in the upgraded nitrided ilmenite sample would ensure lower operational costs (reduced acid consumption) and less generation of iron oxide waste when used in a chemical separation method such as hydrochloric acid leaching.

If the removal of these iron globules from nitrided ilmenite was found to be viable, a process step could be developed to refine nitrided ilmenite before using a chemical separation method such as hydrochloric acid leaching which would remove most of the iron contained in the nitrided ilmenite.

## A2.1 – Materials, methods and equipment used

### A2.1.1 – Sample characteristics

The nitrided ilmenite described in Chapter 3 was used for this procedure. Refer to Chapter 3 for an overview of the sample characteristics and the procedures used to obtain the sample.

Only nitrided ilmenite particles between 71 and 400 µm were used as the standard sample for the experiments conducted in this investigation.

### A2.1.2 – "Heavy" dry milling

The first separation attempt consisted of milling a sample of nitrided ilmenite to see what would happen when a force was applied to the nitrided ilmenite complex and the iron globules on the complex.

This was achieved by adding a 50 g nitrided ilmenite sample to a Lenton single-pot barrel mill for approximately 30 minutes. The milled sample was removed from the barrel mill after 30 minutes and put through a 71 µm screen to capture particles smaller than 71 µm. The sample containing particles smaller than 71 µm was then used to evaluate the separation attempt.

### A2.1.3 – "Light" dry milling

The second attempt involved evaluating the effects of light grinding of the particles against each other. The idea was that the iron globules would separate from the nitrided ilmenite complex and become loose when the light grinding effect was successful.

This was achieved by adding a 20 g nitrided ilmenite sample to a mortar and then lightly grinding the sample with a pestle. Figure A2.2 is a photo of the mortar and pestle used for this experiment.

**Figure A2.2: Mortar and pestle used to simulate light grinding**

The sample was removed from the mortar after approximately 30 minutes of grinding and put through a 36 µm sieve to capture particles smaller than 36 µm. The sample containing particles smaller than 36 µm was then used to evaluate the separation attempt. The particles larger than 36 µm were sent back to the mortar for further grinding. The particles smaller than 36 µm were captured a second time and kept separate for evaluation.

### A2.1.4 – "Light" wet milling

The third attempt involved evaluating the effects of light grinding of the particles against each other in a slurry mixture.

This was achieved by adding 50 g of nitrided ilmenite and 400 ml of water inside a reaction vessel fitted with a VELP Scientifica overhead stirrer (ES) with a propeller shaft. The overhead stirrer mixed the slurry at approximately 1 000 r/min for 3 hours.

After 3 hours, the solution was pumped from the reaction vessel with an Electrolab PP50V peristaltic pump into a separate container.

**Figure A2.3: Mixing vessel to simulate "light" wet milling of nitrided ilmenite**

Figure A2.3 is a photo of the slurry solution inside the reaction vessel and Figure A2.4 is a photo of the vessel into which the solution was pumped.

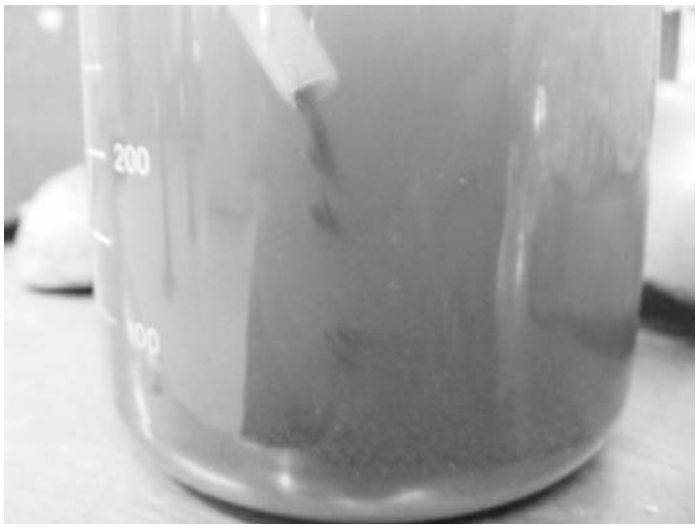


**Figure A2.4: Vessel containing solution pumped from mixing vessel**

The solution decanted from the residue was filtered, dried and kept for evaluation. The residue left behind was also kept for evaluation.

The samples obtained from the separation attempts were all visually evaluated with an Olympus SZ61 stereo microscope for the presence of separated iron globules.

These samples were also treated by means of the magnetic separation procedure described in Appendix 1 to determine whether some of the sample had lost its magnetic properties.

## A2.2 – Results and discussion

### A2.2.1 – "Heavy" dry milling

The first separation attempt involved milling a sample to see what would happen to the complex and the iron globules when milled by a high-energy mill.

The result of this attempt was that the sample became too "fine" and effectively caused the iron globules to smear together with the nitrided ilmenite complex.

The milling action seemed to have the opposite effect to what was intended. Instead of separating the iron globules from the complex, it made them "blend" into the complex and effectively made it impossible to consider mechanical separation of the iron globules from the complex.

### A2.2.2 – "Light" dry milling

The second attempt involved evaluating the effects of light grinding of the particles against each other. The idea was that the iron globules would separate from the nitrided ilmenite complex and become loose if the light grinding effect was successful.

The results showed that iron globules and other fine particles do separate from the complex, but that both substances are magnetic. This indicated that the surface of the nitrided ilmenite complex consists of small nitrided ilmenite extrusions that also came loose during the grinding action. These small complexes must therefore also contain some iron, which precluded the use of a magnetic separation procedure. Figure A2.1 is a SEM photograph of the surface of a large nitrided ilmenite complex showing both the iron globules and smaller particles present.

The precise quantity of fine particles that came loose could not be determined due to recovery losses. However, a recovery of less than 1% (mass) of the original sample is estimated.

The small quantity of iron globules liberated with "light milling" is therefore assumed to be insufficient to justify the addition of another separation step to the process.

### A2.2.3 – "Light" wet milling

The third attempt was involved evaluating the effects of natural grinding of the particles against each other in a slurry mixture.

The results obtained from this attempt agreed with those found in the previous section. Fine particles were again liberated, but this time most of them oxidised in solution to form a "rust" solution. The thick "rust" solution that was removed from the slurry can be clearly seen as it is pumped into the vessel in Figure A2.4. The iron globules that came loose oxidised in the slurry mixture due to the presence of oxygen in the water. This aerated water is the result of excessive agitation introduced by the overhead stirrer.

At first it seemed that a large amount of iron oxide (rust) had formed, but after filtration and drying, it was again found to be insufficient to justify any further investigation.

Figure A2.5 is a photograph showing the residue obtained from the wet-milling attempt; the figure also shows the presence of fine rust particles on the surface of the complex.

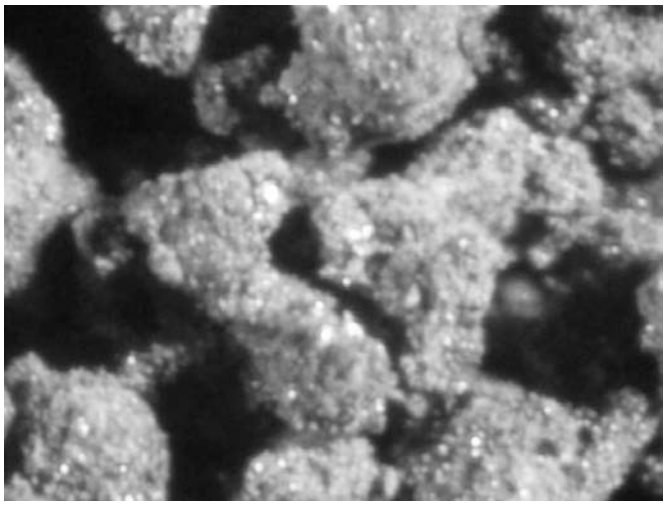

**Figure A2.5: Photograph of residue obtained from wet milling (Approx. x50 magnification)**

## A2.3 – Conclusions

The objective of this study was to determine the viability of removing iron globules from the surface of nitrided ilmenite complexes and whether it would then be possible to separate them from the sample.

Various separation attempts were evaluated. The results suggested that although it is possible to liberate the iron globules from the surface, it would be difficult to separate the them from the other fine particles that also came loose.

The overall conclusion was, however, that it is not viable to use a mechanical separation step due to the insufficient quantity of fine particles that are liberated from the nitrided ilmenite complexes. Less than 1% (mass) of the original sample is estimated to be recovered as fine particles. This is assumed not to justify the addition of another separation step to the process.

# Appendix 3 – Redox titration procedure

The titration procedure used for the determination of Fe(II) in solution is described below (Van Dyk, 1999: 143):

Add 1 ml of sample to approximately 50 ml of water. Acidify the solution with 10 ml of 50/50 $H_2SO_4/H_3PO_4$, then add five drops of diphenylamine sulphonic acid (indicator).

Titrate with 0.1 N of potassium dichromate until the solution turns purple.

The following formula can then be used to determine the Fe(II) in solution:

$$g/L\ Fe(II) = titre \times 5.585$$

* The indicator can be prepared by dissolving 0.4 g of barium diphenylamine sulphonic acid in 100 ml of water.
* The acidifying reagent can be prepared by slowly adding $H_3PO_4$ to $H_2SO_4$. The reaction is extremely exothermic and the solutions are very corrosive.

# Appendix 4 – Austpac ERMS SR process model stream tables

**Table A4.1: Stream table for streams U01-ST01 to U02-ST07**

| | U01-ST01 | U01-ST04 | U01-ST06 | U01-ST07 | U01-ST09 | U01-ST11 | U01-ST12 | U02-ST01 | U02-ST02 | U02-ST04 | U02-ST05 | U02-ST06 | U02-ST07 |
|---|---|---|---|---|---|---|---|---|---|---|---|---|---|
| TOTAL MASS (t/h) | 8.278 | 0.001 | 18.647 | 26.925 | 4.284 | 13.985 | 0.132 | 22.509 | 3.795 | 12.647 | 15.397 | 2.750 | 9.862 |
| TEMPERATURE (°C) | 30 | 25 | 90 | 90 | 25 | 80 | 25 | 90 | 100 | 100 | 100 | 90 | 140 |
| Vapour fraction | 0 | 0 | 0 | 0 | 0 | 0 | 0 | 0 | 1 | 1 | 1 | 1 | 0 |
| GAS PHASE ($Nm^3/h$) | | | | | | | | | | | | | |
| $N_2(g)$ | | | | | | | | | 2 338 | | 829 | 829 | |
| $CO(g)$ | | | | | | | | | | | | | |
| $H_2(g)$ | | | | | | | | | | | | | |
| $CO_2(g)$ | | | | | | | | | | | | | |
| $O_2(g)$ | | | | | | | | | 611 | | | | |
| $HCl(g)$ | | | | | | | | | | 230 | 230 | | |
| $H_2O(g)$ | | | | | | | | | | 15 268 | 17 399 | 2 131 | |
| WATER PHASE (t/h) | | | | | | | | | | | | | |
| $H_2O$ | | | 13.985 | 15.045 | | 13.985 | | 15.045 | | | | | |
| Cl(-) | | 0.001 | 4.533 | 4.525 | | | | 4.525 | | | | | |
| Fe(+2) | | | | 2.161 | | | | 2.161 | | | | | |
| Fe(+3) | | | | 0.664 | | | | 0.664 | | | | | |
| H(+) | | 0.000 | 0.129 | 0.010 | | | | 0.010 | | | | | |
| Al(+3) | | | | 0.008 | | | | 0.008 | | | | | |
| Mg(+2) | | | | 0.021 | | | | 0.021 | | | | | |

**Stream table for streams U01-ST01 to U02-ST07 – Part 2**

| | U01-ST01 | U01-ST04 | U01-ST06 | U01-ST07 | U01-ST09 | U01-ST11 | U01-ST12 | U02-ST01 | U02-ST02 | U02-ST04 | U02-ST05 | U02-ST06 | U02-ST07 |
|---|---|---|---|---|---|---|---|---|---|---|---|---|---|
| WATER PHASE continued | | | | | | | | | | | | | |
| Mn(+2) | | | | 0.039 | | | | 0.039 | | | | | |
| Ca(+2) | | | | 0.000 | | | | 0.000 | | | | | |
| $VO_2$(+) | | | | 0.020 | | | | 0.020 | | | | | |
| $TiCl_2O$(aq) | | | | 0.008 | | | | 0.008 | | | | | |
| $CrCl_3$(aq) | | | | 0.005 | | | | 0.005 | | | | | |
| PURE SUBSTANCES (t/h) | | | | | | | | | | | | | |
| $FeCl_2*2H_2O$ | | | | | | | | | | | | | 6.300 |
| $FeCl_3*6H_2O$ | | | | | | | | | | | | | 3.216 |
| $FeCl_2$ | | | | | | | | | | | | | |
| $FeCl_3$ | | | | | | | | | | | | | |
| C | | | | | | | | | | | | | |
| $TiO_2$ | 4.173 | | | 4.168 | 4.168 | | | | | | | | 0.005 |
| FeO | 2.823 | | | 0.042 | | | 0.042 | | | | | | |
| Fe | | | | | | | | | | | | | |
| $Fe_2O_3$ | 1.002 | | | 0.052 | 0.046 | | 0.006 | | | | | | |
| $Al_2O_3$ | 0.046 | | | 0.030 | 0.006 | | 0.024 | | | | | | |
| MgO | 0.055 | | | 0.020 | 0.001 | | 0.019 | | | | | | |
| MnO | 0.051 | | | 0.000 | 0.000 | | 0.000 | | | | | | |
| CaO | 0.003 | | | 0.003 | 0.000 | | 0.002 | | | | | | |
| $V_2O_5$ | 0.023 | | | 0.001 | 0.001 | | 0.000 | | | | | | |

**Stream table for streams U01-ST01 to U02-ST07 – Part 3**

| | U01-ST01 | U01-ST04 | U01-ST06 | U01-ST07 | U01-ST09 | U01-ST11 | U01-ST12 | U02-ST01 | U02-ST02 | U02-ST04 | U02-ST05 | U02-ST06 | U02-ST07 |
|---|---|---|---|---|---|---|---|---|---|---|---|---|---|
| PURE SUBSTANCES continued | | | | | | | | | | | | | |
| $SiO_2$ | 0.063 | | | 0.063 | 0.034 | | 0.029 | | | | | | |
| $P_2O_5$ | 0.001 | | | 0.001 | 0.001 | | 0.000 | | | | | | |
| $Nb_2O_5$ | 0.009 | | | 0.009 | 0.009 | | | | | | | | |
| $ZrO_2$ | 0.003 | | | 0.003 | 0.000 | | 0.003 | | | | | | |
| $Cr_2O_3$ | 0.007 | | | 0.004 | 0.001 | | 0.004 | | | | | | |
| Other | 0.019 | | | 0.019 | 0.016 | | 0.003 | | | | | | |
| $AlCl_3*6H_2O$ | | | | | | | | | | | | | 0.076 |
| $MgCl_2*2H_2O$ | | | | | | | | | | | | | 0.115 |
| $MnCl_2*2H_2O$ | | | | | | | | | | | | | 0.115 |
| $CaCl_2*2H_2O$ | | | | | | | | | | | | | 0.001 |
| $VO_2Cl$ | | | | | | | | | | | | | 0.029 |
| $AlCl_3$ | | | | | | | | | | | | | |
| $MgCl_2$ | | | | | | | | | | | | | |
| $MnCl_2$ | | | | | | | | | | | | | |
| $CaCl_2$ | | | | | | | | | | | | | |
| $CrCl_3$ | | | | | | | | | | | | | 0.005 |
| Amount Phase 1 (t/h) | | | | | | | | | 3.795 | 12.647 | 15.397 | 2.750 | |
| Amount Phase 2 (t/h) | | 0.001 | 18.647 | 22.509 | | 13.985 | | 22.509 | | | | | |
| Amount Phase 3 (t/h) | 8.278 | | | 4.416 | 4.284 | | 0.132 | | | | | | 9.862 |

**Stream table for streams U01-ST01 to U02-ST07 – Part 4**

| | U01-ST01 | U01-ST04 | U01-ST06 | U01-ST07 | U01-ST09 | U01-ST11 | U01-ST12 | U02-ST01 | U02-ST02 | U02-ST04 | U02-ST05 | U02-ST06 | U02-ST07 |
|---|---|---|---|---|---|---|---|---|---|---|---|---|---|
| ENTHALPY TOTAL (kWh) | -18 995 | -0.70 | -66 769 | -87 099 | -13 976 | -60 741 | -387 | -75 331 | 80 | -45 538 | -51 835 | -6 309 | -18 188 |
| ENTHALPY Phase 1 | | | | | | | | | 80.18 | -45 538 | -51 835 | -6 309 | |
| ENTHALPY Phase 2 | | -0.70 | -66 769 | -72 814 | | -60 741 | | -75 331 | | | | | |
| ENTHALPY Phase 3 | -18 995 | | | -14 284 | -13 976 | | -387 | | | | | | -18 188 |
| GAS DENSITY (kg/m$^3$) | | | | | | | | | 1.29 | 0.82 | 0.83 | 0.93 | |
| WATER DENSITY | 995.61 | 13 18.8 | 10 84.9 | 1 288.5 | 999.80 | 971.67 | 999.80 | 1 345.5 | 958.40 | 958.40 | 958.40 | 965.20 | 929.74 |
| SOLID DENSITY | 48 07.3 | | | 4 223.2 | 4 229.9 | | 4 018.2 | | | | | | 2 391.1 |
| VOLUME Total (m$^3$/h) | 1.722 | 0.000 | 17.187 | 18.513 | 1.013 | 14.393 | 0.033 | 16.729 | | | | | 4.124 |
| VOLUME Phase 2 | | 0.000 | 17.187 | 17.468 | | 14.393 | | 16.729 | | | | | |
| VOLUME Phase 3 | 1.722 | | | 1.046 | 1.013 | | 0.033 | | | | | | 4.124 |
| WATER PHASE mass fraction | | | | | | | | | | | | | |
| HCl | | 1.00 | 0.25 | 0.02 | | | | 0.02 | | | | | |
| $FeCl_2$ | | | | 0.22 | | | | 0.22 | | | | | |
| $FeCl_3$ | | | | 0.09 | | | | 0.09 | | | | | |
| $AlCl_3$ | | | | 0.00 | | | | 0.00 | | | | | |
| $MgCl_2$ | | | | 0.00 | | | | 0.00 | | | | | |
| $MnCl_2$ | | | | 0.00 | | | | 0.00 | | | | | |
| $CaCl_2$ | | | | 0.00 | | | | 0.00 | | | | | |

**Table A4.2: Stream table for streams U02-ST08 to U03-ST08**

| | U02-ST08 | U02-ST09 | U02-ST10 | U02-ST11 | U02-ST12 | U02-ST15 | U02-ST16 | U03-ST01 | U03-ST02 | U03-ST03 | U03-ST04 | U03-ST05 | U03-ST07 | U03-ST08 |
|---|---|---|---|---|---|---|---|---|---|---|---|---|---|---|
| TOTAL MASS (t/h) | 4.172 | 7.036 | 18.646 | 13.985 | 14.360 | 1.037 | 15.654 | 1.567 | 9.078 | 3.767 | 11.049 | 11.858 | 2.958 | 1.347 |
| TEMPERATURE (°C) | 940 | 100 | 70 | 80 | 70 | 80 | 160 | 25 | 40 | 950 | 950 | 930 | 200 | 25 |
| Vapour fraction | 0 | 1 | 0 | 0 | 0 | 1 | 1 | 0 | 1 | 0 | 1 | 1 | 0 | 1 |
| GAS PHASE ($Nm^3/h$) | | | | | | | | | | | | | | |
| $N_2(g)$ | | 829 | | | | 829 | 7 931 | | 5 593 | | 5 593 | 5 593 | | 829 |
| CO(g) | | | | | | | | | | | 2 356 | 1 222 | | |
| $H_2(g)$ | | | | | | | | | | | | | | |
| $CO_2(g)$ | | | | | | | 2 923 | | | | 567 | 1 701 | | |
| $O_2(g)$ | | | | | | | | | 1 461 | | | | | 216 |
| HCl(g) | | 2 634 | | | | | | | | | | | | |
| $H_2O(g)$ | | 2 131 | | | | | | | | | | | | |
| WATER PHASE (t/h) | | | | | | | | | | | | | | |
| $H_2O$ | | | 13.985 | 13.985 | 13.985 | | | | | | | | | |
| Cl(-) | | | 4.532 | | 0.365 | | | | | | | | | |
| Fe(+2) | | | | | | | | | | | | | | |
| Fe(+3) | | | | | | | | | | | | | | |
| H(+) | | | 0.129 | | 0.010 | | | | | | | | | |
| Al(+3) | | | | | | | | | | | | | | |
| Mg(+2) | | | | | | | | | | | | | | |

**Stream table for streams U02-ST08 to U03-ST08 – Part 2**

| | U02-ST08 | U02-ST09 | U02-ST10 | U02-ST11 | U02-ST12 | U02-ST15 | U02-ST16 | U03-ST01 | U03-ST02 | U03-ST03 | U03-ST04 | U03-ST05 | U03-ST07 | U03-ST08 |
|---|---|---|---|---|---|---|---|---|---|---|---|---|---|---|
| WATER PHASE continued | | | | | | | | | | | | | | |
| Mn(+2) | | | | | | | | | | | | | | |
| Ca(+2) | | | | | | | | | | | | | | |
| $VO_2$(+) | | | | | | | | | | | | | | |
| $TiCl_2O$(aq) | | | | | | | | | | | | | | |
| $CrCl_3$(aq) | | | | | | | | | | | | | | |
| PURE SUBSTANCES (t/h) | | | | | | | | | | | | | | |
| $FeCl_2*2H_2O$ | | | | | | | | | | | | | | |
| $FeCl_3*6H_2O$ | | | | | | | | | | | | | | |
| $FeCl_2$ | | | | | | | | | | | | | | |
| $FeCl_3$ | | | | | | | | | | | | | | |
| C | | | | | | | | 1.567 | | | | | | |
| $TiO_2$ | 0.005 | | | | | | | | | 0.005 | | | 0.005 | |
| FeO | | | | | | | | | | 3.635 | | | | |
| Fe | | | | | | | | | | | | | 2.826 | |
| $Fe_2O_3$ | 4.040 | | | | | | | | | | | | | |
| $Al_2O_3$ | 0.016 | | | | | | | | | 0.016 | | | 0.016 | |
| MgO | 0.035 | | | | | | | | | 0.035 | | | 0.035 | |
| MnO | 0.051 | | | | | | | | | 0.051 | | | 0.051 | |
| CaO | | | | | | | | | | | | | | |
| $V_2O_5$ | 0.022 | | | | | | | | | 0.022 | | | 0.022 | |

**Stream table for streams U02-ST08 to U03-ST08 – Part 3**

| | U02-ST08 | U02-ST09 | U02-ST10 | U02-ST11 | U02-ST12 | U02-ST15 | U02-ST16 | U03-ST01 | U03-ST02 | U03-ST03 | U03-ST04 | U03-ST05 | U03-ST07 | U03-ST08 |
|---|---|---|---|---|---|---|---|---|---|---|---|---|---|---|
| PURE SUBSTANCES (t/h) | | | | | | | | | | | | | | |
| $SiO_2$ | | | | | | | | | | | | | | |
| $P_2O_5$ | | | | | | | | | | | | | | |
| $Nb_2O_5$ | | | | | | | | | | | | | | |
| $ZrO_2$ | | | | | | | | | | | | | | |
| $Cr_2O_3$ | 0.003 | | | | | | | | | 0.003 | | | 0.003 | |
| Other | | | | | | | | | | | | | | |
| $AlCl_3*6H_2O$ | | | | | | | | | | | | | | |
| $MgCl_2*2H_2O$ | | | | | | | | | | | | | | |
| $MnCl_2*2H_2O$ | | | | | | | | | | | | | | |
| $CaCl_2*2H_2O$ | | | | | | | | | | | | | | |
| $VO_2Cl$ | | | | | | | | | | | | | | |
| $AlCl_3$ | | | | | | | | | | | | | | |
| $MgCl_2$ | | | | | | | | | | | | | | |
| $MnCl_2$ | | | | | | | | | | | | | | |
| $CaCl_2$ | 0.001 | | | | | | | | | 0.001 | | | 0.001 | |
| $CrCl_3$ | | | | | | | | | | | | | | |
| Amount Phase 1 (t/h) | | 7.036 | | | | 1.037 | 15.654 | | 9.078 | | 11.049 | 11.858 | | 1.347 |
| Amount Phase 2 (t/h) | | | 18.646 | 13.985 | 14.360 | | | | | | | | | |
| Amount Phase 3 (t/h) | 4.172 | | | | | | | 1.567 | | 3.767 | | | 2.958 | |

**Stream table for streams U02-ST08 to U03-ST08 – Part 4**

| | U02-ST08 | U02-ST09 | U02-ST10 | U02-ST11 | U02-ST12 | U02-ST15 | U02-ST16 | U03-ST01 | U03-ST02 | U03-ST03 | U03-ST04 | U03-ST05 | U03-ST07 | U03-ST08 |
|---|---|---|---|---|---|---|---|---|---|---|---|---|---|---|
| ENTHALPY TOTAL (kWh) | -5 229 | -9 240 | -67 016 | -60 741 | -61 396 | 16 | -13 674 | | 38 | -3 426 | -2 813 | -6 639 | -298 | |
| ENTHALPY Phase 1 | | -9 240 | | | | 16 | -13 674 | | 38 | | -2 813 | -6 639 | | |
| ENTHALPY Phase 2 | | | -67 016 | -60 741 | -61 396 | | | | | | | | | |
| ENTHALPY Phase 3 | -5 229 | | | | | | | | | -3 426 | | | -298 | |
| GAS DENSITY (kg/m$^3$) | | 1.26 | | | | 1.25 | 1.44 | | 1.29 | | 1.30 | 1.39 | | 1.29 |
| WATER DENSITY | 9 011 | 958 | 1 095 | 971 | 989 | 971 | 915 | 996 | 992 | 9 327 | 9 327 | 8 704 | 893 | 996 |
| SOLID DENSITY | 5 196 | | | | | | | 2 260 | | 5 907 | | | 7 557 | |
| VOLUME total (m$^3$/h) | 0.803 | | 17.018 | 14.393 | 14.507 | | | 0.693 | | 0.638 | | | 0.391 | |
| VOLUME Phase 2 | | | 17.018 | 14.393 | 14.507 | | | | | | | | | |
| VOLUME Phase 3 | 0.803 | | | | | | | 0.693 | | 0.638 | | | 0.391 | |
| WATER PHASE mass fraction | | | | | | | | | | | | | | |
| HCl | | | 0.25 | | 0.03 | | | | | | | | | |
| $FeCl_2$ | | | | | | | | | | | | | | |
| $FeCl_3$ | | | | | | | | | | | | | | |
| $AlCl_3$ | | | | | | | | | | | | | | |
| $MgCl_2$ | | | | | | | | | | | | | | |
| $MnCl_2$ | | | | | | | | | | | | | | |
| $CaCl_2$ | | | | | | | | | | | | | | |

# Appendix 5 – Experimental data

**Table A5.1: Chemical compositions of feed (as received from UIS Analytical)**

| Constituent | Sample 1 | Sample 2 | Sample 3 |
|---|---|---|---|
| $SiO_2$ | 3.43 | 3.41 | 3.42 |
| $Al_2O_3$ | 1.78 | 1.79 | 1.88 |
| Fe(tot) | 44.60 | 43.40 | 44.10 |
| $Fe_2O_3$ | 63.80 | 62.10 | - |
| Ti(tot) | - | - | 32.11 |
| $TiO_2$ | 51.70 | 53.00 | - |
| CaO | 0.07 | 0.13 | 0.19 |
| MgO | 0.58 | 0.61 | 0.62 |
| $K_2O$ | 0.03 | 0.04 | 0.02 |
| MnO | 1.19 | 1.24 | 1.26 |
| $P_2O_5$ | 0.03 | 0.03 | 0.08 |
| $V_2O_5$ | 0.18 | 0.18 | 0.18 |
| C | 3.45 | 3.40 | 2.99 |
| S | 0.13 | 0.15 | 0.34 |

**Table A5.2: 11% HCl, 25 °C, 20% excess acid (data)**

| Exp # | Time duration (min) | Initial mass (g) | Initial reaction volume (ml) | Reaction volume lost (ml) | Residue mass (g) | Volume titrate required (ml) |
|---|---|---|---|---|---|---|
| | 0 | | | | | |
| | 5 | 7.82 | 50 | 0 | N.A. | 2.56 |
| 43 | 10 | 7.80 | 50 | 0 | N.A. | 4.32 |
| | 20 | 7.81 | 50 | 0 | N.A. | 5.94 |
| 67 | 40 | 15.64 | 100 | 1 | 9.72 | 10.90 |
| 68 | 80 | 15.60 | 100 | 2 | 8.96 | 12.12 |
| 66 | 120 | 15.60 | 100 | 2 | 8.96 | 12.14 |

**Table A5.3: 11% HCl, 60 °C, 20% excess acid (data)**

| Exp # | Time (min) | Initial mass (g) | Initial reaction volume (ml) | Reaction volume lost (ml) | Residue mass (g) | Volume titrant required (ml) |
|---|---|---|---|---|---|---|
| | 0 | | | | | |
| | 5 | 7.83 | 50 | 0 | N.A. | 4.00 |
| 45 | 10 | 7.80 | 50 | 0 | N.A. | 6.79 |
| | 20 | 7.80 | 50 | 0 | N.A. | 9.04 |
| 64 | 40 | 15.61 | 100 | 5 | 8.93 | 12.90 |
| 65 | 80 | 15.60 | 100 | 5 | 8.77 | 13.17 |

**Table A5.4: 11% HCl, 90 °C, 20% excess acid (data)**

| Exp # | Time (min) | Initial mass (g) | Initial reaction volume (ml) | Reaction volume lost (ml) | Residue mass (g) | Volume titrant required (ml) |
|---|---|---|---|---|---|---|
| | 0 | | | | | |
| 46 | 5 | 7.82 | 50 | 0.0 | N.A. | 6.34 |
| | 10 | 7.82 | 50 | 0.0 | N.A. | 8.00 |
| 71 | 25 | 15.61 | 100 | 6.0 | N.A. | 11.66 |
| 59 | 40 | 15.61 | 100 | 9.0 | 8.78 | 13.68 |
| 48 | 60 | 15.60 | 100 | 1.5 | 9.24 | 12.74 |
| 63 | 90 | 15.59 | 100 | 8.0 | 8.67 | 13.98 |

**Table A5.5: 18% HCl, 90 °C, 20% excess acid (data)**

| Exp # | Time (min) | Initial mass (g) | Initial reaction volume (ml) | Reaction volume lost (ml) | Residue mass (g) | Volume titrant required (ml) |
|---|---|---|---|---|---|---|
| | 0 | | | | | |
| 69 | 5 | 13.20 | 50 | 0 | N.A. | 14.23 |
| | 10 | 13.20 | 50 | 0 | N.A. | 15.96 |
| 72 | 25 | 26.43 | 100 | 6 | N.A. | 21.08 |
| 60 | 40 | 26.43 | 100 | 7 | 15.12 | 22.88 |
| 51 | 60 | 26.42 | 100 | 4 | 16.23 | 22.31 |
| 36, 39, 40 | 90 | 132.00 | 500 | 8 | N.A. | N.A. |

**Table A5.6: 25% HCl, 90 °C, 20% excess acid (data)**

| Exp # | Time (min) | Initial mass (g) | Initial reaction volume (ml) | Reaction volume lost (ml) | Residue mass (g) | Volume titrant required (ml) |
|---|---|---|---|---|---|---|
| | 0 | | | | | |
| 70 | 5 | 18.90 | 50 | 0 | N.A. | 17.23 |
| | 10 | 18.90 | 50 | 0 | N.A. | 21.64 |
| 73 | 25 | 37.84 | 100 | 6 | N.A. | 29.56 |
| 61 | 40 | 37.80 | 100 | 7 | 21.95 | 31.97 |
| 54 | 60 | 37.80 | 100 | 1 | 23.93 | 30.72 |
| 62 | 90 | 37.84 | 100 | 7 | 21.24 | 33.06 |

**Table A5.7: Dissolution of other species (data)**

| HCl (%) | Excess acid (%) | Slurry wt % | Solid/ liquid (g/ml) | Exp # | Initial mass (g) | Reaction volume lost (ml) | Residue mass (g) | Volume titrate required (ml) |
|---|---|---|---|---|---|---|---|---|
| 11 | 0 | 16% | 0.20 | 47 | 19.5 | 8.5 | 11.56 | 17.08 |
| | 20 | 13% | 0.16 | 48 | 15.6 | 1.5 | 9.24 | 12.74 |
| | 40 | 10% | 0.12 | 49 | 11.7 | 4.0 | 7.11 | 9.86 |
| 18 | 0 | 23% | 0.33 | 50 | 33.0 | 5.5 | 20.67 | 28.02 |
| | 20 | 20% | 0.26 | 51 | 26.4 | 4.0 | 16.23 | 22.31 |
| | 40 | 15% | 0.20 | 52 | 19.8 | 1.0 | 11.72 | 16.10 |
| 25 | 0 | 30% | 0.47 | 53 | 47.4 | 2.5 | 29.82 | 38.96 |
| | 20 | 25% | 0.38 | 54 | 37.8 | 1.0 | 23.93 | 30.72 |
| | 40 | 20% | 0.29 | 55 | 28.5 | 0.0 | 17.42 | 22.84 |

**Table A5.8: Experimental error for experimental setup #1**

**(18 wt % HCl, 90 °C, $d_{50}$= 185 µm, 100 r/min, 2.5:1 HCl-Fe mole ratio)**

| Exp # | Time (min) | Initial mass (g) | Initial volume (ml) | Volume lost (ml) | Residue mass (g) | Volume titrate required (ml) |
|---|---|---|---|---|---|---|
| 36 | 35 | 132 | 500 | 0 | N.A. | 20.49 |
| 39 | 35 | 132 | 500 | 0 | N.A. | 20.35 |
| 40 | 36 | 132 | 500 | 3 | N.A. | 21.01 |

**Table A5.9: Experimental error for experimental setup #2**

**(11 wt % HCl, 25 °C, $d_{50}$= 185 µm, 25 ml/min, 2.5:1 HCl-Fe mole ratio)**

| Exp # | Time (min) | Initial mass (g) | Initial volume (ml) | Volume lost (ml) | Residue mass (g) | Volume titrate required (ml) |
|---|---|---|---|---|---|---|
| 43 | 5 | 7.82 | 50 | 0 | N.A. | 2.56 |
| 74 | 5 | 7.82 | 50 | 0 | N.A. | 2.66 |
| 75 | 5 | 7.81 | 50 | 0 | N.A. | 2.48 |
| 76 | 5 | 7.84 | 50 | 0 | N.A. | 2.52 |

# Appendix 6 – Calculation examples

## A6.1 – Calculation of experimental error

The experimental error was calculated as follows:

Step 1: Calculate the mean of the data set. This is done with the following equation:

$$\bar{x} = \frac{1}{N}\sum_{i=1}^{N} x_i \qquad [A6.1]$$

where N is the total number of data points and $x_i$ is an individual data point.

Step 2: Calculate the standard deviation of the data set as follows:

$$s = \sqrt{\frac{\sum_{i=1}^{N}\left(x_i - \bar{x}\right)^2}{N-1}} \qquad [A6.2]$$

Step 3: Calculate the standard error of the mean with the following equation:

$$\text{standard } error\ of\ the\ mean = SE = \frac{s}{\sqrt{N}} \qquad [A6.3]$$

Step 4: Calculate the z critical value for a 95% confidence level, i.e. there is a 95% probability that the data points obtained from the experiments lie within the range of the calculated confidence interval. The z critical value is calculated as follows:

$$z = \frac{\bar{x} - \mu}{s/\sqrt{n}} \qquad [A6.4]$$

where μ is the mean value for continuous variable x and n is the number of data points.

Step 5: Calculate the confidence interval with the following equation:

$$\text{confidence interval} = \bar{x} \pm \left(SE \times z\right) \qquad [A6.5]$$

Step 6: Calculate the experimental error with the following equation:

$$Experimental\ error = \frac{2 \times \text{Confidence interval}}{\bar{x}} \times 100 \qquad [A6.6]$$

Table A6.1 shows the calculation of an experimental error.

**Table A6.1: Calculation of the experimental error**

**(18 wt % HCl, 90 °C, $d_{50}$= 185 µm, 100 r/min, 2.5:1 HCl-Fe mole ratio)**

| **Experiment #** | **Experimental Fe conversion** (%) |
|---|---|
| 36 | 93.76 |
| 39 | 93.12 |
| 40 | 95.57 |
| **Average conversion** (%) | 94.15 |
| **Standard deviation** | 1.27 |
| **z critical value** | 3.18 |
| **Confidence interval** (%) | 94.15 ± 4.67 |
| **Experimental error** (%) | 4.96 |

## A6.2 – Derivation of "combined resistance" rate law

*From* Equation 4:

$$-r''_{HCl} = \frac{-1}{S_{ex}} \cdot \frac{dN_{HCl}}{dt} = \bar{k}''_{combined} \cdot C_{HCl,bulk}$$

$$\therefore \frac{-dN_{HCl}}{dt} = S_{ex} \cdot \bar{k}''_{combined} \cdot C_{HCl,bulk}$$

$$and\ \ C_{HCl,bulk} = \frac{N_{HCl,bulk}}{V}$$

*Assume* $H_2$ (g) evolution has negligible effect on reaction volume (V)

$\therefore\ V = V_0$ (i.e. constant reaction volume)

$$\therefore\ \frac{-dN_{HCl}}{dt} = \frac{S_{ex} \cdot \bar{k}''_{combined}}{V_0} \cdot N_{HCl,bulk}$$

$$set\ \alpha = \frac{S_{ex} \cdot \bar{k}''_{combined}}{V_0}$$

$$\therefore\ \frac{-dN_{HCl}}{dt} = \alpha \cdot N_{HCl,bulk} \quad \ldots\ldots\ldots\ldots\ldots\ldots\ldots\ldots\ldots\ldots\ldots\ldots\ldots\ldots\ldots\ldots\ [1]$$

Integrate Equation [1]

$$\therefore\ -\int_{N_{HCl,0}}^{N_{HCl}} \frac{1}{N_{HCl}} dN_{HCl} = \alpha \int_{t=0}^{t} dt \quad \ldots\ldots\ldots\ldots\ldots\ldots\ldots\ldots\ldots\ldots\ldots\ldots\ldots\ldots\ [2]$$

*Equation* [2] becomes:

$$-\ln\left(\frac{N_{HCl}}{N_{HCl,0}}\right) = \alpha \cdot t$$

but

$$\frac{N_{HCl}}{N_{HCl,0}} = 1 - X_{HCl}$$

*and*

$$X_{HCl} = \frac{N_{HCl,0} - N_{HCl}}{N_{HCl,0}}$$

*Iron* is the limiting reactant, but hydrochloric acid is the basis for calculation

$\therefore$ from stoichiometry ($1HCl + 0.5Fe(s) \rightarrow 0.5FeCl_2 + 0.5H_2(g)$, *set* $b = 0.5$)

$$N_{HCl} = \frac{N_{Fe}}{b}$$

$$\therefore \quad -\ln\left(1 - \frac{N_{HCl,0} - \frac{N_{Fe}}{b}}{N_{HCl,0}}\right) = \alpha \cdot t$$

$$with \ \alpha = \frac{S_{ex} \cdot \bar{k}''_{combined}}{V_0}$$

$\therefore$ this equation can be used to solve $\bar{k}''_{combined}$

## A6.3 – Derivation of "combined resistance" conversion equation

$$-\ln\left(1 - \frac{N_{HCL,0} - N_{Fe}/b}{N_{HCL,0}}\right) = \frac{S_{ex} \cdot \bar{k}''_{combined}}{V_0} \cdot t$$

and $N_{Fe} = N_{Fe,0}(1 - X_{Fe})$

$$\therefore \quad -\ln\left(1 - \frac{N_{HCL,0} - \frac{N_{Fe,0}}{b} \cdot (1 - X_{Fe})}{N_{HCL,0}}\right) = \frac{S_{ex} \cdot \bar{k}''_{combined}}{V_0} \cdot t \quad \ldots\ldots\ldots\ldots\ldots\ldots \quad [1]$$

*take the* antilog on both sides

$$\therefore \quad 1-\frac{N_{HCL,0}-\frac{N_{Fe,0}}{b}\cdot(1-X_{Fe})}{N_{HCL,0}}=\exp(-\alpha\cdot t) \quad \text{.....} \quad [2]$$

$$\text{with} \quad \alpha=\frac{S_{ex}\cdot\bar{k}''_{\text{combined}}}{V_0}$$

*after* simplification and re - arangement Equation [2] becomes

$$X_{Fe}=1-\frac{N_{HCL,0}\cdot b}{N_{Fe,0}}\cdot\exp(-\alpha\cdot t)$$

$$\text{with} \quad \alpha=\frac{4\cdot\pi\cdot R_0^2\cdot\bar{k}''_{\text{combined}}(T)}{V} \qquad \text{.....} \qquad [3]$$

*and*, from Equation 12

$$\bar{k}''_{\text{combined}}(T)=1848\cdot\exp\left(\frac{-1137.2}{T}\right)$$

substitute Equation 12 into Equation [3], and simplify

$$\therefore \quad X_{Fe}=1-\frac{N_{HCL,0}\cdot b}{N_{Fe,0}}\cdot\exp(\beta\cdot\phi)$$

$$\text{with } \beta=\frac{-23222.6\cdot R_0{}^2\cdot t}{V} \qquad \text{(t, minutes)}$$

$$\phi=\exp\left(\frac{-1137.2}{T}\right) \qquad \text{(T, Kelvin)}$$

# Appendix 7 – Results

**Table A7.1: 11% HCl, 25 °C, 20% excess acid (results)**

| Time (min) | g/l Fe(II) adjusted | Exp. Conversion (%) | Constant size ash diffusion | constant size reaction | Combined resistance | Calculated conversion (%) |
|---|---|---|---|---|---|---|
| 0 | 0.0 | 0 | 0.000 | 0.000 | 0.225 | 0 |
| 5 | 14.0 | 20 | 0.014 | 0.071 | 0.446 | 20 |
| 10 | 23.7 | 33 | 0.044 | 0.127 | 0.632 | 35 |
| 20 | 32.5 | 46 | 0.090 | 0.185 | 0.841 | 58 |
| 40 | 59.1 | 83 | 0.425 | 0.450 | 2.030 | 83 |
| 80 | 65.0 | 92 | 0.603 | 0.569 | | |
| 120 | 65.1 | 92 | 0.607 | 0.572 | | |

**Table A7.2: 11% HCl, 60 °C, 20% excess acid (results)**

| Time (min) | g/l Fe(II) adjusted | Exp. Conversion (%) | Constant size ash diffusion | constant size reaction | Combined resistance | Calculated conversion (%) |
|---|---|---|---|---|---|---|
| 0 | 0.0 | 0 | 0.000 | 0.000 | 0.225 | 0 |
| 5 | 21.9 | 31 | 0.037 | 0.116 | 0.595 | 28 |
| 10 | 37.2 | 53 | 0.124 | 0.220 | 0.971 | 48 |
| 20 | 49.5 | 70 | 0.256 | 0.331 | 1.429 | 73 |
| 40 | 67.1 | 95 | 0.687 | 0.628 | 3.201 | 93 |
| 80 | 68.5 | 97 | 0.766 | 0.686 | | |

**Table A7.3: 11% HCl, 90 °C, 20% excess acid (results)**

| Time (min) | g/l Fe(II) adjusted | Exp. Conversion (%) | Constant size ash diffusion | constant size reaction | Combined resistance | Calculated conversion (%) |
|---|---|---|---|---|---|---|
| 0 | 0.0 | 0 | 0.000 | 0.000 | 0.224 | 0 |
| 5 | 34.7 | 49 | 0.105 | 0.201 | 0.900 | 35 |
| 10 | 43.8 | 62 | 0.185 | 0.274 | 1.190 | 58 |
| 25 | 60.0 | 85 | 0.450 | 0.467 | 2.113 | 89 |
| 40 | 68.2 | 96 | 0.743 | 0.668 | 3.546 | 97 |
| 60 | 68.7 | 97 | 0.778 | 0.696 | | |
| 90 | 70.4 | 100 | 0.940 | 0.850 | | |

**Table A7.4: 18% HCl, 90 °C, 20% excess acid (results)**

| **Time** (min) | **g/l Fe(II) adjusted** | **Exp. Conversion** (%) | **Constant size ash diffusion** | **Constant size reaction** | **Combined resistance** | **Calculated conversion** (%) |
|---|---|---|---|---|---|---|
| 0 | 0.0 | 0 | 0.000 | 0.000 | 0.223 | 0 |
| 5 | 77.9 | 65 | 0.211 | 0.296 | 1.274 | 35 |
| 10 | 87.4 | 73 | 0.287 | 0.354 | 1.531 | 58 |
| 25 | 108.5 | 91 | 0.567 | 0.545 | 2.586 | 89 |
| 40 | 116.5 | 97 | 0.782 | 0.699 | 3.825 | 97 |
| 60 | 117.3 | 98 | 0.815 | 0.726 | | |
| 90 | 118.5 | 99 | 0.881 | 0.785 | | |

**Table A7.5: 25% HCl, 90 °C, 20% excess acid (results)**

| **Time** (min) | **g/l Fe(II) adjusted** | **Exp. Conversion** (%) | **Constant size ash diffusion** | **Constant size reaction** | **Combined resistance** | **Calculated conversion** (%) |
|---|---|---|---|---|---|---|
| 0 | 0.0 | 0 | 0.000 | 0.000 | 0.225 | 0 |
| 5 | 94.3 | 55 | 0.139 | 0.234 | 1.024 | 35 |
| 10 | 118.5 | 69 | 0.247 | 0.324 | 1.400 | 58 |
| 25 | 152.1 | 89 | 0.525 | 0.517 | 2.411 | 89 |
| 40 | 162.8 | 95 | 0.694 | 0.632 | 3.215 | 97 |
| 60 | 166.5 | 97 | 0.779 | 0.696 | | |
| 90 | 168.3 | 98 | 0.828 | 0.736 | | |

**Table A7.6: Dissolution of other species (liquor analysis results)**

| **wt %** | **11% HCl** | | | **18% HCl** | | | **25% HCl** | | |
|---|---|---|---|---|---|---|---|---|---|
| % excess | 0 | 20 | 40 | 0 | 20 | 40 | 0 | 20 | 40 |
| Al | 1.85 | 2.23 | 2.49 | 1.85 | 2.39 | 2.98 | 2.14 | 2.99 | 3.57 |
| Ca | 0.08 | 0.14 | 0.17 | 0.03 | 0.06 | 0.08 | 0.01 | 0.03 | 0.05 |
| Mg | 0.88 | 1.01 | 1.76 | 0.38 | 0.68 | 1.20 | 0.17 | 0.49 | 0.84 |
| Fe | 96.80 | 97.20 | 97.7 | 96.90 | 97.90 | 97.20 | 96.80 | 97.20 | 96.60 |
| Ti | 0.06 | 0.09 | 0.11 | 0.08 | 0.13 | 0.19 | 0.11 | 0.27 | 0.44 |
| **g/l Species in solution** (adjusted)**:** | | | | | | | | | |
| Al | 0.036 | 0.034 | 0.029 | 0.060 | 0.062 | 0.058 | 0.100 | 0.112 | 0.101 |
| Ca | 0.015 | 0.020 | 0.018 | 0.010 | 0.014 | 0.014 | 0.006 | 0.011 | 0.013 |
| Mg | 0.006 | 0.006 | 0.008 | 0.005 | 0.007 | 0.009 | 0.003 | 0.007 | 0.009 |
| Fe | 85.560 | 68.700 | 51.82 | 144.97 | 117.26 | 87.27 | 207.98 | 166.51 | 125.05 |
| Ti | 0.040 | 0.046 | 0.041 | 0.083 | 0.112 | 0.124 | 0.170 | 0.330 | 0.407 |

**Table A7.7: Dissolution of other species (solids composition results)**

| Exp. # / Constituent | 47 | 48 | 49 | 50 | 51 | 52 | 53 | 54 | 55 |
|---|---|---|---|---|---|---|---|---|---|
| $SiO_2$ | 5.03 | 5.02 | 5.22 | 5.58 | 5.75 | 5.72 | 5.78 | 5.75 | 5.76 |
| $Al_2O_3$ | 3.40 | 3.43 | 3.56 | 3.51 | 3.61 | 3.56 | 3.39 | 3.43 | 3.37 |
| Fe(tot) | 2.33 | 1.92 | 1.75 | 2.19 | 1.46 | 1.40 | 2.05 | 1.45 | 1.29 |
| $Fe_2O_3$ | 3.33 | 2.75 | 2.50 | 3.13 | 2.09 | 2.00 | 2.93 | 2.07 | 1.84 |
| $TiO_2$ | 95.50 | 97.60 | 97.50 | 95.10 | 97.90 | 97.40 | 95.50 | 96.30 | 97.00 |
| CaO | 0.13 | 0.11 | 0.12 | 0.12 | 0.12 | 0.11 | 0.11 | 0.12 | 0.12 |
| MgO | 1.23 | 1.23 | 1.27 | 1.26 | 1.29 | 1.26 | 1.23 | 1.23 | 1.22 |
| $K_2O$ | 0.08 | 0.08 | 0.08 | 0.08 | 0.08 | 0.08 | 0.07 | 0.08 | 0.08 |
| MnO | 1.06 | 1.07 | 1.06 | 1.07 | 1.07 | 1.05 | 1.05 | 1.06 | 1.07 |
| $P_2O_5$ | 0.03 | 0.02 | 0.02 | 0.03 | 0.03 | 0.02 | 0.02 | 0.03 | 0.03 |
| $V_2O_5$ | 0.30 | 0.30 | 0.30 | 0.30 | 0.30 | 0.30 | 0.30 | 0.30 | 0.30 |
| C | 5.11 | 5.16 | 5.36 | 5.03 | 5.05 | 5.25 | 4.92 | 5.05 | 5.17 |
| S | 0.03 | 0.03 | 0.03 | 0.03 | 0.03 | 0.03 | 0.03 | 0.03 | 0.03 |

# Appendix 8 – Proposed process model stream tables

**Table A8.1: Stream table for streams U11-ST01 to U12-ST08**

| | U11-ST01 | U11-ST04 | U11-ST06 | U11-ST07 | U11-ST09 | U11-ST11 | U11-ST12 | U12-ST01 | U12-ST02 | U12-ST04 | U12-ST05 | U12-ST06 | U12-ST07 | U12-ST08 | U12-ST09 |
|---|---|---|---|---|---|---|---|---|---|---|---|---|---|---|---|
| Total mass (t/h) | 8.02 | 1E-05 | 21.047 | 28.94 | 4.34 | 15.79 | 0.04 | 24.56 | 1.31 | 18.57 | 21.46 | 2.89 | 10.58 | 5.18 | 7.64 |
| TEMP (°C) | 30 | 25 | 90 | 90 | 25 | 80 | 25 | 90 | 100 | 100 | 100 | 90 | 140 | 940 | 100 |
| Vapour fraction | 0 | 0 | 0 | 0 | 0 | 0 | 0 | 0 | 1 | 1 | 1 | 1 | 0 | 0 | 1 |
| GAS PHASE ($Nm^3/h$) | | | | | | | | | | | | | | | |
| $N_2(g)$ | | | | | | | | | 807 | 2750 | 4 125 | 1 375 | | | 1 375 |
| $CO(g)$ | | | | | | | | | | | | | | | |
| $H_2(g)$ | | | | | | | | | | | | | | | |
| $CO_2(g)$ | | | | | | | | | | | | | | | |
| $O_2(g)$ | | | | | | | | | 211 | | | | | | |
| $HCl(g)$ | | | | | | | | | | 320 | 320 | | | | 2 915 |
| $H_2O(g)$ | | | | | | | | | | 18 176 | 19 639 | 1 463 | | | 1 463 |
| WATER PHASE (t/h) | | | | | | | | | | | | | | | |
| $H_2O$ | | 3E-06 | 15.785 | 15.801 | | 15.785 | | 15.801 | | | | | | | |
| Cl(-1) | | 6E-06 | 5.116 | 5.116 | | | | 5.116 | | | | | | | |
| Fe(+2) | | | | 3.582 | | | | 3.582 | | | | | | | |
| H(+1) | | 1E-07 | 0.145 | 0.014 | | | | 0.014 | | | | | | | |
| Al(+3) | | | | 0.002 | | | | 0.002 | | | | | | | |
| Mg(+2) | | | | 1E-04 | | | | 1E-04 | | | | | | | |
| Mn(+2) | | | | 0.041 | | | | 0.041 | | | | | | | |
| Ca(+2) | | | | 4E-06 | | | | 4E-06 | | | | | | | |

**Stream table for streams U11-ST01 to U12-ST08 – Part 2**

| | U11-ST01 | U11-ST04 | U11-ST06 | U11-ST07 | U11-ST09 | U11-ST11 | U11-ST12 | U12-ST01 | U12-ST02 | U12-ST04 | U12-ST05 | U12-ST06 | U12-ST07 | U12-ST08 | U12-ST09 |
|---|---|---|---|---|---|---|---|---|---|---|---|---|---|---|---|
| Water phase continued | | | | | | | | | | | | | | | |
| $VO_2(+1)$ | | | | 0.001 | | | | 0.001 | | | | | | | |
| $TiCl_2O(aq)$ | | | | 0.001 | | | | 0.001 | | | | | | | |
| PURE SUBSTANCES (t/h) | | | | | | | | | | | | | | | |
| $FeCl_2*2H_2O$ | | | | | | | | | | | | | 10.440 | | |
| $FeCl_3*6H_2O$ | | | | | | | | | | | | | | | |
| $FeCl_2$ | | | | | | | | | | | | | | | |
| C | | | | | | | | | | | | | | | |
| TiN | 3.232 | | | 3.232 | 3.232 | | | | | | | | | | |
| $TiO_2$ | 0.219 | | | 0.219 | 0.219 | | | | | | | | 5E-04 | 5E-04 | |
| FeO | | | | | | | | | | | | | | | |
| Fe | 3.663 | | | 0.082 | 0.041 | | 0.041 | | | | | | | | |
| $Fe_2O_3$ | | | | | | | | | | | | | | 5.121 | |
| $Al_2O_3$ | 0.151 | | | 0.146 | 0.146 | | | | | | | | | 4E-03 | |
| MgO | 0.050 | | | 0.050 | 0.050 | | | | | | | | | 2E-04 | |
| MnO | 0.102 | | | 0.049 | 0.049 | | | | | | | | | 0.053 | |
| CaO | 0.011 | | | 0.011 | 0.011 | | | | | | | | | | |
| $V_2O_5$ | 0.015 | | | 0.014 | 0.014 | | | | | | | | | 1E-03 | |
| $SiO_2$ | 0.284 | | | 0.284 | 0.284 | | | | | | | | | | |
| other | 0.296 | | | 0.296 | 0.296 | | | | | | | | | | |

**Stream table for streams U11-ST01 to U12-ST08 – Part 3**

| | U11-ST01 | U11-ST04 | U11-ST06 | U11-ST07 | U11-ST09 | U11-ST11 | U11-ST12 | U12-ST01 | U12-ST02 | U12-ST04 | U12-ST05 | U12-ST06 | U12-ST07 | U12-ST08 | U12-ST09 |
|---|---|---|---|---|---|---|---|---|---|---|---|---|---|---|---|
| Pure substances continued | | | | | | | | | | | | | | | |
| $AlCl_3*6H_2O$ | | | | | | | | | | | | | 0.021 | | |
| $MgCl_2*2H_2O$ | | | | | | | | | | | | | 7.940E-04 | | |
| $MnCl_2*2H_2O$ | | | | | | | | | | | | | 0.120 | | |
| $CaCl_2*2H_2O$ | | | | | | | | | | | | | 1.473E-05 | | |
| $VO_2Cl$ | | | | | | | | | | | | | 1.597E-03 | | |
| $AlCl_3$ | | | | | | | | | | | | | | | |
| $MgCl_2$ | | | | | | | | | | | | | | | |
| $MnCl_2$ | | | | | | | | | | | | | | | |
| $CaCl_2$ | | | | | | | | | | | | | | 1.112E-05 | |
| Amount Phase 1 (t/h) | | | | | | | | | 1.310 | 18.567 | 21.461 | 2.895 | | | 7.636 |
| Amount Phase 2 | | 0.000 | 21.047 | 24.559 | | 15.785 | | 24.559 | | | | | | | |
| Amount Phase 3 | 8.023 | | | 4.382 | 4.342 | | 0.041 | | | | | | 10.585 | 5.180 | |

**Stream table for streams U11-ST01 to U12-ST08 – Part 4**

| | U11-ST01 | U11-ST04 | U11-ST06 | U11-ST07 | U11-ST09 | U11-ST11 | U11-ST12 | U12-ST01 | U12-ST02 | U12-ST04 | U12-ST05 | U12-ST06 | U12-ST07 | U12-ST08 | U12-ST09 |
|---|---|---|---|---|---|---|---|---|---|---|---|---|---|---|---|
| ENTHALPY TOTAL (kWh) | -7 929 | | -75 364 | -84 951 | -7 847 | -68 559 | | -77 171 | 27 | -54 185 | -58 487 | -4 312 | -16 888 | -6 296 | -7 557 |
| ENTHALPY Phase 1 | | | | | | | | | 28 | -54 185 | -58 487 | -4 312 | | | -7 557 |
| ENTHALPY Phase 2 | | | -75 364 | -77 171 | | -68 559 | | -77 171 | | | | | | | |
| ENTHALPY Phase 3 | -7 930 | | | -7 779 | -7 847 | | | | | | | | -16 888 | -6 296 | |
| GAS DENSITY (kg/m$^3$) | | | | | | | | | 1.287 | 0.874 | 0.891 | 1.020 | | | 1.327 |
| WATER DENSITY | 995 | 1 302 | 1 084 | 1 330 | 1 000 | 971 | 1 000 | 1 330 | 958 | 958 | 958 | 965 | 929 | 9 011 | 958 |
| SOLID DENSITY | 5 985.727 | | | 5018.707 | 5 002 | | 7 860 | | | | | | 2 390.075 | 5 238.852 | |
| VOLUME Total (m$^3$/h) | 1.340 | | 19.40 | 19.326 | 0.87 | 16.245 | 0.01 | 18.453 | | | | | 4.429 | 0.989 | |
| VOLUME Phase 2 | | | 19.40 | 18.453 | | 16.245 | | 18.453 | | | | | | | |
| VOLUME Phase 3 | 1.340 | | | 0.873 | 0.87 | | 0.01 | | | | | | 4.429 | 0.989 | |
| Mass fraction | | | | | | | | | | | | | | | |
| HCl | | 0.695 | 0.25 | 0.021 | | | | 0.021 | | | | | | | |
| $FeCl_2$ | | | | 0.331 | | | | 0.331 | | | | | | | |
| $MnCl_2$ | | | | 0.004 | | | | 0.004 | | | | | | | |

**Table A8.2: Stream table for streams U12-ST09 to U13-ST08**

| | U12-ST10 | U12-ST11 | U12-ST12 | U12-ST15 | U12-ST17 | U12-ST19 | U13-ST01 | U13-ST02 | U13-ST03 | U13-ST04 | U13-ST05 | U13-ST07 | U13-ST08 |
|---|---|---|---|---|---|---|---|---|---|---|---|---|---|
| Total mass (t/h) | 21.05 | 15.79 | 16.31 | 5.16 | 0.129 | 4.59 | 1.38 | 8.01 | 4.67 | 9.90 | 10.93 | 3.64 | 2.23 |
| TEMP (°C) | 70 | 80 | 70 | 80 | 100 | 160 | 25 | 40 | 950 | 950 | 930 | 200 | 25 |
| Vapour fraction | 0 | 0 | 0 | 1 | 1 | 1 | 0 | 1 | 0 | 1 | 1 | 0 | 1 |
| GAS PHASE ($Nm^3/h$) | | | | | | | | | | | | | |
| $N_2(g)$ | | | | 4 125 | | 2 750 | | 4 933 | | 4 933 | 4 933 | | 1 375 |
| $CO(g)$ | | | | | | | | | | 1 859 | 422 | | |
| $H_2(g)$ | | | | | 1 438 | | | | | | | | |
| $CO_2(g)$ | | | | | | | | | | 719 | 2 156 | | |
| $O_2(g)$ | | | | | | | | 1 289 | | | | | 359 |
| $HCl(g)$ | | | | | | | | | | | | | |
| $H_2O(g)$ | | | | | | 1 438 | | | | | | | |
| WATER PHASE (t/h) | | | | | | | | | | | | | |
| $H_2O$ | 15.785 | 15.785 | 15.785 | | | | | | | | | | |
| Cl(-1) | 5.116 | | 0.506 | | | | | | | | | | |
| Fe(+2) | | | | | | | | | | | | | |
| H(+1) | 0.145 | | 0.014 | | | | | | | | | | |
| Al(+3) | | | | | | | | | | | | | |
| Mg(+2) | | | | | | | | | | | | | |
| Mn(+2) | | | | | | | | | | | | | |
| Ca(+2) | | | | | | | | | | | | | |

**Stream table for streams U12-ST09 to U13-ST08 – Part 2**

| | U12-ST10 | U12-ST11 | U12-ST12 | U12-ST15 | U12-ST17 | U12-ST19 | U13-ST01 | U13-ST02 | U13-ST03 | U13-ST04 | U13-ST05 | U13-ST07 | U13-ST08 |
|---|---|---|---|---|---|---|---|---|---|---|---|---|---|
| WATER PHASE continued | | | | | | | | | | | | | |
| $VO_2$(+1) | | | | | | | | | | | | | |
| $TiCl_2O$(aq) | | | | | | | | | | | | | |
| PURE SUBSTANCES (t/h) | | | | | | | | | | | | | |
| $FeCl_2$*$2H_2O$ | | | | | | | | | | | | | |
| FeCl3*$6H_2O$ | | | | | | | | | | | | | |
| $FeCl_2$ | | | | | | | | | | | | | |
| C | | | | | | | 1.38 | | | | | | |
| TiN | | | | | | | | | | | | | |
| $TiO_2$ | | | | | | | | | 5.916E-04 | | | 0.001 | |
| FeO | | | | | | | | | 4.608 | | | | |
| Fe | | | | | | | | | | | | 3.582 | |
| $Fe_2O_3$ | | | | | | | | | | | | | |
| $Al_2O_3$ | | | | | | | | | 4.512E-03 | | | 0.005 | |
| MgO | | | | | | | | | 2.438E-04 | | | 2.438E-04 | |
| MnO | | | | | | | | | 0.053 | | | 0.053 | |
| CaO | | | | | | | | | | | | | |
| $V_2O_5$ | | | | | | | | | 1.227E-03 | | | 0.001 | |
| $SiO_2$ | | | | | | | | | | | | | |
| other | | | | | | | | | | | | | |

**Stream table for streams U12-ST09 to U13-ST08 – Part 3**

| | U12-ST10 | U12-ST11 | U12-ST12 | U12-ST15 | U12-ST17 | U12-ST19 | U13-ST01 | U13-ST02 | U13-ST03 | U13-ST04 | U13-ST05 | U13-ST07 | U13-ST08 |
|---|---|---|---|---|---|---|---|---|---|---|---|---|---|
| PURE SUBSTANCES continued | | | | | | | | | | | | | |
| $AlCl_3*6H_2O$ | | | | | | | | | | | | | |
| $MgCl_2*2H_2O$ | | | | | | | | | | | | | |
| $MnCl_2*2H_2O$ | | | | | | | | | | | | | |
| $CaCl_2*2H_2O$ | | | | | | | | | | | | | |
| $VO_2Cl$ | | | | | | | | | | | | | |
| $AlCl_3$ | | | | | | | | | | | | | |
| $MgCl_2$ | | | | | | | | | | | | | |
| $MnCl_2$ | | | | | | | | | | | | | |
| $CaCl_2$ | | | | | | | | | 1.11E-05 | | | 1.1E-5 | |
| Amount Phase 1 (t/h) | | | | 5.156 | 0.129 | 4.593 | | 8.005 | | 9.900 | 10.926 | | 2.232 |
| Amount Phase 2 | 21.047 | 15.785 | 16.305 | | | | | | | | | | |
| Amount Phase 3 | | | | | | | 1.382 | | 4.667 | | | 3.641 | |

**Stream table for streams U12-ST09 to U13-ST08 – Part 4**

| | U12-ST10 | U12-ST11 | U12-ST12 | U12-ST15 | U12-ST17 | U12-ST19 | U13-ST01 | U13-ST02 | U13-ST03 | U13-ST04 | U13-ST05 | U13-ST07 | U13-ST08 |
|---|---|---|---|---|---|---|---|---|---|---|---|---|---|
| ENTHALPY TOTAL (kWh) | -75 642 | -68 559 | -69 425 | 82 | 38 | -4 092 | | 33 | -4 011 | -3 203 | -8 025 | -20 | |
| ENTHALPY Phase 1 | | | | 82 | 38 | -4 092 | | 34 | | -3 203 | -8 025 | | |
| ENTHALPY Phase 2 | -75 642 | -68 559 | -69 425 | | | | | | | | | | |
| ENTHALPY Phase 3 | | | | | | | | | -4 011 | | | -20 | |
| GAS DENSITY (kg/m$^3$) | | | | 1.25 | 0.090 | 1.097 | | 1.287 | | 1.318 | 1.455 | | 1.287 |
| WATER DENSITY | 1 095 | 971 | 992 | 972 | 958 | 915 | 996 | 992 | 9 327 | 9 327 | 8 704 | 893 | 996 |
| SOLID DENSITY | | | | | | | 2 260 | | 5 987 | | | 7 793 | |
| VOLUME total (m$^3$/h) | 19.209 | 16.245 | 16.427 | | | | 0.611 | | 0.780 | | | 0.47 | |
| VOLUME Phase 2 | 19.209 | 16.245 | 16.427 | | | | | | | | | | |
| VOLUME Phase 3 | | | | | | | 0.611 | | 0.780 | | | 0.47 | |
| Mass fraction | | | | | | | | | | | | | |
| HCl | 0.250 | | 0.032 | | | | | | | | | | |
| $FeCl_2$ | | | | | | | | | | | | | |
| $MnCl_2$ | | | | | | | | | | | | | |